Searching for New Particles at the Large Hadron Collider: Theory and Methods for Extradimensional Supersymmetry

James Scoville

University College

University of Oxford

A thesis submitted for the degree of

Doctor of Philosophy

Trinity 2015

Abstract

The hierarchy problem of the electroweak scale is an intriguing puzzle which can conceivably be solved during upcoming runs of the Large Hadron Collider (LHC). Supersymmetry (SUSY) is an attractive potential solution to this problem, though the fact that no supersymmetric particles have been discovered thus far raises fine tuning of most models to $\mathcal{O}(1\%)$. Extradimensional SUSY is especially interesting in light of this fact since certain models are easier to reconcile with LHC data. This thesis discusses two different extradimensional SUSY scenarios: auto-concealment and Maximally Natural SUSY (MNSUSY). The auto-concealment mechanism applies when the lightest ordinary supersymmetric particle (LOSP), a brane localized state, promptly decays to the Kaluza-Klein (KK) tower of a bulk lightest supersymmetric particle (LSP). This dynamically realizes the compression mechanism for hiding SUSY as decays into the more numerous heavier KK LSP states are favored. LHC limits on LOSP squarks weaken to $\lesssim 450$ GeV while limits on LOSP right-handed sleptons evaporate. Slepton searches perform poorly in this case because LHC analyses are blind to compressed slepton spectra. To help fill this gap, this thesis presents a monojet-like search sensitive to the very compressed range $3 \text{ GeV} < m_{\tilde{l}} - m_{\tilde{\chi}_1^0} < 24 \text{ GeV}$. The analysis should allow LHC14 with 100 fb^{-1} to search for degenerate left-handed selectrons and smuons in the compressed region up to $m_{\tilde{l}_L} \lesssim 150$ GeV. In addition, it should be sensitive to $m_{\tilde{l}_L} \lesssim 110$ GeV for auto-concealed SUSY. To expand the class of extradimensional SUSY models the LHC is able to test this thesis also describes the Lagrangian and mass matrices of MNSUSY, which are needed to implement this model in the Feynman rules generator program FeynRules for use in Monte Carlo programs for collider simulations. It also describes benchmark scenarios useful for the first collider phenomenology studies.

For my family.

Acknowledgements

I offer my deepest thanks to my advisors John March-Russell and Alan Barr for their incredible dedication, guidance, enthusiasm, advice, and support not only during the preparation of this thesis but during my entire time at Oxford. Without them my research would have been impossible and it was a fantastic privilege and delight to work with both of them.

I also gratefully acknowledge the support and teaching I received from my collaborators at Stanford: Savas Dimopoulos and Kiel Howe. Not only did they enable, strengthen, and refine my research, but they also made my studies far more enjoyable.

I would like to thank the many other people, in Oxford and abroad, who helped fill the numerous gaps in my knowledge and who offered advice on various parts of this work. This includes Juan Rojo, Ulrich Haisch, Guido Bell, Joseph Conlon, Emanuele Re, Isabel García García, Mireia Crispin-Ortuzar, William Kalderon, Alexandru Dafinca, Claire Gwenlan, William Fawcett, Koichi Nagai, and Jonathan Burr. I am also deeply indebted to Jonathan Patterson who worked me through difficulties with the Oxford computing cluster on countless occasions, including many nights and weekends.

Most importantly the gratitude I have towards my family is beyond words. Without my parents' unconditional love and support I would have not reached where I am today. Likewise my wife's family has always been available when I needed them most. My kids are the constant heartbeat of joy in my life and I am grateful for every moment with them. Finally, my wife is the love of my life and the first officer of our home – with her by my side we have conquered the toughest challenges in our lives. Thank God for them all!

Finally, I gratefully acknowledge support from the United States Air Force

Institute of Technology. The views expressed in this work are my own and do not reflect the official policy or position of the United States Air Force, Department of Defense, or the US Government.

Statement of Originality

This thesis is based on original research and contains no material that has already been accepted, or is concurrently being submitted, for any degree or diploma or certificate or other qualification in this university or elsewhere. To the best of my knowledge and belief this thesis contains no material previously published or written by another person, except where due reference is made in the text.

James Scoville 2015

Contents

Chapter 1: Introduction

> The absence of supersymmetry signals at the LHC is not only evidence for supersymmetry but also for extra dimensions. (Savas Dimopoulos[1])

The Standard Model (SM) is an incredibly successful theory of subatomic physics. It has passed a dizzying array of experimental tests, with its most recent success being the discovery of the Higgs boson in 2012 [1, 2]. Nevertheless, there are a number of reasons to expect that it is not the final word in fundamental physics. Notably, it fails to address questions such as: What is the origin and nature of neutrino masses? Do the forces of nature unify? What is dark matter (DM) and dark energy? Why is the electroweak scale so small compared to the Planck scale. The last question is known as the hierarchy or naturalness problem and is a large motivating factor behind this thesis.

While there are a number of competing theories beyond the Standard Model (BSM) which seek to answer some of these questions, none address them all. One of the most popular theories, Supersymmetry (SUSY), manages to tackle several questions by postulating a new symmetry of nature under which every fermion comes with a boson partner, and vice-versa. These new partners are known as superpartners or sparticles. One of the most important phenomenological predictions of SUSY (or at least of SUSY which addresses the hierarchy problem) is the existence of sparticles in a range which should be detectable by the Large Hadron Collider (LHC).

Unfortunately for SUSY supporters there have been no SUSY signals at the LHC so far [3, 4]. This has put into question SUSY's ability to address the hierarchy problem [5]. Recently, however, a number of studies have come forward investigating the phenomenology of extradimensional SUSY to help relieve this tension, either by weakening collider limits on new particles – as in the auto-concealment mechanism [6] – or by reducing the level of fine tuning in the model – as in Maximally Natural Supersymmetry (MNSUSY) [7, 8]. These models have yet to undergo dedicated analysis by the LHC collaborations. This thesis was written to discuss challenges associated with searching for extradimensional SUSY and to introduce tools to help experimentalists confront these theories at the LHC.

[1] In jest, to be sure.

The structure of this work is as follows. Chapter 2 briefly reviews the SM and some of its weaknesses, with a particular focus on the hierarchy problem. Chapter 3 introduces SUSY in higher dimensions. Chapter 4 focuses on both the theory and methods of Monte Carlo collider simulations, which were the primary tools used to conduct the work in this thesis. Chapter 5 gives an overview of the LHC and the ATLAS detector with a specific emphasis on how the design of these machines affects SUSY searches. Chapter 6 then addresses how a specific extradimensional SUSY mechanism known as auto-concealment can weaken current LHC limits on sparticle masses. Chapter 7 introduces a new search strategy designed not only to fill a gap left by auto-concealment, but also to address a blind spot in current searches for less exotic SUSY models. Chapter 8 describes FeynRules code and benchmark models for collider pheno studies of a 5D SUSY model MNSUSY. Finally, ch. 9 summarizes this work.

Chapter 2: Motivations for new physics at the TeV scale

In this chapter we briefly review the main concepts of the SM before moving on to discuss motivations for exploring beyond it. In particular, we will address the hierarchy problem, which is perhaps the strongest reason to expect new physics at the TeV scale. Other open questions in the SM will be covered in less detail. Much of the information covered in the following section can be found in various textbooks – I used ref. [9] extensively.

2.1 The Standard Model

The SM is built upon the machinery of quantum field theory and relies heavily on symmetries to describe subatomic interactions. At its heart lie the global symmetry of Poincaré invariance and three local (gauge) symmetries. The fields in the SM and their interactions can be described via their transformations under specific representations of these symmetry groups.

Under the Poincaré group (or more properly its subgroup, the Lorentz group, which describes boosts and rotations) SM fields fall under one of four representations of the algebra $so(1,3) = su(2) \oplus su(2)$, where the lower-case letters denote the groups' algebras. These representations are summarized in table 2.1.

Fields in the $(0,0)$ representation of $su(2) \oplus su(2)$ transform as scalars under the $SO(3)$ subgroup. The Higgs field H is the only fundamental scalar in the SM. Fields in the representations $(\frac{1}{2},0)$ transform as *left-handed Weyl spinors* while those in $(0,\frac{1}{2})$ transform as *right-handed Weyl spinors* under $SO(3)$. The two are related by conjugation therefore it is notationally convenient to define all right-handed spinors as those appearing

$su(2) \oplus su(2)$	$(0,0)$	$(\frac{1}{2},0)$	$(0,\frac{1}{2})$	$(\frac{1}{2},\frac{1}{2})$
$so(3)$	0	$\frac{1}{2}$	$\frac{1}{2}$	$1 \oplus 0$

Table 2.1: Irreducible representations of the Lorentz algebra $su(2) \oplus su(2)$ and its decomposition into the $so(3)$ subalgebra of rotations. The representation under $so(3)$ describes the particle's spin. Table adapted from [9].

with a dagger $\psi^\dagger$, and left-handed spinors as ψ.[1] The SM has five types of spinors: Q, L, $\overline{e}^\dagger$, $\overline{d}^\dagger$, and $\overline{u}^\dagger$. Consistent with our conventions, we have put daggers on the last three to indicate they are right-handed; the bar above them is simply part of the Weyl spinors' names and does not denote any kind of conjugation. As an example, $\overline{e}^\dagger$ is often called e_R. Defining fields in this way will make the jump to SUSY a bit easier, in which $\overline{e}$ will form part of a left-chiral *superfield*. For each type of spinor field there exists three *generations* or copies of the field, each with a different coupling to the Higgs field – why this should be so is unclear.

Finally, fields in the $(\frac{1}{2}, \frac{1}{2})$ representation transform as a scalar (0) and a vector (1) under $SO(3)$. In fact there are no SM fields which transform as both a scalar and a vector. The scalar must be removed by the correct choice of the kinetic term in the Lagrangian. There are three types of vector fields in the SM represented by B_μ, W_μ, and g_μ.

As already mentioned, in addition to the global Poincaré symmetry of the SM there also exists three local symmetries: $U(1)_Y$, $SU(2)_W$, and $SU(3)_C$. Each of the spinors and scalars transform under these symmetries as $\psi \to U(x)\psi$ with

$$U(x) = \exp(i\alpha^a(x)T^a) \tag{2.1}$$

where U is a representation of the local group (either the fundamental or trivial representation). The matrices T^a form the algebra of this representation. To keep the Lagrangian invariant under this transformation requires replacing ordinary derivatives by covariant derivatives

$$\partial_\mu\psi \to D_\mu\psi = \partial_\mu\psi - igA^a_\mu(x)T^a\psi. \tag{2.2}$$

where the field $A^a_\mu(x)$ transforms as

$$A^a_\mu(x) \to A^a_\mu(x) + \frac{1}{g}\partial_\mu\alpha^a(x) - f^{abc}\alpha^b(x)A^c_\mu(x). \tag{2.3}$$

and the parameter g gives the strength of the coupling between the fields. For abelian fields one may replace T^a by the ψ field's $U(1)$ charge and set f^{abc} to zero.

Thus a local symmetry requires the introduction of a new vector field $A^a_\mu(x)$. This field is in the adjoint representation and must have its own kinetic term. In the SM these vector fields are precisely those already mentioned: B_μ, W_μ, and g_μ corresponding

[1] We adopt the conventions of Martin's SUSY Primer [10] when discussing spinor products.

Name	SU(2) Components	$SO(3)$	$SU(3)_C, SU(2)_W, U(1)_Y$
g_μ	–	1	$(\mathbf{8}, \mathbf{1}, 0)$
W_μ	$(W^1_\mu, W^2_\mu, W^3_\mu)$	1	$(\mathbf{1}, \mathbf{3}, 0)$
B_μ	–	1	$(\mathbf{1}, \mathbf{1}, 0)$
Q_i	(u_{Li}, d_{Li})	$\frac{1}{2}$	$(\mathbf{3}, \mathbf{2}, \frac{1}{6})$
L_i	(ν_{Li}, e_{Li})	$\frac{1}{2}$	$(\mathbf{1}, \mathbf{2}, -\frac{1}{2})$
$\overline{u}^\dagger_i$	–	$\frac{1}{2}$	$(\mathbf{3}, \mathbf{1}, \frac{2}{3})$
$\overline{d}^\dagger_i$	–	$\frac{1}{2}$	$(\mathbf{3}, \mathbf{1}, -\frac{1}{3})$
$\overline{e}^\dagger_i$	–	$\frac{1}{2}$	$(\mathbf{1}, \mathbf{1}, -1)$
H	$(G^+, \frac{1}{\sqrt{2}}(v + h + iG^0)$	0	$(\mathbf{1}, \mathbf{2}, \frac{1}{2})$

Table 2.2: Group transformation properties of the SM Field Content. Following the conventions of ref [10], daggered spinors indicate that they are right-handed and the bar over them is simply part of their name – it does not denote any kind of conjugation. The indices i on the spinors runs from 1 to 3 and indicates that they each come in three generations.

to the gauge groups $U(1)_Y$, $SU(2)_W$, and $SU(3)_C$ respectively. The subscripts stand for *hypercharge, weak, and color* – the names of the forces that result from exchange of the gauge fields. The color force is also called the strong force due to the fact that its coupling g is the largest of the three; so large in fact that perturbation theory breaks down below energies of about 1 GeV – a fact important for its phenomenology. The various group transformation properties of the SM field content are summarized in table 2.2.

The Lagrangian of the SM is renormalizable and satisfies the symmetries just discussed. It is neatly summarized by

$$\begin{aligned}\mathcal{L} = &-\frac{1}{4}F^a_{\mu\nu}F^{a\mu\nu} + i\psi^\dagger_i\overline{\sigma}^\mu D_\mu\psi_i + |D_\mu H|^2 + \mu^2|H|^2 - \lambda|H|^4 - \\ &(\overline{u}_i\mathbf{y}^u_{ij}Q_j\cdot H + \overline{d}_i\mathbf{y}^u_{ij}Q_jH^\dagger + \overline{e}_i\mathbf{y}^e_{ij}L_jH^\dagger + \text{h.c.})\end{aligned} \tag{2.4}$$

where $F^a_{\mu\nu} = \partial_\mu A_\nu - \partial_\nu A_\mu + gf^{abc}A^b_\mu A^c_\nu$ are the gauge field strength tensors, ψ_i are the SM spinor fields, and $Q_j \cdot H = Q_{ja}\epsilon^{ab}H_b = Q_{j1}H_2 - Q_{j2}H_1$ denotes the invariant product over $SU(2)_W$ indices. The spinor-spinor-scalar terms are known as *Yukawa interactions*. Mass terms for the fermions are forbidden for all fields except the Higgs by gauge invariance. Interestingly, the field content of the SM is such that gauge invariance enforces an accidental global $U(1)_{B-L}$ symmetry where $\psi \to \exp(i(B_\psi - L_\psi)\alpha)\psi$ with

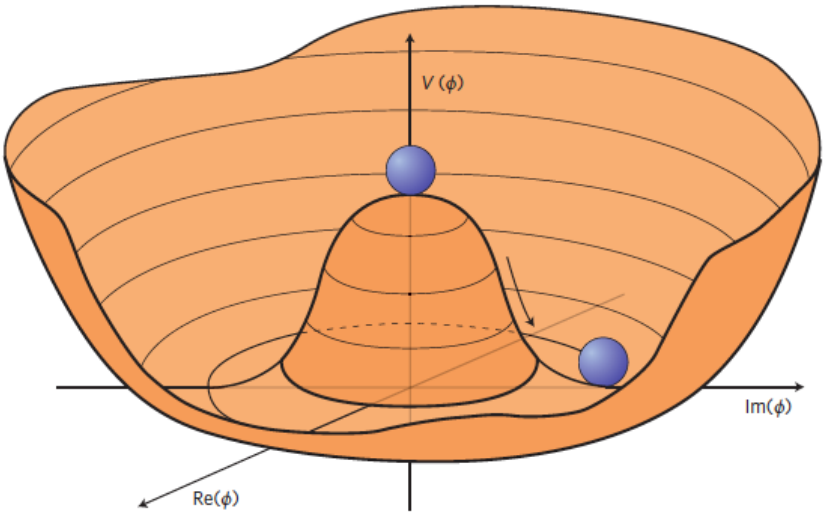

Figure 2.1: Spontaneous symmetry breaking of a complex scalar ϕ field due to a negative quadratic term in its potential $V(\phi)$. The minima of the potential is no longer at $\phi = 0$ (the top of the hill) where the symmetry of the potential is manifest, but rather at the bottom of the potential. Figure taken from [11].

$L_L = L_{\bar{e}^\dagger} = 1$, $B_Q = B_{\bar{u}^\dagger} = B_{\bar{d}^\dagger} = 1/3$, and $B_L = B_{\bar{e}^\dagger} = L_Q = L_{\bar{u}^\dagger} = L_{\bar{d}^\dagger} = 0$. This will be important later.

The theory described thus far is made much richer by the fact that the $SU(2)_W$ symmetry is spontaneously broken by a *vacuum expectation value* (VEV) for the Higgs field – a process known as Electroweak Symmetry Breaking (EWSB). This occurs because the sign of the quadratic term in the Higgs potential $V(H) = -\mu^2|H|^2 + \lambda|H|^4$ is negative (μ^2 is defined to be positive). Why this mass term should be negative is an unanswered question in the SM. Nevertheless, this sign means the vacuum energy is minimized when the Higgs field develops a non-zero VEV. We can choose a $SU(2)$ basis such that

$$\langle h \rangle = \begin{pmatrix} 0 \\ \frac{v}{\sqrt{2}} \end{pmatrix} \tag{2.5}$$

with $v = 247$ GeV. This remarkable fact means that even though the SM Lagrangian has a $SU(2)_W$ gauge invariance, the vacuum does not! This *spontaneous symmetry breaking* can be visualized using the famous "mexican hat" potential shown in fig. 2.1.

Substituting the Higgs VEV back into the Lagrangian one finds that the $W_\mu^{1,2,3}$ gauge bosons mix with the B_μ gauge boson to form three massive vector bosons W_μ^+, W_μ^-, and Z_μ^0 as well as one massless vector boson γ, the photon, which is associated with the residual $U(1)_{\text{EM}}$ gauge symmetry. The $U(1)_{\text{EM}}$ has coupling strength $e = g\sin(\theta_W)$ where

$SO(3)$	Particle Type	Name	Symbol	Mass	$SU(3)_C, U(1)_{\rm EM}$
1	gauge boson	W boson	W	80.39 GeV	$(\mathbf{1}, \pm 1)$
		Z boson	Z	91.19 GeV	$(\mathbf{1}, 0)$
		photon	γ	0	$(\mathbf{1}, 0)$
		gluon	g	0	$(\mathbf{8}, 0)$
1/2	quark	up	u	2.3 MeV	$(\mathbf{3}, +2/3)$
		charm	c	1.275 GeV	
		top	t	173.2 GeV	
		down	d	4.8 MeV	$(\mathbf{3}, -1/3)$
		strange	s	95 MeV	
		bottom	b	4.18 GeV	
	lepton	electron	e	0.511 MeV	$(\mathbf{1}, -1)$
		muon	μ	105.7 MeV	
		tau	τ	1.778 GeV	
		electron neutrino	ν_e	< 2 eV	$(\mathbf{1}, 0)$
		muon neutrino	ν_μ	< 2 eV	
		tau neutrino	ν_τ	< 2 eV	
0	Higgs boson	Higgs	h	125.7 GeV	$(\mathbf{1}, 0)$

Table 2.3: Physical particle content of the SM. Masses are taken from the Particle Data Group [12].

$\tan(\theta_W) = g'/g$ is the ratio of the $U(1)_Y$ to $SU(2)_W$ couplings. Three of the complex Higgs doublet's degrees of freedom $G^\pm, G^0$ provide the extra degrees of freedom necessary for the vector bosons to become massive. One neutral scalar Higgs field h remains with a mass $m_h^2 = 2\lambda v^2 = 2\mu^2$. Additionally, the fermions acquire Dirac masses proportional to the strength of their Yukawa couplings. When the dust settles after EWSB the physical spectrum consists of one real scalar field h, types of massless vector bosons γ and g_μ^a, three massive vector bosons W_μ^+, W_μ^-, and Z_μ^0, three u-type Dirac fermions, three d-type Dirac fermions, three e-type Dirac fermions, and three ν-type fermions. This is summarized in table 2.3

As a final note in discussing the SM content, it's worth mentioning that since the discovery of neutrino oscillations, it is now well known that the SM must be augmented by a mechanism for generating neutrino masses [12]. There are several ways of doing so, either through higher dimensional operators, Yukawa interactions involving a gauge singlet $\overline{\nu}^\dagger$, and (optionally) a Majorana mass for $\overline{\nu}^\dagger$ along with the see-saw mechanism. Since it is not yet known whether the neutrino mass is Dirac or Majorana one cannot say which method is correct.

2.2 Open problems in the Standard Model

The SM has been beautifully confirmed in countless experiments since its inception, with its capstone placed in 2012 when the LHC discovered the Higgs boson [1, 2] – the last missing particle in the theory. Nevertheless, the SM has a number of unexplained features which demand attention. Perhaps one of the most frequently discussed has ironically become more urgent after the discovery of the Higgs. This is the infamous hierarchy or naturalness problem. Though it is not necessarily the largest open problem in the SM it is the best reason to expect new physics at the TeV scale within reach of the LHC. Therefore, we address this problem in the following section. Other open questions in the SM are mentioned in sec. 2.2.2.

2.2.1 The hierarchy problem

Ken Wilson taught us that coefficients of operators with dimension less than four are *relevant* in the sense that they are sensitive to the details of short distance physics which describes the UV completion of a theory [13]. Thus, if any new physics exists at energies above the EW scale, the details of this theory should have a large impact on the only relevant operator in the SM: $\mu^2|H|^2$, or equivalently the Higgs mass (or any other measure of the EW scale, such as the Z mass). This is a concern because we expect new physics at energies above the EW scale – if nothing else a UV completion to gravity should exist at the Planck scale around 10^{19} GeV.

This problem can be made clearer by considering the size of quantum corrections to the mass m_s of a scalar ϕ arising from a new fermion f of mass $m_f \gg m_s$ due to the interaction $\lambda_f \phi f f$. Writing $m_s^2 = m_{s\ \text{bare}}^2 + \Sigma_s$ we obtain

$i\Sigma_s =$ 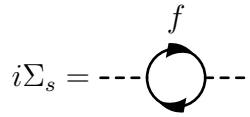

$$= i\frac{\lambda_f^2}{8\pi^2}\left(\Lambda^2 - 3m_f^2 \log\left(\frac{\Lambda^2}{m_f^2}\right) + ...\right). \tag{2.6}$$

where we have introduced a cut-off Λ to regulate the integral.

Two problems become evident when looking at this expression. The first is that

quantum corrections to the Higgs mass squared appear to have a quadratic sensitivity to the cut-off Λ. However this sensitivity is not present in all renormalization schemes. Indeed, this divergence appears as the typical $1/\epsilon$ when using dimensional regularization and can be removed using counter terms as usual. Thus it is not clear that the first term in this expression really denotes a sensitivity to UV physics.

The second term, however, appears regardless of the regularization scheme and is definitely a problem. This term is proportional to the square of the fermion mass m_f^2, which we are assuming to be much heavier than the Higgs. Thus the Higgs mass appears to be highly sensitive to UV physics.

This sensitivity to high scale physics is in stark contrast to quantum corrections to the mass of a fermion. In this case the size of the correction is proportional to the fermion's own mass. Going through the same exercise as before we obtain

$$i\Sigma_f = \quad \phi$$
$$= i\frac{m_f \lambda_f^2}{16\pi^2} \log\left(\frac{\Lambda^2}{m_s^2}\right) + ... \tag{2.7}$$

A simple way to see why this must be so is to notice that left and right-handed fermions such as e_L and $\overline{e}^\dagger$ are only coupled via their mass (or equivalently, their Yukawa interactions) – as in $m_e(e_L\overline{e} + \text{h.c.})$. If one sets $m_e \to 0$, then an additional *custodial* symmetry appears under which e_L and $\overline{e}^\dagger$ have opposite charge: $e_L \to e^{-i\alpha}e_L$ and $\overline{e}^\dagger \to e^{i\alpha}\overline{e}^\dagger$. Since this symmetry is exact, m_e will stay zero to all orders in perturbation theory. If we once again introduce m_e then every diagram which violates custodial symmetry must be proportional to the only thing which does the violating: m_e. Therefore, quantum corrections to m_e must be proportional to m_e itself. If this parameter starts off small then quantum corrections will not do much to change this. The mass of a fermion is *technically natural* [14].

To quantify the Higgs' sensitivity to UV physics it is useful to introduce the concept of fine tuning [15]. Fine tuning is defined as the fractional sensitivity of an observable $\mathcal{O}$ (like the Higgs mass) due to a change in a UV parameter α (such as the mass of a heavy

fermion) divided by the fractional change in that UV parameter. Or more succinctly

$$\begin{aligned} \mathrm{FT}_{\mathcal{O}} =& \frac{\%\text{change in } \mathcal{O}}{\%\text{change in } \alpha} \\ =& \frac{\partial \log \mathcal{O}}{\partial \log \alpha}. \end{aligned} \tag{2.8}$$

If there is more than one relevant variable α_i then the total fine tuning with respect to each of these variables is usually added in quadrature.

As an example, suppose that a new fermion near the Planck scale $\sim 10^{19}$GeV couples to the Higgs with an order one coupling. Then adjusting this parameter by a factor of 10^{-34} will result in an order one change to the quantum correction for the Higgs mass and a fine tuning of 10^{34}. This rather extreme example shows that there must be a very fine cancellation of parameters to arrive at a Higgs mass so much lower than the Planck scale. This would appear to be quite an unnatural situation.

There are a number of ways to deal with this problem. It could be, for instance, that the Higgs is not a fundamental particle but is rather composite as in Technicolor models [16]. Or it could be that the fundamental UV cutoff is much lower than the Planck scale, or that there is simply no new physics between the EW scale and the Planck scale. If none of these are true then one is lead to assume that either the universe is fundamentally unnatural or there must be some new symmetry responsible for the miraculous cancellations between quantum corrections which could feed into the Higgs mass. One such new symmetry is SUSY, which we discuss in ch. 3.

2.2.2 Other open problems in the Standard Model

Besides the hierarchy problem there are a number of other open questions in the SM. We discuss two for which SUSY offers a possible explanation in order to provide context for later discussions.

The first problem or question comes from the fact that the three gauge couplings have drastically different values at low energies. In particular the strong force coupling becomes non-perturbative at energies below about a GeV – the *confinement scale* where bound states of quarks (hadrons) form. However, the gauge couplings experience different renormalization group runnings and come intriguingly close to the same value near the

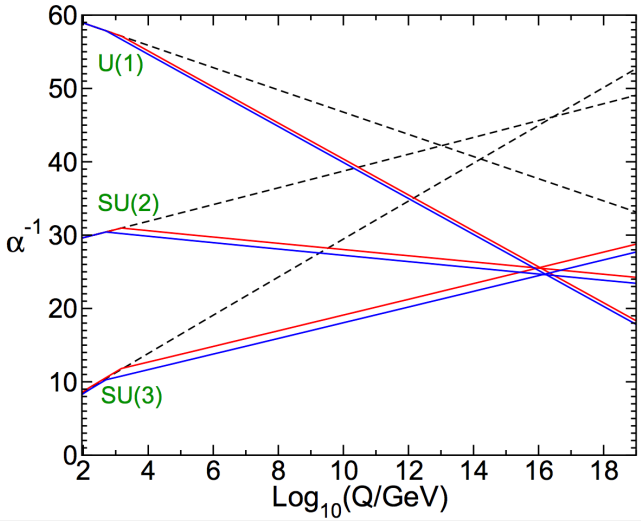

Figure 2.2: RG running of $\alpha^{-1} = 4\pi/g^2$ for all three gauge couplings. The dotted lines show the RG running in the SM, while the solid lines show the running in the MSSM (addressed in ch. 3). Figure taken from [10].

Grand Unified Theory (GUT) scale of 10^{16} GeV. This has lead many to speculate that the three gauge forces may in fact be one force which is spontaneously broken at the GUT scale [17–19]. In this case three free parameters in the SM are reduced to one – a very attractive picture. The simplest SUSY model, the Minimal Supersymmetric Standard Model discussed in ch. 3, brings the couplings into near perfect agreement, as shown in fig. 2.2 .

The second issue we mention is the apparent existence of Dark Matter (DM). DM neither absorbs nor emits light to any significant degree but its presence can be inferred from gravitational effects on galaxy rotation rates, galaxy clusters, gravitational lensing, big bang nucleosynthesis, structure formation, and the cosmic microwave background [20]. Unfortunately, the SM provides no viable DM candidates. However, the lightest supersymmetric particle (LSP) can be one if it is neutral.

There are a few other open problems in the SM which certain SUSY models can explain such as the muon magnetic moment anomaly [21] and the source of EW symmetry breaking [10, 22]. A discussion of these issues provides less relevant background for the chapters which follow so we pass on it here. Instead we move on to discuss SUSY in both 4D and in higher dimensions.

Chapter 3: Supersymmetry in extra dimensions

3.1 4D supersymmetry

As we discussed in sec. 2.2.1, the hierarchy problem arises from the fact that the squared mass of a scalar particle receives large quantum corrections proportional to the squared mass of any new heavy particles. This is true whether the heavy particle is a boson or a fermion, but with the intriguing difference that a fermion loop carries the opposite sign. This observation leads to one potential solution to the hierarchy problem: perhaps every boson comes with a fermion partner with couplings such that all large quantum corrections to the Higgs mass are canceled.

With this as motivation consider a complex scalar, which we suggestively call a *sfermion* $\tilde{f}$, that couples to the Higgs. Then its contribution to the Higgs mass is

$i\Sigma_s =$ 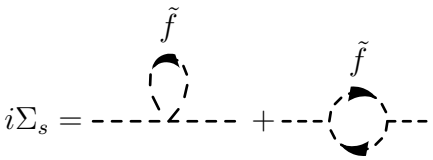

$$= -i\frac{\lambda_{\tilde{f}}}{16\pi^2}\left(\Lambda^2 - m_{\tilde{f}}^2 \log\left(\frac{\Lambda^2}{m_{\tilde{f}}^2}\right)\right) + i\frac{m_f^2\lambda_{\tilde{f}}^2}{8\pi^2\lambda_f^2}\left(\log\left(\frac{\Lambda^2}{m_{\tilde{f}}^2}\right)\right). \tag{3.1}$$

where we have replaced $v \to \sqrt{2}m_f/\lambda_f$ in the last term which is true for SM fermions. Comparing this expression to 2.6 we see that if we had two complex scalars for every Dirac fermion (or equivalently one complex scalar for every Weyl spinor), if $\lambda_{\tilde{f}} = \lambda_f^2$, and if $m_f = m_{\tilde{f}}$ then the radiative corrections would cancel, resolving the hierarchy problem. Such a complex relation between bosons and fermions as well as their couplings implies a new symmetry known as supersymmetry or SUSY. This chapter reviews the basics of 4D SUSY – for more information one should turn to ref. [10], where much of this information can be found.

3.1.1 The structure of SUSY

Schematically, a supersymmetric transformation takes

$$Q|\text{boson}\rangle \to |\text{fermion}\rangle \qquad \text{and} \qquad Q|\text{fermion}\rangle \to |\text{boson}\rangle. \tag{3.2}$$

From the form of 3.2 we see that the generator of SUSY transformations, Q, must itself be a spinor. To be more concrete, the generators Q and $Q^\dagger$ satisfy the algebra [10, 23]

$$\begin{aligned} \{Q_\alpha, Q^\dagger_{\dot\alpha}\} &= -2\sigma^\mu_{\alpha\dot\alpha} P_\mu, \qquad \{Q_\alpha, Q_\beta\} = \{Q^\dagger_{\dot\alpha}, Q^\dagger_{\dot\beta}\} = 0 \\ [Q_\alpha, M^{\mu\nu}] &= \sigma^{\mu\nu\beta}{}_\alpha\, Q_\beta, \qquad [Q_\alpha, P^\mu] = 0 \end{aligned} \tag{3.3}$$

with $M^{\mu\nu}$ obeying the Lorentz algebra

$$[M^{\mu\nu}, M^{\rho\sigma}] = i(M^{\mu\sigma}\eta^{\nu\rho} + M^{\nu\rho}\eta^{\mu\sigma} - M^{\mu\rho}\eta^{\nu\sigma} - M^{\nu\sigma}\eta^{\mu\rho}). \tag{3.4}$$

From $[Q_\alpha, P^\mu] = 0$ we see that SUSY preserves the four momentum p^μ of a particle; therefore particles within a *supermultiplet* should have the same mass. For a massless supermultiplet with $p_\mu = (E, 0, 0, E)$

$$\{Q_\alpha, Q^\dagger_{\dot\alpha}\} = -2\sigma^\mu_{\alpha\dot\alpha} P_\mu \to -2E(\sigma^0 + \sigma^3)_{\alpha\dot\alpha} = -4E \begin{pmatrix} 1 & 0 \\ 0 & 0 \end{pmatrix}_{\alpha\dot\alpha} \tag{3.5}$$

so that $Q_2 = 0$ and $Q_1 \equiv Q$ is the generator of supersymmetric transformations in this representation. The structure $\{Q, Q^\dagger\} \propto 1$ is the same as for ladder operators and the equation $[Q_\alpha, M^{\mu\nu}] = \sigma^{\mu\nu\beta}{}_\alpha\, Q_\beta$ implies

$$\begin{aligned} [Q, J^3] &= \tfrac{1}{2}\sigma^3{}_{11} Q = \tfrac{1}{2} Q \\ \Rightarrow J^3 Q &= Q(J^3 - 1/2) \end{aligned} \tag{3.6}$$

Thus Q lowers the helicity of a particle by $1/2$ while $Q^\dagger$ raises it, in agreement with the schematic form given in eq. 3.2 [23]. Multiple applications of Q and $Q^\dagger$ annihilate the state due to $\{Q_\alpha, Q_\beta\} = 0$. An infinitesimal SUSY transformation can be parameterized using the left-handed Weyl spinor ϵ_α and takes the form $\epsilon Q + \epsilon^\dagger Q^\dagger$.

To understand the Q operators a little more fully we introduce the concept of *superspace*, which we will encounter again in chs. 6 and 8. Superspace makes it especially easy

to write down $\mathcal{N} = 1$ SUSY Lagrangians. It is parameterized by the coordinates

$$(x^\mu, \theta^\alpha, \theta^\dagger_{\dot{\alpha}}) \tag{3.7}$$

where x^μ is the spacetime coordinate, and θ, $\theta^\dagger$ are anticommuting spinor coordinates. The reason we introduce these new coordinates is that it allows us to combine the component fields of a supermultiplet into one object $S(x^\mu, \theta, \theta^\dagger)$ called a *superfield*, and it also allows us to represent supersymmetric transformations as translations over the new coordinate space. In the end it makes building SUSY Lagrangians fairly straightforward.

One can expand $S(x^\mu, \theta, \theta^\dagger)$ in a power series over the anticommuting coordinates. Since there are two independent coordinates in both θ^α and $\theta^\dagger_{\dot{\alpha}}$ the expansion always terminates with at most two θ's and two $\theta^\dagger$'s. Thus a general superfield can be written:

$$S(\theta, \theta^\dagger) = \phi + \sqrt{2}\theta\psi + \sqrt{2}\theta^\dagger\psi'^\dagger + \theta\theta F + \theta^\dagger\theta^\dagger F' + \theta^\dagger\overline{\sigma}^\mu\theta V_\mu + \theta^\dagger\theta^\dagger\theta\lambda + \theta\theta\theta^\dagger\lambda'^\dagger + \frac{1}{2}\theta\theta\theta^\dagger\theta^\dagger D \tag{3.8}$$

where the factors of $\sqrt{2}$ and $1/2$ are added for convenience. Note that the product of superfields can similarly be expanded in terms of Grassmann coordinates and is a superfield in its own right. So, for example, one can ask for the "F-term" or the "θ^2" component of the product superfield $S = s_1 s_2$ by writing [1]

$$S|_{\theta^2} = (s_1 s_2)|_{\theta^2} = \psi_1\psi_2 + \phi_1 F_2 + \phi_2 F_1. \tag{3.9}$$

This type of operation is encountered frequently when constructing a SUSY invariant theory, as we will see shortly.

Just as the operator P_μ generates spacetime translations, Q and $Q^\dagger$ generate translations over the coordinates θ and $\theta^\dagger$ respectively. Similarly, just as one can represent the abstract operator P_μ as a differential operator in spacetime $\mathcal{P}_\mu \equiv -i\partial_\mu$ the operators Q and $Q^\dagger$ can be represented by differential operators in superspace $\mathcal{Q}$ and $\mathcal{Q}^\dagger$. To find the explicit form of the $\mathcal{Q}'s$, consider a group element representing a translation in superspace [24]

$$G(x^\mu, \theta, \theta^\dagger) = \exp\left[i(-x^\mu\mathcal{P}_\mu + \theta\mathcal{Q} + \theta^\dagger\mathcal{Q}^\dagger)\right]. \tag{3.10}$$

[1] Since $\int d\theta\, \theta = 1$ it is also common to see this operation as an integral over the superspace coordinates $\int d^2\theta\, s_1 s_2$.

To find the differential form of $\mathcal{Q}$, we use two subsequent group translations

$$G(0,\epsilon,\epsilon^\dagger)G(x^\mu,\theta,\theta^\dagger) = \exp\left[i(\epsilon\mathcal{Q}+\epsilon^\dagger\mathcal{Q}^\dagger)\right]\exp\left[i(-x^\mu\mathcal{P}_\mu+\theta\mathcal{Q}+\theta^\dagger\mathcal{Q}^\dagger)\right] \tag{3.11}$$

Using the Baker-Campbell-Hausdorff formula

$$e^A e^B = e^{A+B+\frac{1}{2}[A,B]+\text{higher commutations}} \tag{3.12}$$

and the fact that the SUSY algebra with the coordinates θ, $\theta^\dagger$ uses commutators instead of anticommutators

$$\begin{aligned}[\theta\mathcal{Q},\theta^\dagger\mathcal{Q}^\dagger] &= -2\theta\sigma^\mu\theta^\dagger\mathcal{P}_\mu \\ [\theta\mathcal{Q},\mathcal{P}^\mu] &= 0\end{aligned} \tag{3.13}$$

one finds [10, 24]

$$G(0,\epsilon,\epsilon^\dagger)G(x^\mu,\theta,\theta^\dagger) = \exp\left[i\left(-(x^\mu+i\epsilon\sigma^\mu\theta^\dagger+i\epsilon^\dagger\overline{\sigma}^\mu\theta)\mathcal{P}_\mu+(\theta+\epsilon)\mathcal{Q}+(\theta^\dagger+\epsilon^\dagger)\mathcal{Q}^\dagger\right)\right]. \tag{3.14}$$

So a motion in parameter space is given by

$$\begin{aligned} g(\epsilon,\epsilon^\dagger)(x^\mu,\theta,\theta^\dagger) &= (x^\mu+i\epsilon\sigma^\mu\theta^\dagger+i\epsilon^\dagger\overline{\sigma}^\mu\theta,\theta+\epsilon,\theta^\dagger+\epsilon^\dagger) \\ &= \left[\epsilon\left(i\partial_\theta-(\sigma^\mu\theta^\dagger)\partial_\mu\right)+\epsilon^\dagger\left(i\partial_{\theta^\dagger}-(\overline{\sigma}^\mu\theta)\partial_\mu\right)\right](x^\mu,\theta,\theta^\dagger) \\ &= (\epsilon\mathcal{Q}+\epsilon^\dagger\mathcal{Q}^\dagger)(x^\mu,\theta,\theta^\dagger) \\ &\equiv \sqrt{2}\delta_\epsilon(x^\mu,\theta,\theta^\dagger)\end{aligned} \tag{3.15}$$

where the factor of $\sqrt{2}$ in the last line is a convention matching ref. [10], and where

$$\begin{aligned}\mathcal{Q}_\alpha &\equiv i\frac{\partial}{\partial\theta^\alpha}-(\sigma^\mu\theta^\dagger)_\alpha\partial_\mu \\ \mathcal{Q}^{\dagger\dot{\alpha}} &\equiv i\frac{\partial}{\partial\theta^\dagger_{\dot{\alpha}}}-(\overline{\sigma}^\mu\theta^\dagger)^{\dot{\alpha}}\partial_\mu.\end{aligned} \tag{3.16}$$

This is the differential form of the $\mathcal{Q}$ operators which we were seeking. Applying this to

the general superfield in eq. 3.8 we see the SUSY transformations are given by [10]

$$\begin{aligned}
\delta_\epsilon \phi &= \epsilon\psi + \epsilon^\dagger \psi'^\dagger \\
\delta_\epsilon \psi_\alpha &= \epsilon_\alpha F - \frac{1}{2}(\sigma^\mu \epsilon^\dagger)_\alpha (V_\mu + i\partial\phi) \\
\delta_\epsilon \psi'^{\dagger\dot{\alpha}} &= \epsilon^{\dagger\dot{\alpha}} F' + \frac{1}{2}(\overline{\sigma}^\mu \epsilon)^{\dot{\alpha}} (V_\mu - i\partial\phi) \\
\delta_\epsilon F &= \frac{1}{\sqrt{2}}\epsilon^\dagger \lambda'^\dagger - \frac{i}{2}\epsilon^\dagger \overline{\sigma}^\mu \partial_\mu \psi \\
\delta_\epsilon F' &= \frac{1}{\sqrt{2}}\epsilon\lambda - \frac{i}{2}\epsilon\sigma^\mu \partial_\mu \psi'^\dagger \\
\delta_\epsilon V^\mu &= \frac{1}{\sqrt{2}}\left(\epsilon\sigma^\mu \lambda'^\dagger + \epsilon^\dagger \overline{\sigma}^\mu \lambda\right) + \frac{i}{2}\left(-\epsilon\sigma^\nu \overline{\sigma}^\mu \partial_\nu \psi + \epsilon^\dagger \overline{\sigma}^\nu \sigma^\mu \partial_\nu \psi'^\dagger\right) \\
\delta_\epsilon \lambda_\alpha &= \frac{1}{\sqrt{2}}\left(\epsilon_\alpha D - i(\sigma^\mu \epsilon^\dagger)_\alpha \partial_\mu F' - \frac{i}{2}(\sigma^\nu \overline{\sigma}^\mu \epsilon)_\alpha \partial_\mu V_\nu\right) \\
\delta_\epsilon \lambda' &= \frac{1}{\sqrt{2}}\left(\epsilon^{\dagger\dot{\alpha}} D - i(\overline{\sigma}^\mu \epsilon)^{\dot{\alpha}} \partial_\mu F + \frac{i}{2}(\overline{\sigma}^\nu \sigma^\mu \epsilon^\dagger)^{\dot{\alpha}} \partial_\mu V_\nu\right) \\
\delta_\epsilon D &= -\frac{i}{\sqrt{2}}\partial_\mu\left(\epsilon^\dagger \overline{\sigma}^\mu \lambda + \epsilon\sigma^\mu \lambda'^\dagger\right).
\end{aligned} \tag{3.17}$$

Note, in particular, that the SUSY transformation for the D-term is a total derivative, which vanishes when integrated over all space to produce an action. Thus one can build a SUSY invariant theory from the D-term, also known as the θ^4 component, of a superfield (which can itself be the product of multiple superfields)

$$\mathcal{L}_{\text{SUSY}} \supset S(x^\mu, \theta, \theta^\dagger)|_{\theta^4}. \tag{3.18}$$

To construct SUSY invariant Lagrangians a final concept is necessary; one needs a way to take derivatives with respect to the anticommuting coordinates that is SUSY covariant:

$$\delta_\epsilon(D_\alpha S) = D_\alpha(\delta_\epsilon S). \tag{3.19}$$

This can be achieved with [10]

$$\begin{aligned}
D_\alpha &\equiv \frac{\partial}{\partial\theta^\alpha} - i(\sigma^\mu \theta^\dagger)_\alpha \partial_\mu \\
D^\dagger_{\dot{\alpha}} &\equiv -\frac{\partial}{\partial\theta^{\dagger\dot{\alpha}}} + i(\theta\sigma^\mu)_{\dot{\alpha}} \partial_\mu
\end{aligned} \tag{3.20}$$

which satisfies

$$\{\mathcal{Q}_\alpha, D_\beta\} = \{\mathcal{Q}^\dagger_{\dot{\alpha}}, D_\beta\} = \{\mathcal{Q}_\alpha, D^\dagger_{\dot{\beta}}\} = \{\mathcal{Q}^\dagger_{\dot{\alpha}}, D^\dagger_{\dot{\beta}}\} = 0. \tag{3.21}$$

This is useful for defining the most frequently encountered superfield, the *chiral superfield*.

A left chiral superfield is defined by

$$D^\dagger_{\dot\alpha}\Phi \equiv 0. \tag{3.22}$$

The product of multiple left chiral superfields is also a left-chiral superfield due to the Leibnitz property of $D^\dagger$ as a differential operator: $D^\dagger_{\dot\alpha}(\Phi_1\Phi_2) = (D^\dagger_{\dot\alpha}\Phi_1)\Phi_2 + \Phi_1(D^\dagger_{\dot\alpha}\Phi_2) = 0$. One can check [10] that

$$\Phi = \phi + \sqrt{2}\theta\psi + \theta\theta F + i\theta^\dagger\overline{\sigma}^\mu\theta\partial_\mu\phi - \frac{i}{\sqrt{2}}\theta\theta\theta^\dagger\overline{\sigma}^\mu\partial_\mu\psi + \frac{1}{4}\theta\theta\theta^\dagger\theta^\dagger\partial^\mu\partial_\mu\phi \tag{3.23}$$

satisfies eq. 3.22. Looking at this expression it's easier to see why Φ is called left chiral – it contains left handed Weyl fermions but no right handed fermions. Its conjugate $\Phi^\dagger$ is called a right chiral superfield. Φ's field content is two complex scalar fields, ϕ and F, and a left handed Weyl fermion field ψ. We will see shortly that F is a non-dynamical *auxillary* field, which can be removed from the theory by solving it's equation of motion. The purpose of this field will become clearer in a moment.

By inserting the explicit expression for Φ into the general SUSY transformation in eq. 3.17 one obtains

$$\begin{aligned}
\delta\phi &= \epsilon\psi \\
\delta(\psi)_\alpha &= -i(\sigma^\mu\epsilon^\dagger)_\alpha\partial_\mu\phi + \epsilon_\alpha F \\
\delta F &= -i\epsilon^\dagger\overline{\sigma}^\mu\partial_\mu\psi.
\end{aligned} \tag{3.24}$$

This agrees with the schematic SUSY transformation given at the beginning of this section, eq. 3.2; it takes a boson to a fermion and vise versa. The presence of the auxiliary field in the second term is needed to make the SUSY algebra close off-shell. One can see the problem by counting the fermion's off-shell degrees of freedom: four vs. the scalar ϕ's two. F provides the two extra scalar degrees of freedom needed when the fields are off-shell.

One very important point to take from the SUSY transformations 3.24 is that F transforms as a total derivative for a chiral superfield, just as D did for a general superfield. Therefore the F-term of a chiral superfield integrated over spacetime is SUSY invariant and can be used in a SUSY invariant action. Since the product of chiral superfields is also a chiral superfield, the F-term of any holomorphic function of the chiral superfields

$W(\Phi)$ can form part of the Lagrangian. $W(\Phi)$ is called the *superpotential* and for the simplest phenomenologically viable SUSY model, the MSSM, it takes the form

$$W(\Phi) = \frac{1}{2} m_{ij} \Phi_i \Phi_j + \frac{1}{6} y_{ijk} \Phi_i \Phi_j \Phi_k. \tag{3.25}$$

Thus, we can create a real and SUSY invariant action using the Lagrangian

$$\mathcal{L}_{\mathrm{WZ}} = \Phi_i^\dagger \Phi_i|_{\theta^4} + (W(\Phi)|_{\theta^2} + \mathrm{h.c.}). \tag{3.26}$$

This is known as the Wess-Zumino model [25]. Expanding the fields out in component form, one obtains

$$\mathcal{L}_{WZ} = \partial^\mu \phi_i^\dagger \partial_\mu \phi_i + i\psi_i^\dagger \overline{\sigma}^\mu \partial_\mu \psi_i + F_i^\dagger F_i - \frac{1}{2}\left(\psi_i \psi_j \partial_{\phi_i} \partial_{\phi_j} W + F_i \partial_{\phi_i} W + \mathrm{h.c.}\right) \tag{3.27}$$

where $W = \frac{1}{2} m_{ij} \phi_i \phi_j + \frac{1}{6} y_{ijk} \phi_i \phi_j \phi_k$ is the superpotential written in terms of scalar fields. The F's do not have a kinetic term and they can easily be eliminated by solving for their equations of motion: $F_i^\dagger = -\partial_{\phi_i} W$. Substituting this back into the Lagrangian we arrive at

$$\mathcal{L}_{WZ} = \partial^\mu \phi_i^\dagger \partial_\mu \phi_i + i\psi_i^\dagger \overline{\sigma}^\mu \partial_\mu \psi_i - |\partial_{\phi_i} W|^2 - \frac{1}{2}\left(\psi_i \psi_j \partial_{\phi_i} \partial_{\phi_j} W + \mathrm{h.c.}\right). \tag{3.28}$$

We should pause for a moment to take notice of the fact that the form of the terms involving W demand that the scalar quartic couplings are the square of the Yukawa couplings, just as was needed to cancel loop corrections to the Higgs mass!

$$\begin{aligned} |\partial_{\phi_i} W|^2 &= \left| m_{ij} \phi_j + \frac{1}{2} y_{ijk} \phi_j \phi_k \right|^2 \\ -\frac{1}{2} \psi_i \psi_j \partial_{\phi_i} \partial_{\phi_j} W &= -\frac{1}{2}\left(m_{ij} + \frac{1}{2} y_{ijk} \phi_k\right) \psi_i \psi_j \end{aligned} \tag{3.29}$$

Following chiral superfields, the next most important type of superfield are vector superfields. Like regular vector fields they are real and are therefore defined by

$$V = V^\dagger. \tag{3.30}$$

While a detailed derivation of the transformation properties and the Lagrangian of these fields is outside the scope of this chapter it is worth taking a brief look at them so that ch. 8 is made more clear. We will focus mainly on abelian fields. For a more thorough look at vector superfields there are several excellent references [10, 23, 24, 26].

A clever way to write vector superfields is [10]

$$\begin{aligned} V =&\varphi + \theta\xi + \theta^\dagger\xi^\dagger + \theta\theta f + \theta^\dagger\theta^\dagger f^\dagger + \theta^\dagger\overline{\sigma}^\mu\theta V_\mu + \\ &\theta^\dagger\theta^\dagger\theta(\lambda - \frac{i}{2}\sigma^\mu\partial_\mu\xi^\dagger) + \theta\theta\theta^\dagger(\lambda^\dagger - \frac{i}{2}\overline{\sigma}^\mu\partial_\mu\xi) + \theta\theta\theta^\dagger\theta^\dagger(\frac{1}{2}D + \frac{1}{4}\partial^\mu\partial_\mu\varphi). \end{aligned} \tag{3.31}$$

It turns out that the fields φ, ξ, and f are unphysical and can be *supergauged* away. To see this, note that if we shift V by a chiral superfield Ω as in

$$V \to V + i(\Omega^\dagger - \Omega) \tag{3.32}$$

then the components of V in eq. 3.31 transform as [10]

$$\begin{aligned} &\varphi \to \varphi + i(\phi^\dagger - \phi) \\ &\xi \to \xi - i\sqrt{2}\psi \\ &f \to f - iF \\ &V_\mu \to V_\mu + \partial_\mu(\phi + \phi^\dagger) \\ &\lambda \to \lambda \\ &D \to D \end{aligned} \tag{3.33}$$

so that only λ and D remain untransformed while V_μ undergoes a normal gauge transformation. Thus, *if* supergauge transformations are a symmetry of the Lagrangian then normal gauge symmetry is automatically satisfied and one can put the vector superfield in the *Wess-Zumino gauge*

$$V_{WZ} = \theta^\dagger\overline{\sigma}^\mu\theta V_\mu + \theta^\dagger\theta^\dagger\theta\lambda + \theta\theta\theta^\dagger\lambda^\dagger + \frac{1}{2}\theta\theta\theta^\dagger\theta^\dagger D. \tag{3.34}$$

V_μ is the usual gauge vector field, λ is its superpartner known as the *gaugino* and D is a non-propagating auxiliary field which permits the SUSY algebra to close off shell, as F did for chiral superfields.

Given that vector fields transform as normal gauge transformation under a supergauge transformation it is not hard to guess that chiral superfields will transform in an analogous way to the non-supersymmetric case

$$\Phi \to e^{i2gq\Omega}\Phi, \qquad \Phi^\dagger \to e^{i2gq\Omega^\dagger}\Phi^\dagger \tag{3.35}$$

where the factor of two is included to obtain the standard transformations of component

fields. Then to keep the chiral kinetic terms in the Lagrangian supergauge invariant it must be modified to

$$\mathcal{L}_{\text{SUSY}} \supset \Phi^\dagger e^{2gqV}\Phi|_{\theta^4} \tag{3.36}$$

The exponential can be evaluated as a power series in θ's, which terminates after $V^2 = -\frac{1}{2}\theta^\dagger\theta^\dagger\theta\theta V^\mu V_\mu$ for the Wess-Zumino gauge. For non-abelian vector fields this generalizes to

$$\begin{aligned}\mathcal{L}_{\text{SUSY}} \supset\ \Phi^\dagger e^{2gT^aV^a}\Phi|_{\theta^4} =& D^\mu\phi^\dagger D_\mu\phi + i\psi^\dagger\overline{\sigma}^\mu D_\mu\psi + F^\dagger F \\ &- \sqrt{2}g\left((\phi^\dagger T^a\psi)\lambda^a + \text{h.c.}\right) + g(\phi^\dagger T^a\phi)D^a\end{aligned} \tag{3.37}$$

with D_μ the usual gauge-covariant derivative.

Building the kinetic terms for V is a less intuitive process so we will simply quote the results of refs. [10, 23]. They show that the chiral superfield

$$\begin{aligned}\mathcal{W}_\alpha =& -\frac{1}{4}D^\dagger D^\dagger D_\alpha V \\ =& \lambda_\alpha + \theta_\alpha D + \frac{i}{2}(\sigma^\mu\overline{\sigma}^\nu\theta)_\alpha F_{\mu\nu} + i\theta\theta(\sigma^\mu\partial_\mu\lambda^\dagger)_\alpha\end{aligned} \tag{3.38}$$

is supergauge invariant. Since it contains the field strength tensor $F_{\mu\nu}$ the product $\mathcal{W}^\alpha\mathcal{W}_\alpha$, which is also chiral, will contain the kinetic term. As with other chiral superfields, we use the real part of its F-term to obtain the SUSY invariant action.[2].

$$\mathcal{L}_{\text{SUSY}} \supset \frac{1}{4}\mathcal{W}^\alpha\mathcal{W}_\alpha|_{\theta^2} + \text{h.c.} \tag{3.39}$$

or for non-abelian fields (and neglecting the possible Θ term)

$$\frac{1}{4}\mathcal{W}^{a\alpha}\mathcal{W}^a_\alpha|_{\theta^2} + \text{h.c.} = -\frac{1}{4}F^{\mu\nu a}F^a_{\mu\nu} + i\lambda^{\dagger a}\overline{\sigma}^\mu D_\mu\lambda^a + \frac{1}{2}D^aD^a \tag{3.40}$$

with $D_\mu\lambda^a = \partial_\mu\lambda^a + gf^{abc}A^b_\mu\lambda^c$ the covariant derivative of λ^a.

To summarize, one can build a SUSY invariant action with the Lagrangian

$$\begin{aligned}\mathcal{L}_{\text{SUSY}} =& \Phi_i^\dagger e^{2gT^aV^a}\Phi_i|_{\theta^4} + \left(\frac{1}{4}\mathcal{W}^{a\alpha}\mathcal{W}^a_\alpha + W(\Phi_i)\right)\Big|_{\theta^2} + \text{h.c.} \\ =& -\frac{1}{4}F^{\mu\nu a}F^a_{\mu\nu} + i\lambda^{\dagger a}\overline{\sigma}^\mu D_\mu\lambda^a + D^\mu\phi_i^\dagger D_\mu\phi_i + i\psi_i^\dagger\overline{\sigma}^\mu D_\mu\psi_i + \\ &- \sqrt{2}g\left((\phi_i^\dagger T^a\psi_i)\lambda^a + \text{h.c.}\right) - \frac{g^2}{2}(\phi_i^\dagger T^a\phi_i)^2 + \\ &- |\partial_{\phi_i}W|^2 - \frac{1}{2}\left(\psi_i\psi_j\partial_{\phi_i}\partial_{\phi_j}W + \text{h.c.}\right).\end{aligned} \tag{3.41}$$

[2]The D-term $V|_{\theta^4}$ can also show up in the Lagrangian and can play a role in SUSY breaking. For more information see ref. [10]

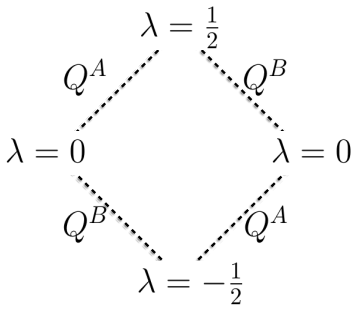

Figure 3.1: Massless hypermultiplet of $\mathcal{N} = 2$ SUSY showing how the generators Q^A, Q^B relate fields of different helicity. This can be decomposed into two $\mathcal{N} = 1$ multiplets.

In this expression we have removed the F's and D^a using their equations of motion. For D^a this is $D^a = -g(\phi_i^\dagger T^a \phi_i)$.

Up to this point we have considered SUSY transformations with a single generator Q, called $\mathcal{N} = 1$ SUSY. It turns out it is possible to build more complex SUSY theories by including additional generators. For the massless case, the SUSY algebra generalizes to $\{Q^A_\alpha, Q^\dagger_{\dot{\beta}B}\} = -2\,\delta^A_B\,\sigma^\mu_{\alpha\dot{\beta}} P_\mu$, where A, B label the generator. SUSY with $\mathcal{N} > 1$ is important when reducing higher dimensional supersymmetric theories to 4D SUSY, as we will see in sec. 3.2. However, when considering phenomenologically viable SUSY theories it is worth noting that it is not possible to have chiral fermions that transform in the fundamental representation of a gauge group (as in the SM) in $\mathcal{N} > 1$ SUSY [23]. This is because higher $\mathcal{N}$ multiplets necessarily contain a spin one particle which transforms in the adjoint representation. The exception to this is the $\mathcal{N} = 2$ *hypermultiplet*, built starting from a helicity $\lambda = -1/2$ particle and applying each of the helicity raising operators once to obtain a supermultiplet with two scalars and two chiral spinors. This is shown schematically in fig. 3.1.

3.1.2 Broken SUSY and phenomenologically viable theories

Though unbroken SUSY solves the hierarchy problem of the EW scale, it cannot be realized in our universe; since superpartners must interact with the same gauge coupling strengths as SM particles they would be quite conspicuously produced in nature and in colliders if they had the same mass as their SM partners. If SUSY does exist it must be broken, though the masses of superpartners should not be too large or else the hierarchy problem is reintroduced. Though there are many ways to perform the necessary breaking

there is no way to see which method (if any) is correct since we have yet to discover any SUSY particles! One method, known as Scherk-Schwarz symmetry breaking, involves the use of boundary conditions for fields in an extra dimension. This is discussed in detail in ch. 8.

Regardless of the method used to break SUSY it can be parameterized by including all possible terms with couplings of positive mass dimension, consistent with the model's symmetries. Dimensionless couplings are not included because otherwise they will reintroduce the hierarchy problem due to an incomplete cancellation of terms, as in

$$\Sigma_h = \frac{1}{8\pi}(\lambda_s - \lambda_f^2)\Lambda^2. \tag{3.42}$$

SUSY breaking with only positive mass dimension couplings is called *soft breaking* and it can introduce mass terms for sfermions $m_{\tilde{f}}^2 \tilde{f}^* \tilde{f}$ and gauginos $\frac{1}{2} m_\lambda (\lambda\lambda + \text{h.c.})$ explaining why superpartners are heavier than their SM cousins.

Parameterizing SUSY breaking in this way one can write down the simplest phenomenologically realistic SUSY theory – the Minimal Supersymmetric Standard Model (MSSM). The MSSM field content is shown in table 3.1, and its superpotential is

$$W = \mu H_u H_d + \overline{u}\mathbf{y^u} Q H_u - \overline{d}\mathbf{y^d} Q H_d - \overline{e}\mathbf{y^e} L H_d. \tag{3.43}$$

Note that since W must be holomorphic the MSSM uses another Higgs field H_d (which also acquires a VEV) to give mass to the down-type quarks and leptons.

Unfortunately, unlike the SM Yukawa terms the MSSM superpotential does not include all possible renormalizable gauge invariant terms. One could also include, for instance, $\lambda_1 LQ\overline{d} + \lambda_2 \overline{u}\overline{d}\,\overline{d}$. Both terms have a non-zero $B-L$ and if allowed would mediate tree level proton decay making us all rather short-lived. In the SM these types of terms were forbidden by the accidental $B - L$ symmetry.

To prevent these dangerous terms one usually assumes a conserved *R-parity* $P_R = (-1)^{3(B-L)+2s}$ where s is the particle's spin. Including spin in this parity definition has the nice property of giving all SM particles $P_R = +1$ and their superpartners $P_R = -1$. If R-parity is conserved then the lightest superpartner is stable. If it is also neutral then it provides a nice DM candidate. For collider physics the important phenomenological consequence of this is that sparticles must be produced in pairs and each must decay

Type	Name	$SU(3)_C, SU(2)_W, U(1)_Y$
Vector Multiplet	g	$(\mathbf{8}, \mathbf{1}, 0)$
	W	$(\mathbf{1}, \mathbf{3}, 0)$
	B	$(\mathbf{1}, \mathbf{1}, 0)$
Chiral Multiplet	Q	$(\mathbf{3}, \mathbf{2}, \frac{1}{6})$
	$\overline{u}$	$(\overline{\mathbf{3}}, \mathbf{1}, -\frac{2}{3})$
	$\overline{d}$	$(\overline{\mathbf{3}}, \mathbf{1}, \frac{1}{3})$
	L	$(\mathbf{1}, \mathbf{2}, -\frac{1}{2})$
	$\overline{e}$	$(\mathbf{1}, \mathbf{1}, 1)$
	H_u	$(\mathbf{1}, \mathbf{2}, \frac{1}{2})$
	H_d	$(\mathbf{1}, \mathbf{2}, -\frac{1}{2})$

Table 3.1: MSSM supermultiplet content. Note that by convention all chiral multiplets are defined to be left-handed. Excluding H_u and H_d the chiral multiplets each come in three generations.

to an odd number of sparticles. If the sparticle decay is prompt then the neutral LSPs, which are invisible to a detector, can carry away large amounts of momentum so that the detected momenta does not sum to zero. We will discuss this and other classic SUSY signatures in ch. 5.

As we mentioned in ch. 1, SUSY signals have yet to be found at the LHC. If SUSY does exist it seems sparticles must be a bit heavier than was initially hoped, reintroducing the hierarchy problem. Some attempts to alleviate the tension between natural SUSY and LHC data rely on extradimensional SUSY [6, 7], a topic which we turn to next.

3.2 Extradimensional SUSY

To extend SUSY to higher dimensions one must consider how component fields of a multiplet change with extra dimensions. Scalars are easiest: one simply replaces $\phi(x^\mu)$ with $\phi(x^M)$ where M runs over all the space-time dimensions. Vectors get slightly more complex – they gain a new degree of freedom for each new dimension as one goes from $A_\mu(x^\nu)$ to $A_M(x^N)$, but the form of the equations doesn't change otherwise.

Spinors, on the other hand, require a bit more work. One requires a set of gamma

matrices Γ^M to write down the Dirac equation $(\Gamma^M \partial_M - m)\psi = 0$. As in four dimensions, the gamma matrices are defined by the Clifford Algebra

$$\{\Gamma^M, \Gamma^N\} = 2\eta^{MN} \tag{3.44}$$

which can be used to construct generators of $SO(1, D-1)$ [23, 26]

$$\Sigma^{MN} = \frac{i}{4}[\Gamma^M, \Gamma^N]. \tag{3.45}$$

These satisfy the Lorentz algebra 3.4 as usual.

Explicit representations of the Dirac Matrices can be built out of Pauli matrices, though it is easiest to do so if one starts by assumes a Euclidean metric

$$\{\Gamma^M, \Gamma^N\} = 2\delta^{MN}. \tag{3.46}$$

For example, the generalized Weyl basis for arbitrary spacetime dimension is as follows:

1. Start with $\gamma^0 = \sigma^1$, $\gamma^1 = \sigma^2$, $\gamma^2 = \sigma^3$. These satisfy eq. 3.46.

2. For even spacetime dimension $2n$

$$\begin{aligned} \Gamma^0 &= \sigma^1 \otimes \mathbb{1} \\ \Gamma^{m+1} &= \sigma^2 \otimes \gamma^m \\ \Gamma_* &= -\sigma^3 \otimes \mathbb{1} \end{aligned} \tag{3.47}$$

   where γ^m are the Euclidean gamma matrices of $2n-1$ spacetime dimensions, the rank of $\mathbb{1}$ matches γ^m, and Γ_* is the generalization of γ^5 (the $-$ sign matches the convention $P_{R,L} = \frac{1}{2}(\mathbb{1} \pm \Gamma_*)$). It is not too difficult to see that these Γ's also satisfy 3.46.

3. For odd spacetime dimensions $2n+1$ use Γ_* for the next highest Dirac matrix. The sign is arbitrary.

4. Repeat steps 2-3 until reaching the desired spacetime dimension. Then multiply all the space-like Γ^M by i for the 'mostly minus' metric $\eta^{MN} = \text{diag}(1, -1, -1, ...)$.

When complete the Dirac matrices take the usual form

$$\begin{aligned}\Gamma^M &= \begin{pmatrix} 0 & \sigma^M \\ \overline{\sigma}^M & 0 \end{pmatrix}, \quad M \in \{0, 1, ...2n-1\} \\ \Gamma_* &= (-)i\Gamma^{2n} = \begin{pmatrix} -\mathbb{1} & 0 \\ 0 & \mathbb{1} \end{pmatrix}\end{aligned} \tag{3.48}$$

with generalized σ matrices

$$\sigma^M = \{\mathbb{1}, \gamma^m\}, \quad \overline{\sigma}^M = \{\mathbb{1}, -\gamma^m\}. \tag{3.49}$$

As an explicit example the five dimensional Euclidean gamma matrices are

$$\begin{aligned}\gamma^0 &= \sigma^1 \otimes \mathbb{1} \\ \gamma^1 &= \sigma^2 \otimes \sigma^1 \\ \gamma^2 &= \sigma^2 \otimes \sigma^2 \\ \gamma^3 &= \sigma^2 \otimes \sigma^3 \\ \gamma^4 &= \sigma^3 \otimes \mathbb{1}.\end{aligned} \tag{3.50}$$

If we multiply the last four of these by i then $\gamma^0 - \gamma^3$ are the normal four dimensional Weyl representation gamma matrices we are familiar with. Going up to six spacetime dimensions the Euclidean gamma's are

$$\begin{aligned}\Gamma^0 &= \sigma^1 \otimes \mathbb{1} = \sigma^1 \otimes \mathbb{1} \otimes \mathbb{1} \\ \Gamma^1 &= \sigma^2 \otimes \gamma^0 = \sigma^2 \otimes \sigma^1 \otimes \mathbb{1} \\ \Gamma^2 &= \sigma^2 \otimes \gamma^1 = \sigma^2 \otimes \sigma^2 \otimes \sigma^1 \\ \Gamma^3 &= \sigma^2 \otimes \gamma^2 = \sigma^2 \otimes \sigma^2 \otimes \sigma^2 \\ \Gamma^4 &= \sigma^2 \otimes \gamma^3 = \sigma^2 \otimes \sigma^2 \otimes \sigma^3 \\ \Gamma^5 &= \sigma^2 \otimes \gamma^4 = \sigma^2 \otimes \sigma^3 \otimes \mathbb{1} \\ \Gamma_* &= -\sigma^3 \otimes \mathbb{1} = -\sigma^3 \otimes \mathbb{1} \otimes \mathbb{1}.\end{aligned} \tag{3.51}$$

Again, multiplying the space-like gamma's $\Gamma^1 - \Gamma^5$ by i we obtain the correct Minkowski metric in the Clifford Algebra.

From this it is easy to see that for even space-time dimensions one can build off block-diagonal Γ's which produce block diagonal Σ's. In other words the Lorentz algebra

dim	Majorana	Weyl	Dirac rank	min components
2	yes	self	2	1
3	yes	-	2	2
4	yes	complex	4	4
5	-	-	4	8
6	-	self	8	8
7	-	-	8	16
8	yes	complex	16	16
9	yes	-	16	16
10	yes	self	32	16
11	yes	-	32	32

Table 3.2: Properties of spinors in various dimensions. Weyl spinors labeled as "self" are conjugate to themselves while those labeled "complex" are conjugate to each other [27].

is reducible and spinors in even dimension can be chiral. However, for odd dimensions one must use the Γ_* matrix to build the new space-like Γ^{2n+1} and the Lorentz algebra becomes irreducible – Weyl spinors do not exist in odd dimensions.

More general arguments which don't rely on a specific representation can be made using symmetries of the Γ^M [26] or raising and lowering operators [23]. The bottom line is that in even $D = 2n$ and odd $D = 2n + 1$ dimensions the size of the Dirac basis is 2^n with 2^{n+1} real components. Weyl spinors, which can only exist in even dimensions, have half the number or real degrees of freedom and can thus be considered more fundamental.

Majorana spinors, which satisfy the condition $\psi^* = C\Gamma^0\psi$ where C is the charge conjugation matrix defined by $C\Gamma^M C^{-1} = \pm(\Gamma^M)^T$, also have half the degrees of freedom of a Dirac spinor and so can be considered more fundamental. To be consistent, $C\Gamma^0 C\Gamma^0 \stackrel{!}{=} \mathbb{1}$, which turns out to only be possible if $D = 0, 1, 2, 3, 4 \mod 8$. For $D = 2 \mod 8$ a spinor can be both Majorana and Weyl [23]. Table 3.2 summarizes the types of spinors possible in various dimensions, along with the number of real components the minimal spinor has.

Spinors, vectors and scalars are the only particle types we will need in our review of higher dimensional fields. To see how these fields behave in 4D we must discuss *dimensional reduction*, the process of recovering the four dimensional theory from a higher dimensional one. Gravitational experiments rule out extra dimension larger than about $\mathcal{O}(10)$ μm [28]. Thus extra dimensions must be smaller than this and the behavior of fields in the extra dimensions is specified by their boundary conditions therein. The simplest case to consider is one extra dimension y which is *compactified* to a circle with radius r. Since y is periodic, fields which propagate in this extra dimension have discrete

Fourier modes

$$\phi(x^\mu, y) = \sum_n \phi_n(x^\mu) \exp\left(\frac{iny}{r}\right). \tag{3.52}$$

Then the 5D action for a massless free scalar field becomes [23]

$$\begin{aligned} S_{5D} &= \int d^5x\, \partial^M \phi^*(x^\mu, y) \partial_M \phi(x^\mu, y) \\ &= \int d^4x \int dy \sum_n \left(\partial^\mu \phi_n^*(x^\mu) \partial_\mu \phi_n(x^\mu) - \left(\frac{n}{r}\right)^2 |\phi_n(x^\mu)|^2 \right) \\ &= \sum_n 2\pi r \int d^4x \left(\partial^\mu \phi_n^*(x^\mu) \partial_\mu \phi_n(x^\mu) - \left(\frac{n}{r}\right)^2 |\phi_n(x^\mu)|^2 \right). \end{aligned} \tag{3.53}$$

The factor of $2\pi r$ can be absorbed into the definition of ϕ. We see in the end that this type of compactification results in a *Kaluza-Klein* (KK) *tower* of massive states starting with zero mass and increasing as (n/r). Other types of compactification schemes are possible – we will meet a more complex example in ch. 8.

When a 5D vector field is dimensionally reduced the extra degree of freedom separates into a scalar

$$A^M = \begin{cases} A^\mu \\ \\ A^4 \end{cases}. \tag{3.54}$$

Spinors will also split. In the 5D case a spinor splits cleanly into massless left and right-handed Weyl fields and massive Dirac spinors,

$$\begin{aligned} S_{5D} &= \int d^5x\, i\overline{\Psi} \Gamma^M \partial_M \Psi \\ &= \sum_n 2\pi r \int d^4x \left(i\psi_{A\,n}^\dagger \overline{\sigma}^\mu \partial_\mu \psi_{A\,n} + i\psi_{B\,n}^\dagger \overline{\sigma}^\mu \partial_\mu \psi_{B\,n} - \frac{n}{r}(\psi_{A\,n}\psi_{B\,n} + \text{h.c.}) \right). \end{aligned} \tag{3.55}$$

The easiest way to determine the field content of an extradimensional $\mathcal{N} = 1$ SUSY multiplet is to consider the minimum spinor degrees of freedom the multiplet must have. For instance, in five dimensions the simplest $\mathcal{N} = 1$ SUSY multiplet contains one fermion with eight real degrees of freedom off-shell. Since this corresponds to two 4D Weyl fermions the field content must be the same as 4D $\mathcal{N} = 2$ SUSY after dimensional reduction. As a simple example we consider a $5D$ abelian vector supermultiplet. The Lagrangian for this multiplet is

$$\mathcal{L}_{5D} = -\frac{1}{4} F^{MN} F_{MN} + \frac{1}{2} |\partial_M \phi|^2 + i\overline{\lambda} \Gamma^M \partial_M \lambda + \frac{1}{2} X^a X^a \tag{3.56}$$

where X^a is a triplet of auxiliary fields and ϕ is a real scalar field [29]. After dimensional

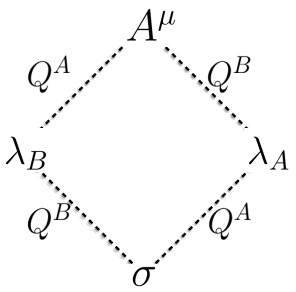

Figure 3.2: Four dimension $\mathcal{N} = 2$ vector multiplet, which is equivalent to a 5D $\mathcal{N} = 1$ vector multiplet after dimensional reduction. This can be further decomposed into one 4D $\mathcal{N} = 1$ vector multiplet and one chiral multiplet.

reduction the extra scalar field from A^M combines with ϕ to form a complex scalar σ. It is σ which completes the 4D $\mathcal{N} = 2$ multiplet as show in fig. 3.2.

We conclude this chapter by noting that higher dimensional SUSY theories can be efficiently written down in terms of 4D $\mathcal{N} = 1$ superfields. We will take advantage of this fact in ch. 8.

Chapter 4: Monte Carlo simulations of hadron colliders

The ability to compare SM and SUSY theoretical results to actual data from colliders relies heavily on Monte Carlo simulations of particle collisions. In this chapter we will outline the tools available to perform such simulations, from Lagrangian to exclusion/discovery. We will also cover some of the important theory behind the tools.

4.1 From Lagrangian to Feynman rules

Before any simulation can begin the Feynman rules associated with a given model must be worked out in detail, as must the physical spectrum. Deriving the Feynman rules for a new model has been made much simpler by the invention of two Mathematica based codes built for this purpose: FeynRules [30] and SARAH [31]. Currently, computation of Feynman rules is only possible at leading order, though work is underway that will enable NLO computations of many types of BSM models [32]. Both SARAH and FeynRules require (at minimum) particle content, local symmetries, and a Lagrangian written in four-dimensional space-time. Each is capable of handling supersymmetric theories, though their approach to doing so is different and gives each distinct strengths and weaknesses. This author found SARAH to be a far easier to use, while FeynRules is a bit more flexible in terms of the types of models it can handle.

To determine the physical particle spectrum (*i.e.* masses and mixings) both codes rely on support from external programs. FeynRules uses ASperGe to perform automatic mass diagonalization while SARAH uses SPheno [33,34]. Impressively, SARAH calculates two-loop renormalization group equations (RGEs) for SPheno to allow for parameter running when calculating masses.

4.2 From Feynman rules to simulated collisions

Once the Feynman rules for a model have been computed they can be imported into a Monte Carlo event generator capable of simulating collisions between particles and all the

physics contained within this process. There are several Monte Carlo event generators on the market, each with differing capabilities in terms of handling BSM models, working beyond leading order, and treating infrared (IR) physics like hadronization. These programs include MadGraph5_aMC@NLO [35], Sherpa [36], CalcHEP [37], Whizard [38,39], Pythia [40], and Herwig++ [41].

Monte Carlo techniques are ideal for collider simulations in part because they provide an efficient way to perform the high dimensional phase space integration necessary to calculate cross sections. Feynman rules for a given model are used to generate Feynman diagrams corresponding to the user-defined initial and final states, which then define the matrix element. Roughly speaking, to calculate a cross section the Monte Carlo generates random four-momenta for the final state particles and weights these by the matrix element. In fact, the process is more complex than this and the Monte Carlo adapts to the analytic structure of the matrix element by generating more "random" four-momenta where the amplitude is largest. Details of this process can be found in [42].

Though this process can accurately model the interaction of a few particles it starts to be computationally impractical when the final state includes more than about a half-dozen particles, due to the large phase space. Moreover, it is unsuitable in regions where the matrix element develops singularities or when the relevant coupling constant become non-perturbative. Since hadrons are inherently non-perturbative objects and since final states of hard collisions typically involve a great deal of particles, the physics and methods one needs for an accurate simulation can be quite involved. We give a brief overview of what is needed in what follows. Much of what is contained within this can be found in refs. [9, 28, 43].

4.2.1 Parton distribution functions

A proton consists of group of interacting quarks and gluons collectively known as *partons*. At energies below $\Lambda_{\text{QCD}} \sim m_p$ the strong coupling constant becomes large and calculations for parton interactions using perturbation theory break down. On the other hand, the strong coupling constant is weaker (and perturbative) at the higher energy Q at which hard collisions take place. Since momentum is exchanged between proton constituents at

time scales of $\sim \Lambda_{\mathrm{QCD}}^{-1}$ while hard collisions take place at time scales $\sim Q^{-1}$, one might hope that hard scale physics would happen so fast as to decouple from the IR physics within the proton. In this case, one could treat the proton's constituents as essentially free particles and could account for the low-energy parts of the problem using classical probabilities $f_i(x)dx$ for a particle to interact with a parton species i carrying a fraction x of the proton's momentum. Then the total cross section for a particle to interact with a proton is given by

$$\sigma = \sum_i \int_0^1 dx f_i(x)\sigma_i + \mathcal{O}\left(\frac{\Lambda_{\mathrm{QCD}}}{Q}\right) \tag{4.1}$$

where σ_i is the cross section for an interaction with parton i. The ability to separate low scale physics from high scale physics in this way is known as *factorization*.

In fact factorization has been proven for a few examples and appears well justified by experiments such as deep inelastic scattering [44]. The low energy physics of protons can be encapsulated in the $f_i(x)$, known as *parton distribution functions* (PDFs). These functions have some scale dependence in them which can be computed in perturbative QCD. Once the functions are measured at one scale, they can be computed at another using renormalization group techniques. The *DGLAP evolution equation*, which governs the evolution of $f(x, \mu)$ from one scale to another, is given by

$$\mu \frac{d}{d\mu} f_i(x, \mu) = \frac{\alpha_s}{\pi} \int_x^1 \frac{d\xi}{\xi} P_{ij}(x/\xi) f_j(\xi, \mu) \tag{4.2}$$

where the $P_{ij}(z)$ are known as *DGLAP splitting functions*, calculable from perturbation theory [45–47]. The DGLAP evolution equation is actually a set of coupled integro-differential equations relating multiple PDFs.

The parton distribution functions for several particle types at two different energy scales are shown in Figure 4.1. One important observation from this figure is that for low x the gluon PDF is far larger than that of the quarks (the scale for the gluon PDF has been divided by 10 so that it is visible on the plot), especially at higher energies. Thus the LHC is mainly a gluon collider.

In summary, PDFs provide a way to treat initial state protons in terms of its constituent partons, so that instead of modeling $pp \to q\overline{q}$ one can model (for instance) $gg \to q\overline{q}$. This can be done for all the proton constituents, weighted by PDFs to get a

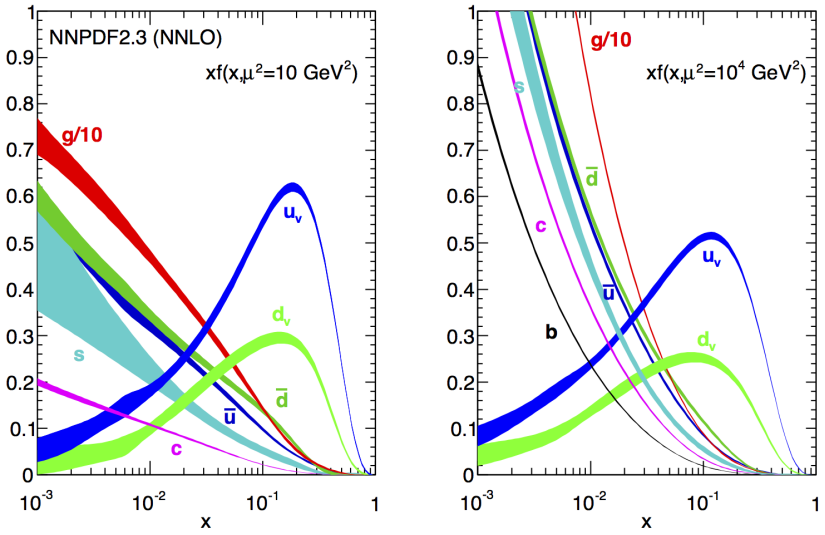

Figure 4.1: Parton distribution functions at the scales 10 GeV (left) and 10^4 GeV (right). Note that the gluon line is divided by 10 so that it is visible on the graph. Figure taken from NNPDF set described in [48].

total cross section. Unfortunately, this is still not enough to accurately model hadron collisions since partons will shower many particles as they evolve from one scale to another (in a similar way to electrons emitting photons as they are accelerated) and due to the fact that one cannot actually measure a final state such as $q\bar{q}$ due to confinement. We will set aside the latter problem for the moment and focus on the former.

4.2.2 Parton showers

The origin of a parton shower can be quickly understood from the matrix element for the splitting process

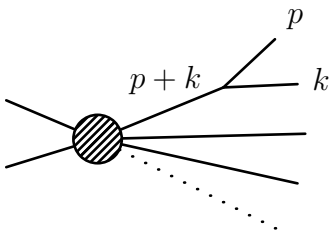

$$\sim \frac{1}{t} = \frac{1}{(p+k)^2} = \frac{1}{2E^2 z(1-z)\sin^2\theta} \tag{4.3}$$

where t is the *virtuality* of the mother parton, θ is the angle between the daughter partons, z and $(1-z)$ are the fractions of the mother parton's energy carried by the daughters, and this expression is valid for massless partons. The matrix element diverges when either z (or $1-z$) is small (soft) or θ is small (collinear). Physically, it represents the fact that partons, once produced at a hard scale Q, will emit a large number of soft and collinear quarks and gluons in a collimated spray known as a *jet* until they reach the hadronization scale Λ_{QCD}. The dominant effects of this process are reasonably modeled using *parton*

showers [9, 28].

Parton showers work in the limit $t \ll Q$. If the differential cross section before splitting was $d\sigma_n$ then in this limit the cross section after splitting $d\sigma_{N+1}$ is approximated by

$$d\sigma_{n+1} = d\sigma_n \frac{dt}{t} dz \left(\frac{\alpha_s}{2\pi} P_{ij}(z) + \mathcal{O}\left(\frac{t}{Q^2} \right) \right), \tag{4.4}$$

where $P_{ij}(z)$ is the same splitting function encountered earlier and gives the distribution of the fraction z of energy of the mother parton i carried by the daughter j [9, 28]. Here, t is known as the *evolution variable* which we will assume is the virtuality but can, in principle, be any variable such as p_{T}^2 or θ that causes the matrix element 4.3 to diverge in the collinear limit. The splitting cannot take place with all the partons on-shell and the dominant contributions come from configurations where t is *strongly ordered* so that it is largest near the hard subprocess and decrease as the shower evolves away from this, emitting further partons as it goes. The upper limit on t is set by the momentum transfer at Q, while the lower limit is usually at the hadronization scale $t_0 = \Lambda_{QCD}$.

The expression 4.4, while encapsulating the dominant physics of splitting, does not account for virtual corrections at the same order. These are accounted for by running couplings and by multiplying each line that ends in a split by the *Sudakov form-factor* given by

$$\Delta_i(t_1, t_2) = \exp\left[-\int_{t_2}^{t_1} \frac{dt}{t} \frac{\alpha_s}{2\pi} \int_{z_{min}(t,t_0)}^{z_{max}(t,t_0)} dz \sum_j P_{ij}(z) dz \right] \tag{4.5}$$

which can be interpreted as the probability for a parton *not* to split as it evolves from t_1 to t_2. Then modeling a parton shower in a Monte Carlo can proceed as follows. For a each parton produced in a hard process, generate a random between 0 and 1 as the probability for this parton not to split, $\Delta_i(t_1, t_2)$. Use this to calculate the corresponding t_2 at which the parton splitting occurs. Repeat this for the daughter partons, stopping the process once they reach $t = t_0$. The total cross section is then given by the hard cross section multiplied by 4.4 and 4.5 for each intermediate parton which ends at a split.

If the initial state particles are also partons – as in a hadron collider – then a similar process has to be accomplished for the initial state. This proceeds backwards from the hard process so that the initial particles gain energy and lose virtuality as they evolve backwards in time. Besides this the only other major difference from the final state parton

shower is that the Sudakov factor must be modified to include the ratio of the parton distribution functions at the two scales to account for the probability that the parton being evolved would have come from the proton to begin with.

4.2.3 Jet matching

Though the parton shower scheme accurately models jet evolution in the dominant region $t \ll Q$ it fails when $t \sim Q$. Specifically, parton showers typically under-produce events with widely separated energetic jets. Fortunately, this is precisely where the matrix element method works well. Therefore one can include events with extra jets in this region of phase space during the matrix element calculation to help fill the gap. One is able, for instance, to combine the process $p\,p \to t\,\bar{t}$ with $p\,p \to t\,\bar{t} + j$ (where j represents a mother parton which will evolve into a jet) to model top pair production along with a possible extra jet. Unfortunately, after putting $p\,p \to t\,\bar{t}$ through the parton shower it will sometimes gain an extra jet in a region of phase space already covered by $p\,p \to t\,\bar{t} + j$, effectively double counting this process. This double counting must be accounted for and removed by a process known as *jet matching*.

Just as there are several evolution variables one can use to perform the parton shower there are several jet matching schemes. One, called the *shower $k_\perp$ scheme* [49], uses the ordering variable p_{T} (as measured from mother parton) and demands that any additional jets that the matrix element generator produces are greater than some intermediate cutoff scale Q_{cut}. These events are then fed into the parton shower. If the parton shower for one of the lower multiplicity inputs ($p\,p \to t\,\bar{t}$ in our example) produces a new splitting with p_{T} larger than Q_{cut} then the event is rejected. For the highest multiplicity state ($p\,p \to t\,\bar{t} + j$ in our example) shower p_{T}'s may be larger than Q_{cut} and are only rejected if greater than the softest parton p_{T} produced by the matrix element generator.

Though jet matching may seem like a technical detail, in practice it is important for the average physicist wishing to study collider search strategies for BSM models. In such cases it is common to use one program to generate the hard process and another to handle the parton shower. Then one must take a very hands-on approach to jet matching. For SM processes this is less of an issue as many programs combine the matrix element-

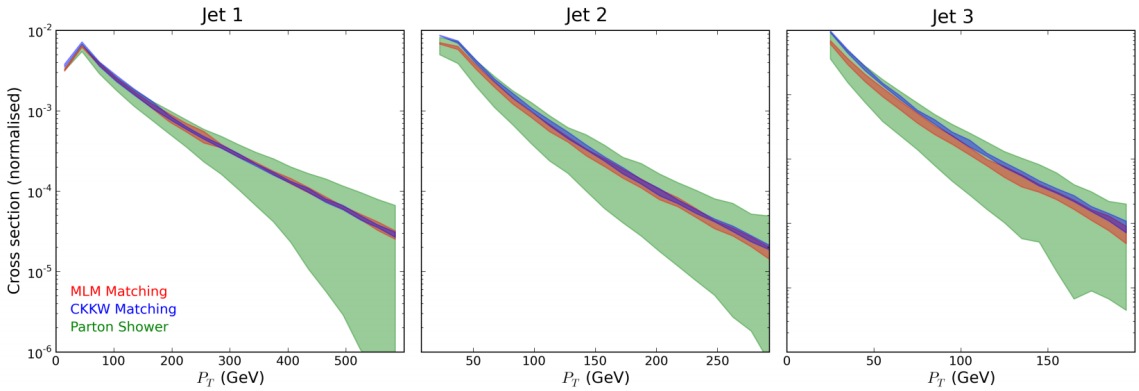

Figure 4.2: Uncertainty on ISR jet p_{T} distribution (as measured from the beam) for squark pair production ($m_{\tilde{q}} = 500$ GeV). Uncertainty is given for the first, second, and third hardest jets, from left to right. Green shows parton shower uncertainty (from Pythia) while red and blue show matched jet uncertainties for two different matching schemes. Uncertainties were obtained by varying algorithm parameters such as Q_{cut} by factors of two, which should have no effect on the physics. Figure taken from [50].

parton shower matching into a single package. Fig. 4.2 shows the effect of matching vs. not matching on jet p_{T} uncertainty for squark pair production with initial state radiation (ISR).

4.2.4 Hadronization and decays

As we stated previously, hadronization is a non-perturbative process. Modeling this using rigorous but computationally expensive techniques such as lattice QCD is out of the question for large scale Monte Carlo simulations so researchers must instead content themselves with capturing the essential features of this process using phenomenological models based on general features of QCD.

There are several models of hadronization employed by different MCs. One of the most commonly used, known as the *Lund string model* [51] implemented in Pythia, is based on the fact that in lattice QCD simulations the potential energy between quarks increases linearly with distance. This is apparently due to gluon self-attraction which causes the gluon field to collapse into a string or flux tube. The string model simulates this flux tube with a string of constant potential energy per unit length. The string model is easiest to visualize with a quark-antiquark pair. As the pair is created the particles fly apart stretching the flux tube between them. The potential energy of the tube grows until it becomes energetically favorable to break the tube by producing a new quark-antiquark

pair. These pair up with the original quarks in color singlet states which fly apart and may repeat the process.

After hadronization the final step in the collision simulation is to decay any resulting unstable hadrons. MC generators rely on large tables of experimental data for this purpose. Since this data is incomplete and occasionally contradictory MC authors must make choices to ensure (for example) branching ratios add to one. Differences between programs also arise in how accurately decays are treated – whether, for instance, spin correlations are included for a given process or not. In the end no one generator addresses all of these issues better than the others.

4.3 From simulated collisions to analysis

Following the MC event generation, large numbers of events can be imported into one of several particle detector simulations. Those in widest use among theorists are Delphes [52], PGS [53], and AcerDet [54] – experimentalists use proprietary simulations to model their own detectors. Various properties of the simulated detector such as tracking coverage and resolutions are configurable to more accurately match an actual detector's performance. Details of the LHC's ATLAS detector are given in ch. 5, and may help some readers more closely follow the discussion below.

For every final state particle, detector simulations create a simulated track (if the particle is charged) and a calorimeter deposit (if it leaves one). From this information physical objects such as electrons, photons, muons, and jets are reconstructed just as in actual high energy physics experiments. Detector simulations introduce effects such as jet energy smearing and jet type tagging efficiency (tau-jet, b-jet, ...) which may be important in determining the effectiveness of a proposed new collider search strategy. Most will not, however, include effects such as pileup.

After the detector simulation, an analysis of the data is needed to determine if one is able to differentiate the events produced by particles in a given BSM model from the (usually large) background of similar events produced by particles within the SM, and if so over what range of parameters this is possible. This is a highly non-trivial task, though we will cover some of the basics of BSM search strategies in ch. 5. Suffice it to say

that unless the analysis code and associated backgrounds are publicly available, recasting existing searches to look for particles in a new model can be a very time consuming process requiring simulations of both the BSM signal one was looking for, as well as many different types of SM processes. However, the release of the relatively new program CheckMATE changes this [55]. Within this code is a Delphes detector simulation more highly tuned to match the performance of the ATLAS detector. More importantly, it comes with many existing ATLAS (and a few CMS) analyses built in, along with experiment event counts and a statistical package to make a final 95% confidence "excluded" or not determination for a given model. Another program called Rivet exists to compare SM measurements to event generators [56] and includes many more analyses.

To summarize, using the Monte Carlo tools described within this chapter one is able to determine if a given process in a specific BSM model with a specific parameter set is excluded by the LHC starting from the model Lagrangian. More importantly, new search strategies can be invented and tested within this framework. We emphasize, however, that final exclusion determination must still be left to experimentalists with access to more accurate detector simulations and actual data.

Chapter 5: LHC, ATLAS, and BSM search strategies

5.1 LHC and the ATLAS detector

The LHC is a true wonder of science – one of the most complex machines ever built by mankind. It is a circular proton-proton collider which sits in a 27 km circumference tunnel between the borders of Switzerland and France and is part of the European Organization for Nuclear Research (CERN) complex. It is the most powerful particle accelerator built to date with a center of mass energy initially at 7 TeV (3.5 TeV per beam), rising to 8 TeV by the end of Run 1 and currently at 13 TeV in Run 2. It has a planned integrated luminosity of 300 fb^{-1} after the first ten years of its life, a figure that will rise by an order of magnitude after the High Luminosity (HL) upgrade [57].

LHC beams consist of short bunches of protons – in Run 1 bunches contained about 10^{11} protons. Many bunches circle the collider at once with a maximum number of 1374 during Run 1 with intersections occurring every 50 ns. Multiple protons collide during each bunch crossing (a situation known as *pileup*) – for Run 1 the maximum average rate was 37 per bunch [58]. Up to 1000 particles emerge from each collision vertex [57].

Situated along the main ring are the 'big-four' experiments ATLAS, CMS, LHCb, and ALICE, inside of which the particle collisions take place. ATLAS and CMS are both general purpose experiments designed to study the SM and search for physics beyond it. LHCb specializes in heavy flavor physics while ALICE studies lead-lead ion collisions. Though ATLAS and CMS are broadly similar in their designs and objectives it is ATLAS which I will focus on due to my close working relationship with ATLAS members. Much of the information about the ATLAS detector presented here can be found in ref. [59].

ATLAS (A Toroidal LHC ApparatuS) is a large multi-layered detector with fast radiation-hard electronics and sensor elements. Its main detector elements are the inner tracker, the electromagnetic calorimeter, the hadronic calorimeter, and the muon tracker. Both the inner and muon trackers are immersed in strong magnetic fields (from a superconducting solenoid and toroid respectively) to measure particle charges and momenta.

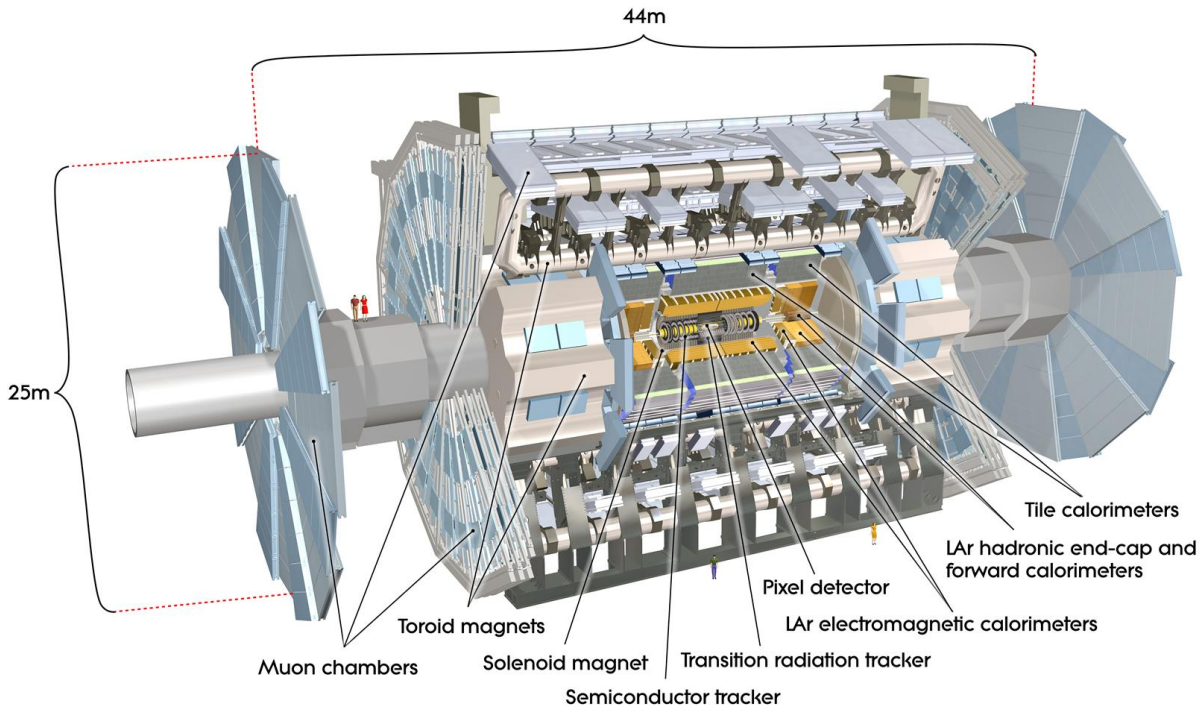

Figure 5.1: Cutaway view of the ATLAS detector with major components labeled. Figure taken from reference [59].

The coordinate system used to describe the detector has z starting at the center and running along the beam axis with the $x-y$ axis in the transverse plane. The azimuthal angle ϕ is measured around the beam axis and the polar angle θ is measured from the beam. The pseudorapidity is defined as $\eta = -\log(\tan(\theta/2))$ and the distance ΔR is defined as $\Delta R = \sqrt{\Delta\eta^2 + \Delta\phi^2}$.

The inner detector is itself a layered system. Starting at a radius of 5 cm from the central axis, 7 layers of silicon detectors (pixel and strip) form concentric cylinders around the beam[1]. Outside this a large number of straw-tubes, filled with a xenon-based gas mixture, are able to generate and detect transition radiation. Together, these systems precisely track particles as they leave the impact point, and allow for secondary vertex site determination for heavy-flavor and τ lepton tagging. Tracking is possible up to $|\eta| < 2.5$. The 2 T magnetic field combined with the precise instrumentation allows for a transverse momentum resolution on the order of 1%.

The high granularity electromagnetic calorimeter is liquid argon (LAr) and covers the pseudorapidity range $|\eta| < 3.2$. The hadronic calorimeter uses a mix of LAr technology

[1]During the LHC Run 2 upgrade ATLAS installed the Insertable B-Layer; a new pixel layer with an inner radius of 3.1 cm [60]

Category	Luminosity [$cm^{-2}s^{-1}$]:	3×10^{30}	2×10^{31}	2×10^{32}
		p_{T} threshold [GeV], selection		
Single muon		4, none	10, none	13,tight
Di-muon		4, none	6, none	6,loose
Single electron		10, medium	15, medium	15, medium
Di-electron		3, loose	5, medium	10, loose
Single photon		15, loose	30, loose	40, loose
Di-photon		5, loose	15, loose	15, loose
Single tau		20, loose	50, loose	84, loose
Single jet		30, none	75, loose	95, loose
$E_{\mathrm{T}}^{\mathrm{miss}}$		25, tight	30, loose	40,loose
B-physics		mu4_DiMu	mu4_DiMu	2mu4_DiMu

Table 5.1: Examples of p_{T} thresholds and object identification criteria for various triggers at three Luminosities. Table taken from [61].

along with a scintillator-tile detector and covers a range $|\eta| < 4.9$ (including the forward calorimeter). It has coarser granularity that the EM calorimeter as it is designed primarily for jet reconstruction and $E_{\mathrm{T}}^{\mathrm{miss}}$ measurements. Both calorimeters are generally thick enough to provide protection against punch-through into the muon system.

The muon spectrometer, with dimensions roughly 25 m $\times$ 25 m $\times$ 44 m, is quite large and combined with its strong magnetic field is able to provide enough bending power to resolve 1 TeV transverse momenta to 10%, independent of the inner tracker. It covers a region $|\eta| < 2.7$.

One critical limitation for both ATLAS and CMS is an inability to write information to disk at close to the speed at which it is collected from the detector. At the LHC's design luminosity the proton-proton interaction rate is about 1 GHz while technology and resources constrains the event data recording rate to about 200 Hz. This situation necessitates the use of triggers which decide, real time, weather to discard an event or keep it for further processing. ATLAS uses three trigger levels. The Level-1 (L1) trigger uses a subset of the detector information to decide whether to continue processing an event. Following this are the Level-2 (L2) trigger and event filter, which collectively reduce the data rate to a manageable 200 Hz. Together the triggers form a *trigger chain*, of which there are several hundred different types within ATLAS [61].

Triggers can look for single objects, multiple objects, or for patterns in several regions within the detector. They are extremely important for physics studies because without a trigger for the type of signal one is looking for the desired information will not be saved

to disk. An example of various trigger thresholds is show in Table 5.1.

The object identification criteria listed in this table (*e.g.*, loose, medium, tight) describe the degree of certainty the detector has on a given object classification. Tight criteria rely on more stringent rules to label an object and contain fewer false positives; however they also incorrectly reject more false negative events. The reasons for using a particular set of identification criteria vary based on the desired signal and the relevant backgrounds.

We will discuss more details about object identification in the next section.

5.2 Object identification

As was introduced in the discussion of ATLAS triggers above, the identification of objects within a detector, though well understood, is not always straightforward. Perhaps the largest limitation of a hadron collider, in contrast to lepton colliders, is that the true center of mass and collision energy of the process of most interest is unknown. This is due to the fact that on the time scale of collisions each of the hadrons acts like a loose bag of partons, with each parton carrying an unknown fraction the hadron's overall momentum. Nevertheless, the momentum transverse to the beam is known (zero by definition) providing enough information to help object identification.

The five main categories of objects identifiable at ATLAS are muons, electrons, photons, jets, and missing transverse momentum. We will briefly describe how these are identified in what follows. This discussion is made easier to follow by referring to Figure 5.2, which is a greatly simplified view of the signature left by various objects in the detector.

Muons are perhaps the easiest fundamental particles for ATLAS to identify since (in the absence of punch-through) they are the only objects which leave tracks in the muon chamber. They can be reconstructed either from the muon chamber alone or by matching muon chamber tracks with those in the inner detector tracks [62].

Following this, electrons and photons are fairly easy to identify from their shower profile in the EM calorimeter. The two are distinguished by the track the electron leaves in the inner detector which is absent for the neutral photon [63, 64].

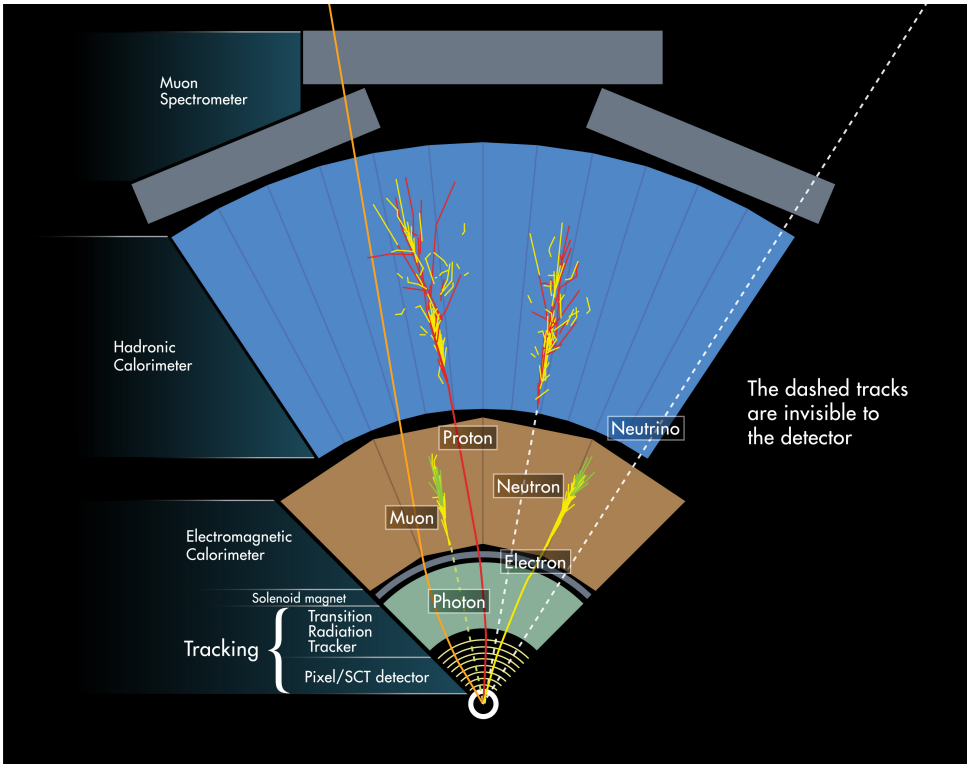

Figure 5.2: Schematic of particle signals left in various portions of the ATLAS detector. Figure taken from ref. [62].

Hadrons, while leaving quite obvious signals in the calorimeter, nevertheless require subtle treatment. As discussed in ch. 4, if a hard parton is produced in an event it will result in a collimated spray of particles (a jet) which leave a tell-tale cluster of energy in the hadronic calorimeter. Of course there are a wealth of soft hadrons spraying out from collisions, and there can be many jets, so identifying individual jets requires an algorithm. There are several types of algorithms, but for most purposes the anti-k_{T} is the favorite [65,66]. It is IR and collinear safe, in that emissions of this sort do not change the observable. This algorithm uses the distance measure d_{ij} between two particles i and j to sequentially combine particles with the lowest d_{ij} into jets, until the d_{ij} reach a size R. For the anti-k_{T} algorithm d_{ij} is given by

$$d_{ij} = \min(k_{\mathrm{T}i}^{-2}, k_{\mathrm{T}j}^{-2}) \frac{\Delta y_{ij}^2 + \Delta\phi_{ij}^2}{R}, \tag{5.1}$$

where k_{T} is the transverse momentum, Δy_{ij} is the difference in rapidity, and $\Delta\phi$ is the azimuthal separation. ATLAS often uses a size $R = 0.4$ and requires $p_{\mathrm{T}} > 20$ GeV for its jets.

Obviously, knowing what sort of particle produced a given jet is enormously helpful

in physics studies. While this is not always possible, algorithms exist to identify particles based on their jet energy profiles or displaced vertices. For instance, b quark tagging algorithms rely on the fact that hadrons containing these particles live long enough to move a detectable distance before decaying. They "connect the dots" between hits in the inner detector to determine if the particles emerged from a *secondary vertex* some distance from the primary vertex. For b quarks this requires finding a secondary vertex about ~ 0.1 mm from a primary vertex. Incredibly, ATLAS is able to locate vertices to an $\mathcal{O}(10\ \mu\text{m})$ accuracy, enabling such algorithms [67] – quite a feat considering the inner detector starts at a 5 cm radius.

The last major category of identifiable objects at ATLAS is missing transverse momentum, or missing transverse energy (commonly $\vec{E}_{\text{T}}^{\text{miss}}$, but also $\vec{p}_{\text{T}}^{\text{miss}}$ or MET). It is the only "signal" left by neutral weakly interacting particles such as neutrinos, and is identifiable by that the fact that transverse momentum in the detector should sum to zero. Though the name is a bit of a misnomer since it implies energy is a vector, it makes a bit more sense when one considers that it is primarily measured using calorimeter information. To avoid confusion we will call $\vec{p}_{\text{T}}^{\text{miss}}$ the vector quantity and $E_{\text{T}}^{\text{miss}}$ its magnitude, implicitly assuming that the particles involved may be treated as massless. Then $\vec{p}^{\text{miss}}$ (not transverse) is defined as

$$\vec{p}^{miss} = -\left(\sum_{\text{calo cell } i} E_i \vec{u}_i + \sum_{\text{muon } j} \vec{p}_j \right) \tag{5.2}$$

were $\vec{u}_i$ is a unit vector to the i^{th} calorimeter cell with a reconstructed object calibrated energy E_i, and $\vec{p}_j$ are the muons' momenta as measured in the muon spectrometer (since muons are not stopped in the calorimeter) [68]. Then $\vec{p}_{\text{T}}^{\text{miss}}$ is the component of $\vec{p}^{\text{miss}}$ transverse to the beam. Systematic uncertainties in $\vec{p}_{\text{T}}^{\text{miss}}$ come primarily from jet energy mismeasurement (particularly from soft jets) and calorimeter cell energy mis-measurement for cells not associated with reconstructed objects.

5.3 Classic SUSY search strategies

By reconstructing physical objects within the ATLAS detector and comparing the number of and distributions of these objects as compared to theory, one is able to make accurate

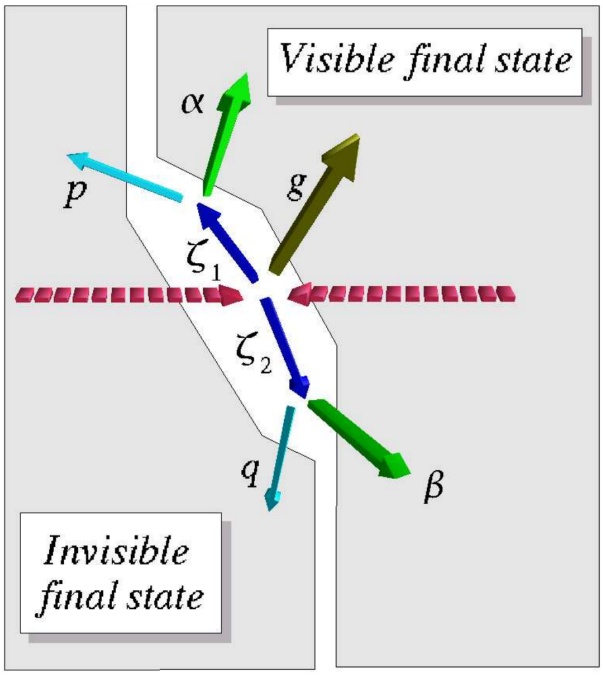

Figure 5.3: Schematic of generic signal for SUSY production in a collider. Two sparticles $\zeta_{1,2}$ are produced, decaying to visible final states α and β, and invisible final states p and q. In addition to these, further debris or ISR from the collision may be produced, represented by g. Figure taken from [69].

tests of the SM. Large excesses in the production of certain objects can point to new physics or indicate a weakness in theoretical calculations. Modeling of both the SM and new physics at the LHC relies heavily on Monte Carlo simulations, as we discussed in ch. 4. In this chapter we focus on a few of the techniques which can be used to separate SUSY from large SM backgrounds.

As we discussed in ch. 3, SUSY theories with R parity demand that sparticles are produced in pairs and, if they decay, will each do so to an odd number of sparticles. The LSP is usually assumed to be neutral and will leave the 'detectable' signal of missing transverse momentum as it leaves the detector. Therefore, typical SUSY searches usually assume sparticle pair production, where each sparticle is fairly massive (heavier than LEP limits, usually ~ 100 GeV [3]) and promptly decays into at least one neutral stable sparticle. The primary signal, then, is energetic SM decay products in association with missing transverse momentum. This is shown schematically in fig. 5.3.

The sort of SM processes which mimic this signal often involve neutrinos or mis-measured jets (resulting in missing transverse momentum) produced as a result of, or in association with, heavy SM particles. Top quarks, Ws, and Zs each fit the bill for a heavy SM particle and are all capable of producing neutrinos during their decays; therefore these

often constitute significant backgrounds.

Since a SUSY signal and its backgrounds each produce the same types of objects in a detector one must use differences in their kinematics to separate them. There is a very large (and still growing) list of kinematic variables which aid in this process. One well known variable is m_{T2},[2] colloquially called the 'stransverse mass' for its similarity to the transverse mass m_{T} and its ability assist in sparticle identification [69–71].

Transverse mass m_{T} is similar to the invariant mass of a parent particle m_{parent} which decays to two daughters with energy-momentum p_1 and p_2

$$m_{\mathrm{parent}}^2 = (p_1 + p_2)^2 = m_1^2 + m_2^2 + 2(E_1 E_2 - \vec{p}_1 \cdot \vec{p}_2). \tag{5.3}$$

This expression is useful for reconstructing the parent mass when one knows the energy-momentum of both of the daughters, however it is less useful when one of the daughters is invisible and the center of mass is unknown, as is the case in a hadron collider. Then the best one can do is provide a event-by-event lower bound on the parent mass using the transverse information in the detector,

$$m_{\mathrm{parent}}^2 \geq m_{\mathrm{T}}^2 \equiv m_1^2 + m_{\mathrm{miss}}^2 + 2(E_{1\,\mathrm{T}} E_{\mathrm{T}}^{\mathrm{miss}} - \vec{p}_{1\,\mathrm{T}} \cdot \vec{p}_{\mathrm{T}}^{\,\mathrm{miss}}), \tag{5.4}$$

where $E_{\mathrm{T}} \equiv \sqrt{p_{\mathrm{T}}^2 + m^2}$. If there are two parents each decaying semi-invisibly then things become more complex since p_T^{miss} must somehow be shared between two invisible particles. Nevertheless, one can still construct a maximum lower bound on the parent mass using

$$m_{\mathrm{T2}}(p_{\mathrm{T}\,1}, p_{\mathrm{T}\,2}; m_{\mathrm{inv}}) = \min_{q_{\mathrm{T}}} \Big[\max \Big(m_{\mathrm{T}}(p_{\mathrm{T}\,1}, q_{\mathrm{T}}; m_{\mathrm{inv}}), m_{\mathrm{T}}(p_{\mathrm{T}\,2}, p_{\mathrm{T}}^{\mathrm{miss}} - q_{\mathrm{T}}; m_{\mathrm{inv}}) \Big) \Big] \tag{5.5}$$

which is also implicitly dependent on m_1 and m_2.

One can use Monte Carlo simulations to plot m_{T2} distributions of both SUSY models and SM background processes to determine if there are regions where sparticle production will be detectable. Where SM processes dominate events are 'cut away' leaving only regions in which new physics should produce a significant number of events. If there are no large data excesses in these regions then one may be able to exclude some portion of the parameter space for a given SUSY model. Fig. 5.4 shows an example of this in an ATLAS search for slepton pair and chargino pair production, with each sparticle decaying to a

[2] A variable as glamorous as its proponents – take a look at the first page of Barr et al. [69].

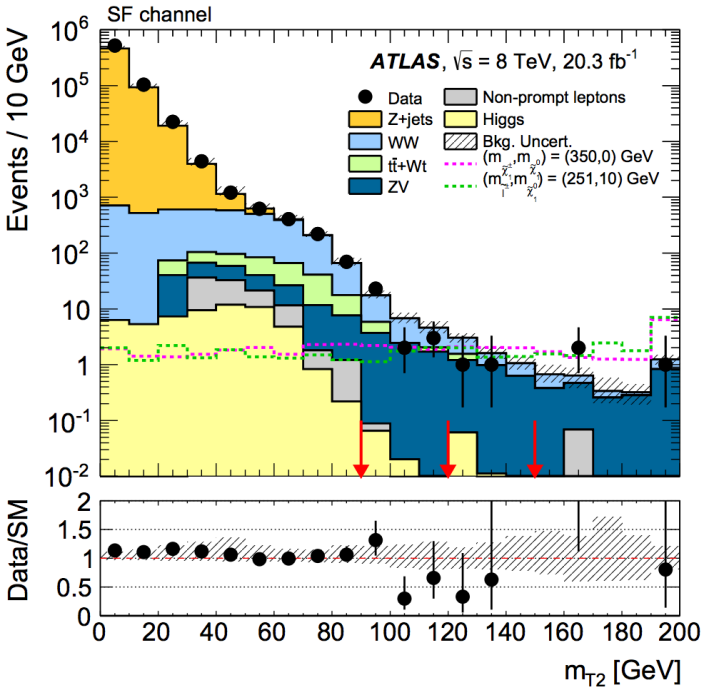

Figure 5.4: m_{T2} distributions for two representative SUSY signals and SM backgrounds in an ATLAS SUSY search for charginos and sleptons. The objects used for constructing m_{T2} are two same-flavor leptons + $E_{\mathrm{T}}^{\mathrm{miss}}$. m_{miss} is assumed to be zero, appropriate for the backgrounds involving neutrinos. Standard model backgrounds dominate below ~ 90 GeV, therefore events with m_{T2} less than this are cut. Figure taken from [72].

lepton plus neutralino LSP. Significant backgrounds from W pair production, for instance, are removed by taking only events with $m_{\mathrm{T2}} > m_W$ (in actuality the requirement is a bit higher than this).

In practice one usually uses several kinematic discriminants, the list of which may or may not include m_{T2}, to separate signal from background. For a generic SUSY search this usually results in limits with general features similar to those shown in fig. 5.5. The process considered for this schematic plot is sparticle pair production with each sparticle $\tilde{\chi}$ promptly decaying to a SM particle (which may undergo further splittings or decays) and a neutral LSP $\tilde{\chi}_1^0$. As the trial mass of the sparticle $\tilde{\chi}$ increases its production cross section decreases since PDFs mostly decrease with momentum fraction. This results in fewer expected SUSY events and thus weakened sensitivity to models as $m_{\tilde{\chi}}$ increases. On the other hand, many searches also lose sensitivity to models as $m_{\tilde{\chi}}$ approaches the kinematic limit $m_{\tilde{\chi}} \geq m_{\tilde{\chi}_1^0} + m_{\text{SM particle}}$, which is represented by a dashed line in fig. 5.5. This is because the decay products lose momentum in this limit making them harder to pick out of backgrounds or causing them to fail trigger requirements. Exactly when a search loses sensitivity in this region depends heavily on the nature of the backgrounds

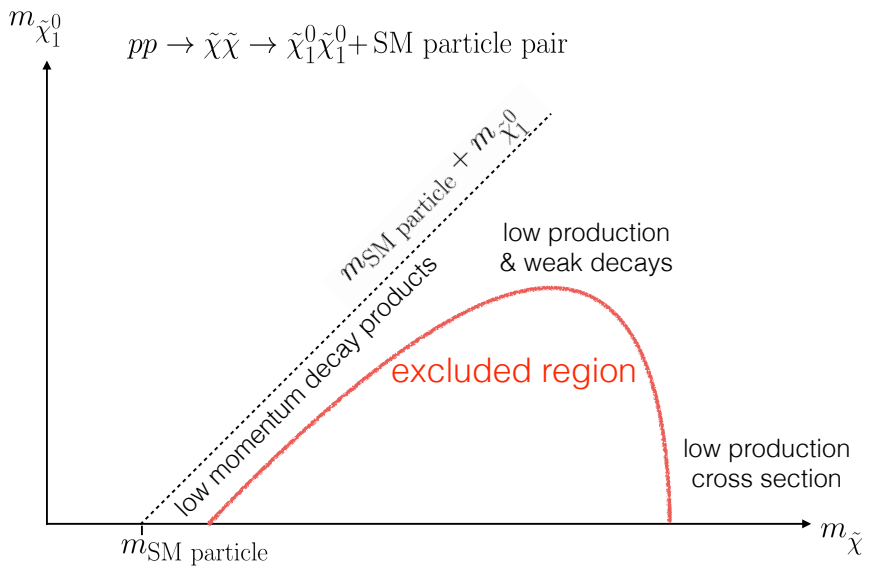

Figure 5.5: Generic form of SUSY limits plot and reasons for exclusion weaknesses. In this representative example, a pair of sparticles $\tilde{\chi}$ each decay to a LSP $\tilde{\chi}_1^0$ plus a SM particle, which may or may not undergo further decays or hadronization. Searches will not have sensitivity to new physics when the production cross section is too low (because the mass of the new particle $m_{\tilde{\chi}}$ is too high) or when the decay products have such low momentum that they drown in SM backgrounds or fall below the detector's trigger levels.

and on the trigger levels.

One technique to get around the problem of weak decay products and to fill in the gap just described is to search for ISR instead of sparticle decay products. This also works in searches for invisible particles, such as $\tilde{\chi}_1^0$ pair production. In short, before the hard collision takes place one of the partons may emit an energetic transverse jet as it evolves in virtuality from the scale of the proton to the hard scale. This will boost the heavy particle center-of-mass along with the final state particles in the transverse direction. If the final state particles are invisible then the signal will be a single hard jet and missing transverse momentum. This strategy is used in generic DM searches such as those described in [73, 74]. On the other hand, if the final state particles are visible they can be boosted and may be used to assist the analysis [75–77].

The strategies discussed here, while giving a general idea of how a generic SUSY search works, is by no means comprehensive. Still, it is enough to understand what is covered in the rest of this thesis. We will now proceed to investigate how an extradimensional scenario known as auto-concealment affects current ATLAS SUSY limits.

Chapter 6: Auto-concealment of supersymmetry in extra dimensions

This chapter is based on [6]*, work done in collaboration with Savas Dimopoulos, Kiel Howe, and John March-Russell.*

6.1 Introduction

In this chapter we present a mechanism by which SUSY signals at a hadron collider are dynamically degraded. We consider a framework in which the SM particles and their SUSY-partners live on a brane that is embedded in a (flat) $4 + d$-dimensional supersymmetric bulk whose dimensions are bigger than $\sim 10^{-14}$cm $\sim 1/(\text{few GeV})$. SUSY breaking is felt softly on the brane, and the MSSM superpartners may be produced at colliders[1]. As we will show, many realizations of this scenario have additional light bulk states that are associated with SUSY breaking or additional sequestered sectors. In such cases, the lightest R-parity odd sparticle, the 'bulk LSP', will propagate in the $4 + d$ extra dimensions, and the lightest ordinary-sector SUSY particle (LOSP) will decay to this state.

Couplings between bulk and brane states are necessarily higher dimensional operators, and if the fundamental scale, M_*, is not too high, decays of the LOSP can occur on collider timescales. From a 4D perspective, the LOSP decays to a distribution of KK-modes of the bulk LSP of mass m_n with bulk phase space factor $\sim m_n^{d-1}$. This favors decays to the heaviest KK states, thus suppressing both visible energy and E_T^{miss} in the decay, and so, as we will argue in detail, severely weakening LHC limits on SUSY for certain classes of visible sparticle spectra. The basic mechanism is illustrated in Figure 6.1.

Specifically, we show that two-body decays of the brane-localized LOSP of mass (M) to a SM state and a bulk LSP are typically dominated by decays to bulk KK-modes with masses $m_n \gtrsim 0.4M - 0.8M$ depending on the nature of the coupling and the dimension of the bulk. This leads automatically to signatures similar to a compressed spectrum,

[1]In contrast, studies of brane-worlds with supersymmetric bulks have focused mostly on the case that SUSY is realized only non-linearly on the brane [78–85].

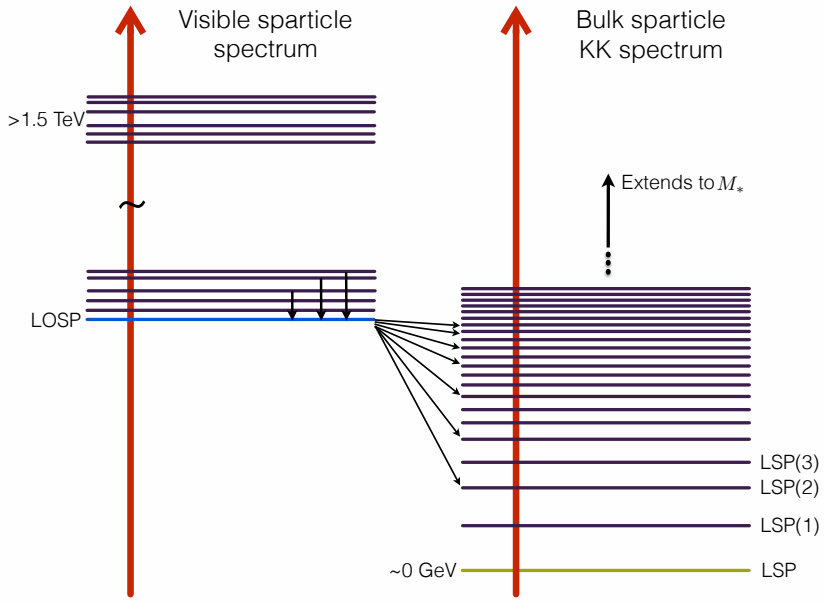

Figure 6.1: Schematic representation of the basic idea behind the auto-concealment mechanism, in which the LSP is a bulk state propagating in $d \geq 1$ extra dimensions. The visible sparticle spectrum has a lightest state, the LOSP, which decays promptly to the full tower of KK excitations of the LSP. As the spectral density of KK excitations behaves as $\sim m_n^{d-1}$ (as a function of the KK mass, m_n), decays to the heavier KK states are favored, dynamically realizing the compressed spectrum mechanism of hiding SUSY with reduced E_T^{miss} and visible energy. As the masses of the KK-tower of the LSP extend from ~ 0 GeV to the underlying gravitational scale M_* the LOSP mass is automatically within this tower. Transitions from visible sector to the bulk sector are prompt if M_* is not too high depending on the nature of the bulk LSP. In the case that transitions are not prompt, the auto-concealment mechanism no longer functions, but instead the decays of the LOSP can provide a powerful search method for extra dimensions.

where super-partners with large production cross sections are concealed if they decay to a nearly degenerate invisible LSP [50,86–92]. Cascade decays that produce a highly boosted LOSP are not as effectively hidden, but nonetheless we find that a variety of motivated and potentially low-fine-tuned spectra are successfully auto-concealed. In this work, we focus primarily on limits from searches for prompt decays, which restricts M_* from above. For higher scales of M_*, searches for displaced vertices and out-of-time stopped decays become relevant, and their sensitivity is also likely to be affected, though a study of this possibility is beyond the scope of this work.

If superpartners *are* discovered at future colliders, then observations of the LOSP decay can be the leading signature of the extra-dimensional nature of the theory. Some probes of the properties of bulk states through prompt decays of a new non-supersymmetric colored states have been studied in refs. [93,94]. Because the visible sparticles are charged under the SM gauge group and brane-localized, their production and subsequent decay

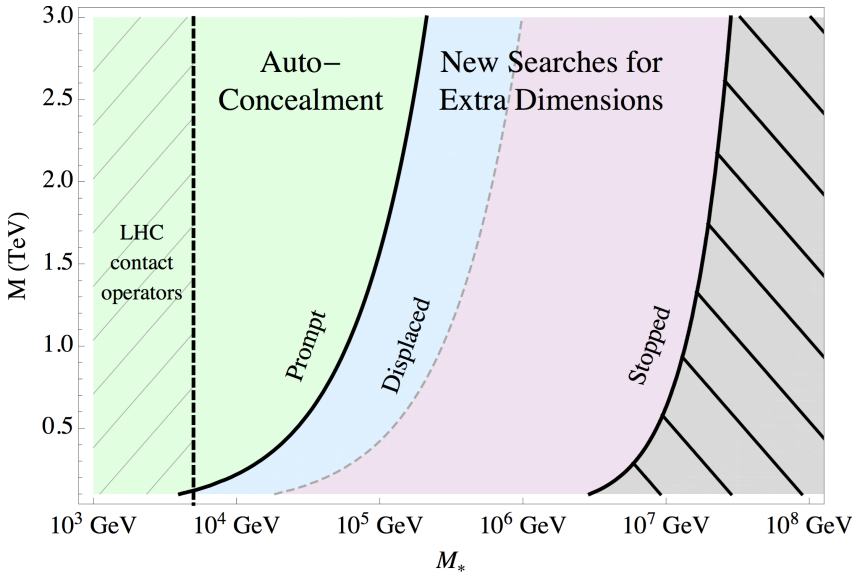

Figure 6.2: Colored regions display the form of LOSP decay as a function of the LOSP mass, M, and the fundamental gravitational scale, M_*. The bulk LSP is taken to be a modulino, the LOSP to be a sfermion, and we show the case $d = 4$. The auto-concealment mechanism applies in the region of prompt decays. In the regions of displaced decays or stopped LOSP out-of-time decays the auto-concealment mechanism no longer functions, but the decays of the LOSP can provide a new search mechanism for extra-dimensions with reach much greater than that provided by contact operators. In the gray hatched region to the far right, the splitting between KK states becomes large compared to the mass of the LOSP, $1/(ML) \gtrsim 0.1$ (all of the decays to the left of this region have lifetimes $\tau \lesssim 1$ yr). The hatched region to the far left shows the range of M_* excluded by current LHC contact operator searches for extra-dimensions.

will be the dominant production mechanism for bulk modes, especially when M_* is so large that the LOSP decay is displaced or occurs after the LOSP is stopped in a detector. This can extend the reach for the fundamental gravitational scale as high as $M_* \lesssim 10^9$ GeV, far above the reach of the usual contact-operator based searches for extra dimensions. As an example of the scales of interest, in Figure 6.2 we show the relevant regions of the M_*-M plane for the case of a bulk modulino LSP with $d = 4$ extra dimensions (Figure 6.9 in Section 6.4 shows the $d = 2, 6$ cases).

6.2 Decays to the bulk

We now turn to a detailed discussion of the mechanism. The decay of a brane-localized LOSP of mass M into a bulk state propagating in d extra dimensions of size $L \gg 1/M$ can be described by an effective theory for the bulk-brane interactions [95–101]. The description of the brane states as point-localized objects in the d bulk dimensions is taken to be valid up to a scale $\Lambda_b < M_*$, where M_* is the fundamental gravitational scale

of the theory, and $M < \Lambda_b$ by assumption so that the decay is well described by the effective theory.[2]

To be concrete we start by studying the decays of a brane-localized $\tilde{e}_R$ LOSP to the fermion ψ of a bulk chiral multiplet[3] Φ. While we now focus on this case as a simple example, there are a variety of other strongly motivated possibilities. In addition to a slepton LOSP, the case of a stop/sbottom LOSP and the case of degenerate first and second generation squark LOSPs provide particularly interesting examples from the point of view of collider phenomenology which we study in detail in the following section. The results derived in this section apply to any sfermion decaying to its massless SM fermion partner and a bulk modulino.

6.2.1 Bulk spectrum and profiles

We study the bulk states by expanding in KK-modes in the extra dimensions,

$$\psi = \sum_n \frac{1}{\sqrt{V}} f_n(y_i)\psi_n(x),$$

where x are the (3+1) coordinates, y_i are the extra bulk coordinates, V is the volume of the bulk, and each KK mode has mass m_n. In flat extra dimensions and in the absence of any bulk mass terms for the state, there is a zero mode, $m_0 = 0$ and the splittings between KK-modes are of order the size of the bulk $\Delta m_n \approx 1/L$. We will be interested in cases where the decays from the brane states are highly-localized compared to the size of the bulk; in this case, the decays are insensitive to the exact form of the boundary conditions for bulk fields far away from the MSSM brane and can be well described in the continuum approximation, $\Delta m_n \to 0$.

The spectrum of KK masses and profiles of a bulk multiplet will be perturbed by the presence of mass terms, which may be spread along the entire $4 + d$ dimensional space occupied by the bulk state or be localized in some of the extra dimensions (for

[2] At distances shorter than $1/\Lambda_b$, the embedding of the brane in the d bulk dimensions may be non-trivial; these effects could be taken into account by the presence of higher dimensional operators including terms with bulk derivatives. The scale Λ_b could correspond to the fundamental gravitational scale M_* or to an intermediate scale related to the extension of the brane embedding in the transverse directions.

[3] The bulk theory has at least $N = 2$ extended SUSY from the 4D perspective, and this N=1 'chiral multiplet' must in fact have bulk partners that fill out a full higher dimensional hyper-multiplet or vector multiplet, although these states need not couple to the brane. We use the N=1 superfield field notation of Ref. [97].

example localized on the MSSM brane). A mass term m_{4+d} spread along the full $(4+d)$ dimensional space lifts the start of the KK-tower to m_{4+d}. We assume such terms are negligible compared to the mass scale of the decays. Mass terms that are localized in some of the d dimensions have their effects suppressed by the volume of the remaining space, and are generally only relevant if they are localized near the MSSM brane, in which case they can affect the wave function profiles near the brane $f_n(0)$.

For example, a mass term for the fermion components of Φ localized on the MSSM brane has the form

$$\mathcal{L} = \delta^d(y)\frac{(\mu\psi\psi)}{\Lambda_b^d} + h.c. \tag{6.1}$$

where the fermion ψ is normalized as a bulk field with mass dimension $(3+d)/2$. The effect of the on-brane mass is to reduce the profile $f_n(0)$ of the KK states near the brane, which suppresses the coupling to brane-localized states. For KK masses $m_n \ll \Lambda_b$ and co-dimension $d \geq 3$, the perturbation of the wave function at the brane $f_n(0)$ is independent of m_n: for small perturbations $\mu \lesssim \Lambda_b$, $f_n(0)$ is unsuppressed, while for large perturbations $\mu \gg \Lambda_b$, $f_n(0) \to 0$ and the leading operators coupling brane fields to the bulk field will be those containing bulk derivatives $\sim \frac{\nabla_y \psi}{\Lambda_b}$ (this latter case is the correct description for instance when orbifold conditions in the fundamental theory force the wave function to vanish on the brane). For co-dimension $d = 1$, $f_n(0) \sim \frac{m_n}{\mu}$ for $m_n \lesssim \mu$, and for $d = 2$ there is a logarithmic dependence on m_n. Overall, the localized mass terms typically increases the efficiency of auto-concealment by decreasing the relative coupling of lighter KK-modes to the MSSM brane states. As the sizes of the localized mass terms μ are only weakly constrained, to be conservative we assume they are negligible for the rest of this work.

6.2.2 Brane couplings and decays

For a simple and well-motivated example, we take Φ to couple to the MSSM states as a modulus in the Kahler potential with a gravitationally suppressed coupling

$$\mathcal{L} = \delta^d(y)\,\frac{1}{2}\left[\frac{(\Phi+\Phi^*){e_R}^* e_R}{M_*^{(d+2)/2}}\right]\Bigg|_{\theta^4}. \tag{6.2}$$

After making the KK expansion, the decay rate of a selectron with mass M to each

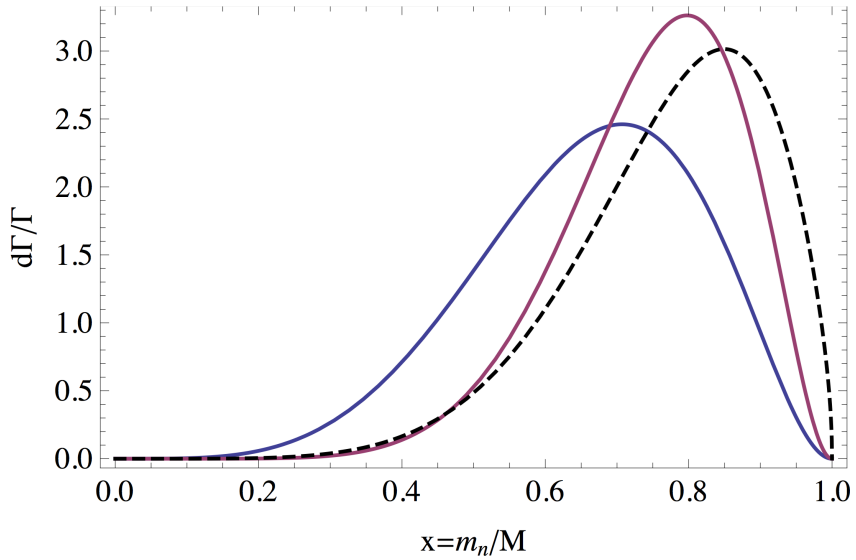

Figure 6.3: Differential distribution of KK masses for the decay $\tilde{e}_R \to e + \psi$ from Eq.(6.4) for $d = (3, 6)$ (solid curves with peaks from left to right, respectively). Also shown dashed is the distribution for a 500 GeV stop decaying in $d = 6$ as $\tilde{t}_R \to t + \psi$, with the definition $x \equiv m_n/(m_{\tilde{t}_R} - m_t)$.

individual mode of mass $m_n < M$ that follows from Eq.(6.2) is

$$\Gamma_n = \frac{M^3}{8\pi M_*^{2+d} V} \frac{m_n^2}{M^2} \left(1 - \frac{m_n^2}{M^2}\right)^2 . \tag{6.3}$$

For co-dimension d, the number of states with mass $\sim m_n$ grows as $\sim m_n^{d-1}$ (this assumes the extra d-dimensions are flat—we later comment on the more general case [102]). For this particular example, the rate to heavier KK states is further enhanced by a factor m_n^2/M^2 due to a helicity suppression of decays to lighter modes. Therefore, even in $d = 1$ the distribution will be peaked towards higher KK masses – the extra-dimensional nature of the LSP is still crucial to provide the continuum of accessible states, but the enhancement of decays to heavier states is due completely to the matrix element. Going to the continuum limit, the total decay rate is

$$\Gamma_{\rm tot} = \sum_n^{m_n < M} \Gamma_n = \frac{M^{3+d}}{8\pi M_*^{2+d}} \frac{\Omega_d}{(2\pi)^d} \int_0^1 x^{d+1}(1 - x^2)^2 dx, \tag{6.4}$$

where Ω_d is the surface area of a $(d-1)$-sphere and $x \equiv m_n/M$. The resulting differential decay rate with respect to the KK mass of the modulino is shown in Figure 6.3. The most likely KK mass is $\sim (0.6 - 0.8)M$, and this can have striking observable consequences for collider phenomenology. (For the case of a stop LOSP with decay $\tilde{t} \to t + \psi$, the non-negligible top mass modifies the distribution as shown in Figure 6.3.)

6.3 SUSY limits and auto-concealment

To understand the effect of auto-concealment on collider searches, it is useful to consider the limit that the LOSP decays to a very narrow distribution of bulk LSP KK states peaked at $m_n \approx M$. In this case there is no visible energy from the LOSP decay[4], and events involving only direct pair production of the LOSP are invisible at colliders. This is identical to the case of exactly degenerate compressed spectra [50]. In this kinematic limit, missing and visible transverse energy arise only when the system recoils against a radiated jet or photon – dominantly ISR – and SUSY searches are significantly weakened.

A realistic distribution of KK masses as shown in Figure 6.3 does not completely realize this limit; the distributions peak below M and they have a non-negligible width. Nonetheless, they remain in the regime where most LOSP decays produce little visible energy and pair production events with large missing and visible energy are still dominantly due to hard ISR. The effect on experimental limits remains substantial. To illustrate this, we re-interpret existing 8 TeV LHC sparticle searches for three interesting cases of LOSP pair production followed by decays to a bulk modulino LSP: a right-handed slepton LOSP $\tilde{e}_R/\tilde{\mu}_R \to e/\mu+\psi$, a right-handed stop LOSP $\tilde{t}_R \to t+\psi$, and degenerate first and second generation squarks $\tilde{q}_{u,d,c,s} \to q+\psi$. We simulate sfermion pair production processes with MadGraph5 [103] with shower and decays[5] in Pythia6 [40] and MLM matching of up to one additional jet. With one exception,[6] experimental limits were recast using validated analyses in CheckMATE [52, 55, 65, 66, 105, 106]. While we expect the results of these simulations to broadly characterize how auto-concealment affects current SUSY search limits, it is up to the experimental collaborations to set definitive bounds.

The first process we consider is pair production of degenerate right-handed sleptons decaying to a bulk modulino $\tilde{e}_R/\tilde{\mu}_R \to e/\mu + \psi$. The dominant limit is from a 20.3 fb^{-1} ATLAS $l^+l^- + E_T^{\rm miss}$ search [107] based on the kinematic variable $m_{\rm T2}$ [69–71]. The effect

[4]Decays of the bulk KK states among themselves producing visible energy on the brane are possible, but they are irrelevant on collider time scales due to the volume suppression of couplings to the brane.

[5]To implement LOSP decays to a KK-tower of fermion LSPs we introduced $N \sim 20$ new gauge neutral spin 1/2 states in Pythia. The masses of these states m_j fell into N evenly spaced bins from 0 to the LOSP mass M. The mass m_j of the $j^{\rm th}$ state was given by the branching ratio-weighted average of masses in the $j^{\rm th}$ bin, and the branching fraction to this state was determined by the integrated width over the bin.

[6]With the exception of [104], all of the analysis used in this chapter to recast limits have been validated by CheckMATE. It was felt important to include this unvalidated analysis since it provided the only exclusion limits for stops decaying to a modulino in $d = 6$.

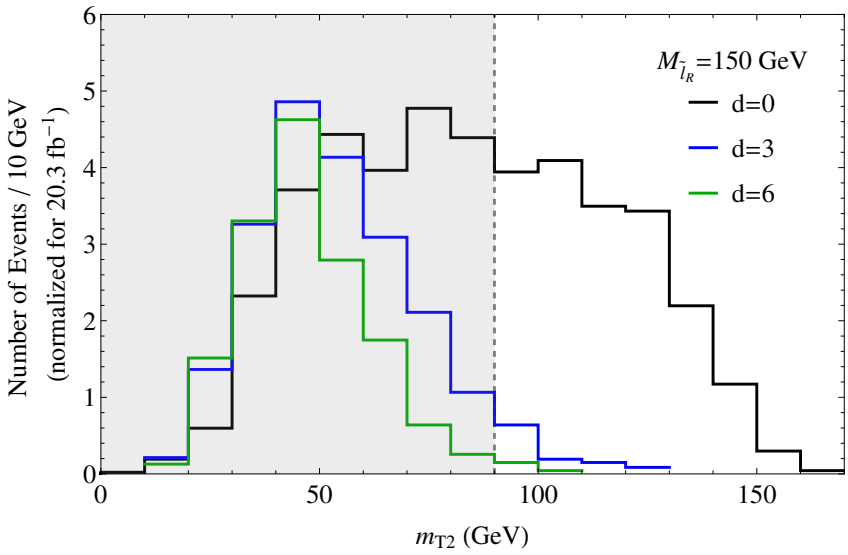

Figure 6.4: Differential distribution in stransverse mass m_{T2} for the decay $\tilde{e}_R \to e + \psi$ for a slepton of mass $M = 150$ GeV to a single massless LSP (black) and a bulk modulino LSP (blue and green) as in Eq.(6.4) for $d = 3, 6$. The preselections of Ref. [107] have been applied, including a cut on missing energy, $E_T^{\mathrm{miss,rel}} > 40$ GeV, which leads to the different total number of events for each case. Shown by a dashed line is the signal region cut $m_{\mathrm{T2}} > 90$ GeV used to reduce backgrounds such as W^+W^- production. Definitions of $E_T^{\mathrm{miss,rel}}$ and m_{T2} can be found within Ref. [107].

of auto-concealment on missing energy-related observables is dramatic, as illustrated in Figure 6.4, which shows the signal m_{T2} distribution after typical cuts used to reduce backgrounds. For the case of $d = 3$, the number of events satisfying the signal region cuts is very significantly reduced, while for $d = 6$ essentially no events pass cuts for the illustrated case of $M_{\tilde{l}_R} = 150$ GeV and 20.3 fb^{-1}. The effect on exclusion limits is predictable. Figure 6.5 shows the strongest cross section exclusion limit (at 95% CL$_{\mathrm{S}}$) from the ATLAS searches [107,108]. A monojet search [109] was also considered to pick up ISR but the analysis had no effect on limits as it vetoed events with isolated leptons. The existing LHC8 limits of $M_{\tilde{l}_R} \gtrsim 225$ GeV for direct production of right-handed sleptons decaying to a massless LSP are completely eliminated, with only the much weaker LEPII limit of $M_{\tilde{l}_R} \gtrsim 95$ GeV for very compressed slepton decays still applying [111–115].[7]

Limits on 3rd generation squark production can also be dramatically reduced. We studied $\tilde{t}_R$ pair production with $\tilde{t}_R \to t + \psi$. As depicted in Figure 6.3, the distribution of KK states in the decay is slightly modified from the result for a massless SM fermion

[7]Note that direct production of left-handed sleptons is already concealed independent of the existence of a bulk LSP as the EW symmetry breaking mass splitting between the heavier charged and lighter neutral members of the LH slepton doublet is small enough that a compressed spectrum is automatically realized.

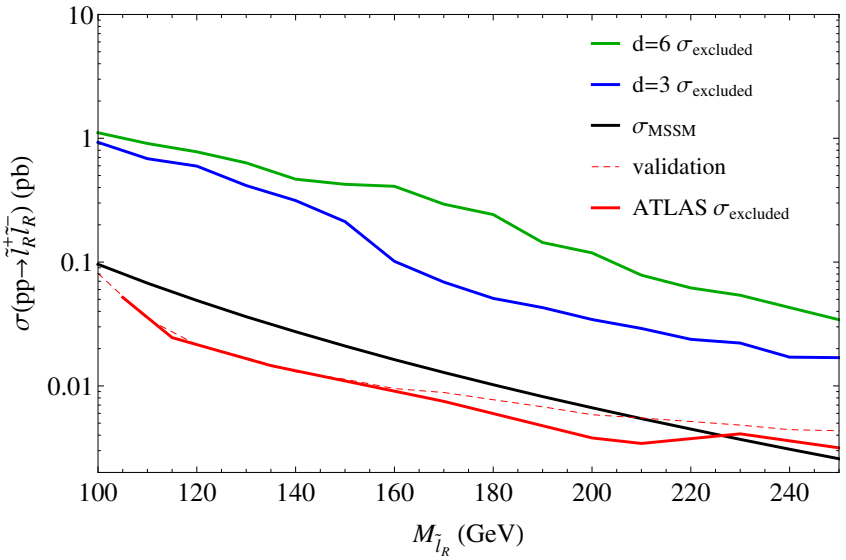

Figure 6.5: Strongest upper bound on degenerate $\tilde{\mu}_R, \tilde{e}_R$ slepton pair production cross sections from ATLAS $l^+l^- + E_T^{\rm miss}$ $m_{\rm T2}$ [107] and razor analyses [108]. A monojet search was also considered [109] but did not affect limits. The top two curves corresponds to sleptons promptly decaying to the KK-tower of a massless modulino in $d = 3$ (blue) and $d = 6$ (green) extra dimensions. The $m_{\rm T2}$ analysis is more effective at higher masses; below 140 GeV (170 GeV) for $d = 3$ ($d = 6$) the razor analysis sets stronger limits. Solid red (lowest) curve gives the observed ATLAS upper bound on the RH slepton production cross section from [107] for decays to a massless LSP. For validation, a dashed red curve gives the same bound using our simulation. Black curve gives the predicted NLO direct production cross section [110] with other superpartners decoupled, illustrating that RH sleptons are excluded up to $\sim$ 225 GeV for decays to a massless LSP. For the searches considered, present limits on direct production of RH sleptons evaporate in the presence of the auto-concealment mechanism.

fermion, eq.(6.4), due to the non-negligible top mass. The dominant validated analysis in CheckMATE was the ATLAS 20.3 fb^{-1} all hadronic 6 (2 b) jet $+E_T^{\rm miss}$ search [116], while the unvalidated 2 lepton stop search [104] provided the strongest limits below $\sim$ 360 GeV. Figure 6.6 shows cross section limits for these searches. For prompt decays to a massless LSP the limit is $m_{\tilde{t}} \gtrsim 680$GeV, while limits reduce to $\sim 350 - 410$ GeV for decays to a bulk modulino in $d = 3, 6$. A number of other searches are expected to provide similar limits, for example the ATLAS and CMS semi-leptonic searches [117, 121] and the most recent all-hadronic searches [121, 122] which perform better than [116] at low stop masses in the compressed region.

We finally study pair production of degenerate first and second generation squarks with $\tilde{q}_i \to q_i + \psi$ assuming the gluinos and 3rd generation squarks are decoupled. The dominant limits shown in Figure 6.7 are from the ATLAS 20.3 fb^{-1} $2-6$ jets $+E_T^{\rm miss}$ analysis [123], except for squarks below 200 GeV where limits are driven by the monojet search [109]. These searches have hard cuts on missing and visible energy and are sub-

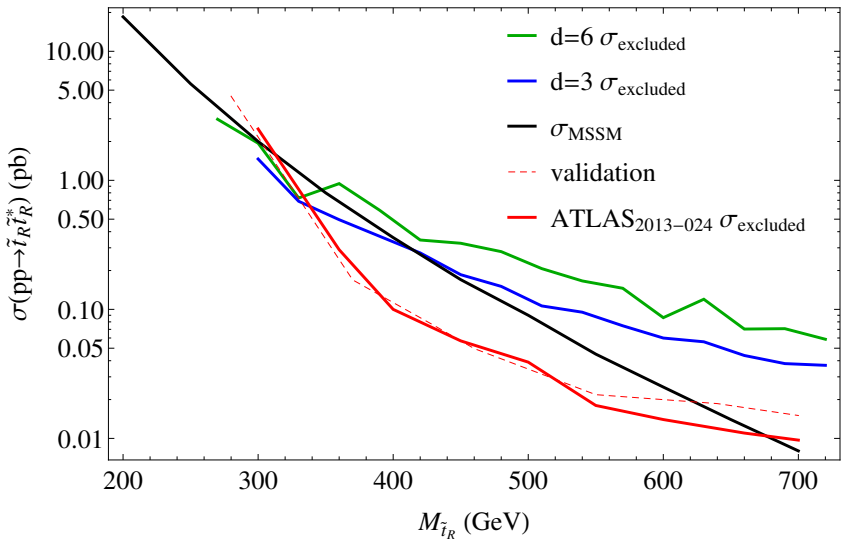

Figure 6.6: Strongest upper bound on stop pair production cross sections from ATLAS 6 (2 b) jet + E_T^{miss} [116] and 2 lepton stop [104] searches. A razor analysis [108], a one lepton stop search [117], and two monojet searches [109, 118] were also considered but did not strengthen the exclusion limits. The upper two curves corresponds to stops promptly decaying to a top + the KK-tower of a massless modulino in $d = 3$ (blue) and $d = 6$ (green) extra dimensions. The all hadronic analysis is more effective at higher masses; below ~ 360 GeV the two lepton analysis sets stronger limits, however it should be noted that this analysis is not yet validated by CheckMATE. Solid red (lowest) curve gives the observed ATLAS upper bound on the stop production cross section from [116] assuming prompt decay to a top + a massless LSP. For validation, a dashed red curve gives the same bound using our simulation. Black curve gives the predicted NLO direct production cross section [119,120], thus illustrating that stops are excluded up to ~ 680 GeV for a single massless LSP. For the search considered, present limits on direct production of stops drop to $\sim 350 - 410$ GeV in the presence of the auto-concealment mechanism.

stantially affected by auto-concealment. While for a decay to a single massless LSP the limit is $M \gtrsim 800$ GeV, for decays to a bulk modulino in $d = 3, 6$ the limit is reduced to only ~ 450 GeV. We have assumed no D-term splitting leading to decays between the left-handed squarks, but we do not expect that these soft decays would significantly affect the results.

We have seen that auto-concealment significantly reduces bounds on direct production of superpartners, dynamically realizing the signatures of a compressed spectrum where a single LSP is nearly degenerate with the LOSP. It is important to emphasize that the auto-concealment mechanism, like the compressed case, does *not* alleviate bounds on all forms of visible sparticle spectra. This is because of the possibility of highly energetic cascade decays before the decay of the LOSP. To distinguish the bad cases from the good it is useful to define *deep* cascade decays as ones where the splitting between the parent visible-sector sparticle and the LOSP are large, $\Delta\tilde{m} \gtrsim M$, and conversely, *shallow*

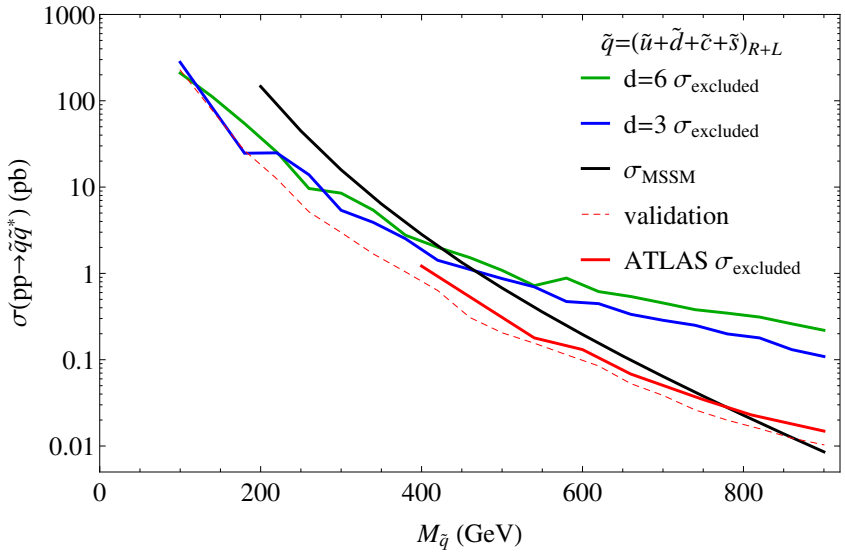

Figure 6.7: Strongest upper bound on pair production cross sections for degenerate first and second generation squarks from ATLAS $2-6$ jets + $E_T^{\rm miss}$ [123] and monojet [109] searches. A razor analysis was also considered [108] but its limits were weaker. The top two curves corresponds to squarks promptly decaying to the KK-tower of a modulino in $d=3$ (blue) and $d=6$ (green) extra dimensions. The hadronic search is the more effective of the two analysis except below ~ 200 GeV. Solid red (lowest) curve gives the observed ATLAS upper bound on the squark production cross section from [123] assuming prompt decay to a LSP with mass ~ 40 GeV. Dashed red curve gives our bounds for a single massless LSP for validation. Black curve gives the predicted NLO direct production cross section when gluinos are decoupled [119, 120], thus illustrating that degenerate squarks are excluded up to ~ 775 GeV for a single massless LSP. For the searches considered, present limits on direct production of squarks drops to ~ 450 GeV for $d=3,6$ in the presence of the auto-concealment mechanism.

cascade decays as ones involving parent-LOSP splittings $\Delta\tilde{m} \lesssim M$. Auto-concealment does not substantially ease bounds on spectra driven by large cross-sections for deep cascade decays to the LOSP. The reason for the failure of efficient auto-concealment in this case is that deep cascades produce highly energetic visible particles (*e.g.*, jets or leptons) recoiling from a highly boosted LOSP, which is transformed primarily into $E_T^{\rm miss}$ in the final decay of the LOSP to the LSP KK-tower.

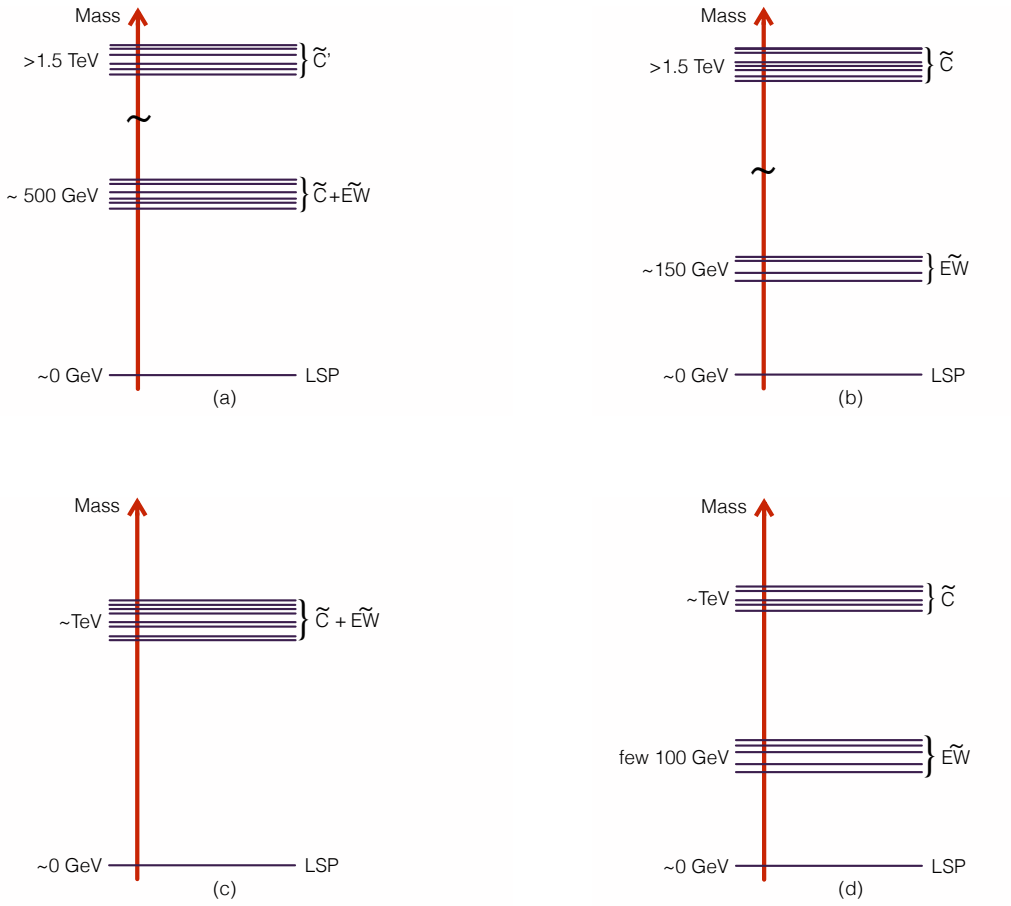

Figure 6.8: Schematic sparticle spectra for which efficient auto-concealment applies, cases (a)-(c), and for which it fails (d). In case (d) colored particles, here generically denoted $\tilde{C}$, are light enough, $\sim$ 1 TeV, that they can be copiously pair produced at the LHC and simultaneously EW sparticles, among which is the LOSP, are substantially less massive, $\sim$ few $\times\, 10^2$ GeV. In this situation there are many deep cascade decays of the heavier colored particles to the LOSP producing both highly energetic jets, and a boosted LOSP which leads to a boost of the $E_T^{\rm miss}$ produced in the final decay of the LOSP. Conversely, in case (a) all the heavier colored sparticles, $\tilde{C}'$ are so massive as to have small pair production cross sections at the LHC, while the lighter colored sparticles (*e.g.*, the 3rd generation squarks) are not too far separated from the EW sparticles, so only leading to shallow cascade decays before the final decay of the LOSP to the LSP KK-tower. In (b) all colored particles are too heavy to be substantially produced at the LHC $m_{\tilde{C}} \gtrsim 1.5$ TeV, while the copiously produced light EW sparticles have only shallow cascade decays before LOSP decay. In case (c) all sparticles apart from the LSP are moderately heavy and roughly comparable in mass, and the dominant production through the colored states undergoes only shallow cascades to the LOSP.

A common example where auto-concealment fails to weaken limits is when squark LOSPs of mass M are accompanied by a gluino of mass $\lesssim 2M$ [5]; even though direct production limits could allow squark LOSPs as light as $\sim$ 450GeV, we estimate gluino pair and associated production with decays to squarks sets much stronger limits $M_g \gtrsim (1.5 - 2)$ TeV $\gg 2 \times (450$ GeV$)$. On the other hand there are a variety of visible-sector sparticle spectra for which auto-concealment is efficient. For example Dirac gluinos can naturally have a mass $M_g \gg 2M$, yielding a sufficiently small production cross section for deep

cascades that auto-concealment is effective. To illustrate this point more generally we show in Figure 6.8 four examples of visible-sector spectra, one of which (d) fails the condition for efficient auto-concealment, while (a)-(c) satisfy the condition.

A number of search strategies using leptons to detect compressed SUSY spectra have been developed (since leptons typically have softer p_T cuts than jets) and will likely be useful in detecting shallow decays and discovering auto-concealment signatures. For this purpose ref. [124] developed a $ll + E_T^{\text{miss}}$ "super-razor" search, while ref. [125] proposed modifying cuts on existing lepton searches. Additionally, refs. [75, 126, 127] have suggested modifying monojet searches to include soft leptons as a way of picking out shallow electroweak decays with hard ISR.

6.4 Probing extra dimensions

While decays of the LOSP to a KK-tower of a bulk LSP can erode limits from standard promptly decaying super-partner searches, they also have the potential to open a new window for probing extra dimensions if SUSY particles are discovered. Decays of the LOSP are potentially observable over a wide range of lifetimes through prompt decays in the detector, in-flight decays (1 mm $\lesssim c\tau \lesssim$ 10 m), or decays of stopped particles (100 ns $\lesssim \tau \lesssim$ 1 yr). As shown in Figs. 6.2 ($d = 4$) and 6.9 ($d = 2, 6$), this corresponds to a range of fundamental scales that can far exceed the current reach[8] $M_* \gtrsim 5$ TeV [128,129] of traditional collider searches for KK graviton emission and contact operators[9] [131–137] and searches for the effects of Higgs mixing with bulk states [138]. This reach can also greatly exceed that of astrophysical searches[10] [139] and reaches values of M_* which are consistent with cosmological limits for a large range of reheat temperatures. This motivates studying strategies to distinguish decays to a bulk LSP from other scenarios, for instance two- and three-body decays to a single massive LSP, and further to distinguish different numbers of bulk dimensions and different bulk LSP candidates. A detailed study

[8] We assume the contact operators have $\mathcal{O}(1)$ coefficients suppressed by the scale M_*, corresponding to a weakly coupled UV completion of gravity.

[9] In addition to contact operators for SM states, operators contributing to sfermion production have also been studied in refs. [101, 130]. The lower dimension contact operators contributing to sfermion production described in ref. [101] can set stronger bounds for certain SUSY spectra, but can also be forbidden if some R-symmetries are preserved near the brane to energies below the fundamental scale.

[10] Astrophysical searches can also easily be avoided by modifying the low energy KK spectrum [102,137].

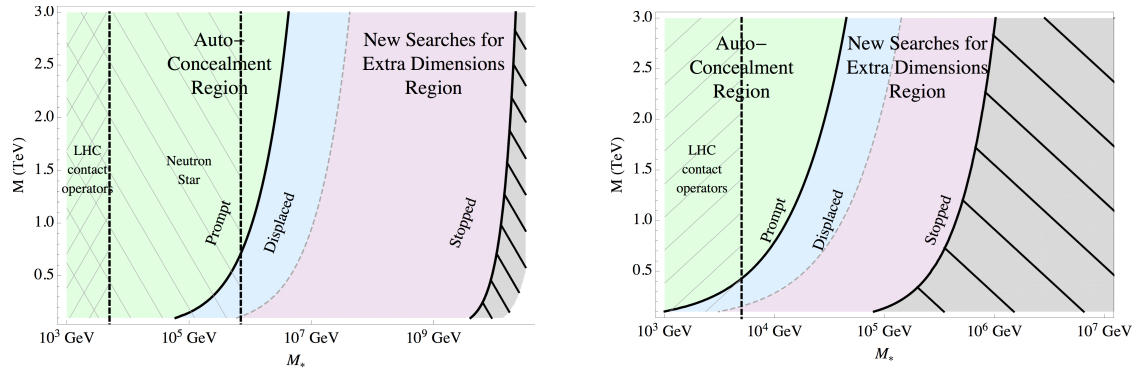

Figure 6.9: Companion to Figure 6.2 in the Introduction. Colored regions display the form of LOSP decay as a function of the LOSP mass, M, and the fundamental gravitational scale, M_*, for $d = 2$ (left panel) and $d = 6$ (right panel). In the gray hatched region to the far right, the splitting between KK states becomes large compared to the mass of the LOSP, $1/(ML) \gtrsim 0.1$ (all of the decays to the left of this region have lifetimes $\tau \lesssim 1$ yr). The hatched region to the far left shows the range of M_* excluded by current LHC contact operator searches for extra-dimensions. In the left panel we also show the region that can potentially be excluded by neutron star observations [139]. This exclusion, however, depends on the far IR part, $m_{KK} \lesssim 100$ MeV, of the KK spectrum of the graviton which is highly dependent on the assumption of perfectly flat extra dimensions. In the more general case of curved (but still unwarped) extra dimensions the neutron star limits no longer apply [102, 137].

of this possibility is beyond the scope of this work, but we describe briefly some of the relevant issues.

For prompt decays, a variety of LHC studies have demonstrated that features of m_{T2} and similar generalized distributions could determine the LSP mass in some spectra (for a review, see ref. [140]) using $100 - 1000$ BSM events after cuts (corresponding to $\sim 2.0 - 2.5$ TeV squarks and gluinos at the high luminosity LHC13). Such observations should be sensitive to the absence of a single mass for the LSP, and may be adaptable to identify a bulk LSP. The possibility of measuring the properties of a distribution of DM particles with different masses at the LHC has been studied in the particular case of three-body decays of a scalar color octet in Refs. [93,94]. For a light enough or electroweak dominated spectrum, measurements at a e^+e^- collider may be more promising [141–144].

If the LOSP decay is displaced in the detector or is long-lived on collider time scales then a great deal more information becomes accessible. The lifetime can be directly measured [145–147] and if the LOSP is charged or colored, its mass is directly observable through timing and ionization measurements [148–151]. Proposals have been made to study the kinematics of production and in-flight decays [151–155] as well as decays of charged/colored LOSPs stopped in the existing LHC detectors [145–147, 156–158] or a dedicated stopper-detector [159, 160]. Tracking of particles from in-flight decays with

large displacements or decays of LOSPs stopped in dense regions of detector material may be challenging. However, measurements of the kinematic features of in-flight and stopped decays have two primary advantages compared to techniques for prompt decays: i) backgrounds are very small and require fewer cuts which affect the kinematic distributions of the decay, ii) the rest frame and mass of the parent particle can be determined independently from the decay. Combining sufficiently precise measurements of the LOSP decay with mass and lifetime measurements could give strong evidence for the nature of the bulk LSP, the number of bulk dimensions, and the scale M_*!

6.5 Conclusions

We have presented a mechanism – auto-concealment in extra dimensions – which significantly weakens present search limits for some SUSY models. Auto-concealment applies to theories wherein the LOSP is a brane localized state while the LSP is a bulk state, producing a dense KK-tower of LSP excitations with increasing mass, m_n, that automatically brackets the LOSP mass without further tuning. The increased density of states at higher mass due to the bulk phase space factor $\sim m_n^{d-1}$ favors LOSP decays to the heaviest KK states, dynamically generating a quasi-compressed spectra, as discussed in Section 6.2.2 and shown in Figures 6.1 and 6.3. If the scale M_* is such that decays from the LOSP to the LSP are prompt, typical handles used in SUSY searches such as visible energy and $E_T^{\rm miss}$ are then dynamically suppressed as we discussed in Section 6.3. This reduces both $E_T^{\rm miss}$ and visible energy in SUSY events (unlike R-parity violation for example, which increases visible energy).

Auto-concealment can occur for a variety of visible-sector LOSP candidates. In particular, we find that LHC limits on right-handed slepton LOSPs evaporate in the case of prompt decays to a bulk modulino (see Figure 6.5), while the LHC limits on stop LOSPs weakens to $\sim 350 - 410$ GeV (see Figure 6.6). Present LHC limits on direct production of degenerate first and second generation squarks similarly drop to ~ 450 GeV (see Figure 6.7).

As discussed in Section 6.3 the mechanism is effective for a variety of visible-sector superpartner spectra, but not for all kinds. In particular, auto-concealment does not

significantly weaken limits driven by deep cascade decays to the LOSP. In addition, the mechanism is most effective when the bulk LSP propagates in > 2 large extra dimensions. Thus we find that a wide variety of visible-sector SUSY spectra and LOSP candidates lead to efficient auto-concealment. The auto-concealment mechanism also applies to more than just SUSY theories, broadly speaking to any theory wherein a discrete quantum number is shared between brane and bulk states and where the analog of the LSP is a bulk state.

Though discovery becomes more difficult for SUSY spectra without common deep cascade decays to the LOSP, it is not impossible. For the examples of stops and squarks of the first two generations we found searches designed to pick out compressed spectra [104] and monojets [109] remain effective, albeit at lower masses than traditional searches. For the case of sleptons, searches modified to keep lower-energy leptons in the signal region [75, 124–127] could be useful.

If superpartners are eventually discovered then observations of LOSP decays may prove to be a powerful window into extra dimensions. This is especially true if the scale M_* is large enough to lead to LOSP tracks in the detector, displaced vertices, or stopped out-of-time decays. As we discussed in Section 6.4 searches for such signals could probe the underlying gravitational mass scale up to $M_* \lesssim 10^9$ GeV!

Finally, we caution the reader that although we expect the limits obtained from validated CheckMATE analyses to provide a good estimate of the best current limits from the LHC experiments, there may be increased uncertainty because these searches are particularly sensitive to the tails of kinematic distributions and some of the most recent analysis updates are not presently available. We hope that this work motivates further study of these signals by the experimental collaborations.

Chapter 7: Monojet-like search for compressed sleptons at LHC14

This chapter is based on [77]*, work done in collaboration with Alan Barr.*

7.1 Introduction

In R-parity-conserving SUSY, in which the LSP is stable and invisible to the detector, methods commonly used to separate signal from backgrounds take advantage of the signal's large missing transverse momentum ($E_{\mathrm{T}}^{\mathrm{miss}}$), numerous jets from emitted partons, or highly energetic leptons [161]. However, this becomes more challenging in the case of electroweak (EW) SUSY production where cross sections are modest, and is especially difficult for compressed EW SUSY scenarios in which the mass difference between the produced sparticle and the LSP is small. Compressed SUSY scenarios result in less energetic final state radiation and less $E_{\mathrm{T}}^{\mathrm{miss}}$. Not only are such processes harder to pick out of backgrounds during an analysis, but they may not even pass trigger requirements for the LHC detectors. As a result, both CMS and ATLAS remain insensitive to compressed EW SUSY scenarios involving sleptons with $m_{\tilde{l}} - m_{\tilde{\chi}_1^0} \equiv \Delta m \lesssim 60$ GeV [72, 162].

One way to circumvent the challenges of compressed SUSY is to search for events with an energetic jet from ISR [50, 163–165]. In such events the sparticles will recoil against the ISR, increasing both the energy of visible decay products and $E_{\mathrm{T}}^{\mathrm{miss}}$. Such a strategy was used, for instance, by both ATLAS and CMS to search for top squarks with masses close to the LSP [118, 166]. However monojet searches are typically not designed to find EW sparticles and therefore those analyses veto events containing leptons in order to suppress unwanted backgrounds. Recently, several groups investigated the possibility of using a monojet, large $E_{\mathrm{T}}^{\mathrm{miss}}$, and soft leptons to pick out Higgsinos in a compressed spectrum [75, 127, 167]. Motivated by their strategy and the current absence of slepton limits from the LHC for compressed models, we investigate the possibility of performing a similar search to discover sleptons.

We rely on a high-p_{T} ISR jet to boost pair-produced sleptons, which promptly decay to

two neutralino LSPs and a same flavor opposite sign (SFOS) lepton pair ($pp \to \tilde{l}^+\tilde{l}^- j \to l^+l^-\tilde{\chi}_1^0\tilde{\chi}_1^0 j$). Like refs. [75,167] we search for a hard jet in the central rapidity region, large $E_{\mathrm{T}}^{\mathrm{miss}}$, and a soft SFOS lepton pair. However, unlike these studies we find it difficult to pick the signal out of the large backgrounds from leptonically decaying $t\bar{t}$ and $W^+W^- j$ using a veto on large m_{ll} alone; since signal leptons come from opposite legs of the decay chains their angular separation is not always small. Therefore, we use the leptons' 'stransverse' mass m_{T2} [69–71] to compress signal events into a narrow window and make the signal competitive with backgrounds.

However, even this is insufficient to pick out the signal if there is $\mathcal{O}(20\%)$ systematic uncertainty in the remaining backgrounds. Thus we use a different-flavor lepton pair control region (i.e. $e\mu$) to subtract away these backgrounds, similar to the CMS study in ref. [168]. With this we are able to investigate the potential exclusion reach of the LHC at $\sqrt{s} = 14$ TeV (LHC14) with 100 fb^{-1} if no excess in signal events are seen.

In addition to the normal compressed spectrum scenario, we also consider one of the auto-concealed (AC) SUSY scenarios that we investigated in ch. 6. As we discussed in that chapter, in this extra-dimensional SUSY model the slepton can decay to a nearly continuous Kaluza-Klein (KK) tower of neutral states, with a denser number of states closer to the parent mass $m_{\tilde{l}}$. The effect of the multiple states is phenomenologically similar at colliders to a compressed spectrum of near-degenerate particles. The result is that current LHC searches are not sensitive to direct slepton production in auto-concealed scenarios [6].[1]

7.2 Simulation

7.2.1 Tools

We investigated the prospect of discovering slepton production in near-degenerate slepton/LSP scenarios at the LHC using simulations of pp at $\sqrt{s} = 14$ TeV, assuming an

[1] During the preparation of the paper upon which this chapter was based, two searches were published which also attacked the compressed spectrum slepton problem. The first to do so [169] used vector boson fusion and missing transverse momentum to reduce SM backgrounds, but required around 3000 fb^{-1} of data. The second [76] proposed a solution remarkably similar to ours, also using a high-p_{T} monojet to help generate $E_{\mathrm{T}}^{\mathrm{miss}}$ and employing a moving m_{T2} window to distinguish signal from background. However some of the details of signal selection differ and in particular they do not address background systematics as we do in this chapter using the different flavor control region.

integrated luminosity of 100 fb^{-1}. To generate signal events and SM backgrounds we used MadGraph5_aMC@NLO [35] at tree level paired with Pythia 6 [40] for showering and hadronization. With the exception of taus, decays into leptons were done at the matrix element level (within MadGraph5) thus retaining spin correlations and increasing generator efficiency. Taus were decayed using Tauola [170] within Pythia.

For both the SUSY signal ($pp \to \tilde{l}^+\tilde{l}^- j$) and the dominant background ($pp \to t\bar{t}$) we used MLM matching with up to one additional jet (e.g. $pp \to \tilde{l}^+\tilde{l}^- jj$). For all backgrounds we used a generator level cut $R_{ll} \equiv \sqrt{\Delta\eta^2 + \Delta\phi^2} > 1.0$ between leptons and for all non-MLM matched processes we used a generator level cut on the leading jet $p_{\mathrm{T}} > 80$ GeV to increase efficiency (both of which were looser than the final analysis level cuts and were checked to not impact the results).

Events were then fed into an analysis built by the authors within the program CheckMATE [55, 65, 106], which includes an improved ATLAS detector simulation in Delphes [52]. In our analysis, jets and isolated leptons were assigned as follows:

- Jets were defined using the anti-k_{T} algorithm [66, 105] with a distance parameter 0.4, $|\eta| < 4.5$, and $p_{\mathrm{T}} > 20$ GeV. The assumed b-jet tagging efficiency is 80%. Further details on the b-tagger can be found in ref. [55].

- Isolated leptons were defined to mimic ref. [171]. Electrons (muons) were required to have $|\eta| < 2.47$, $p_{\mathrm{T}} > 7$ GeV and to not be within $R < 0.4$ of a reconstructed jet or $R < 0.1$ of another isolated lepton. The p_{T} sum of tracks above 0.4(1) GeV within $R < 0.3$ was required to be less than 16(12)% of the lepton p_{T}. Electrons had the additional requirement that the sum of energies within $R < 0.3$ was required to be less than 18% of the electron energy.

7.2.2 Slepton signal

We consider two cases: a classic compressed SUSY scenario and an auto-concealed SUSY scenario, described in further detail below. For the classic scenario we use a simplified model with a bino LSP and degenerate selectrons and smuons, both left or right-handed, with all other sparticles decoupled. The sleptons decay with a 100% branching ratio to a lepton of the same flavor plus the LSP. In this simplified model at leading-order slepton

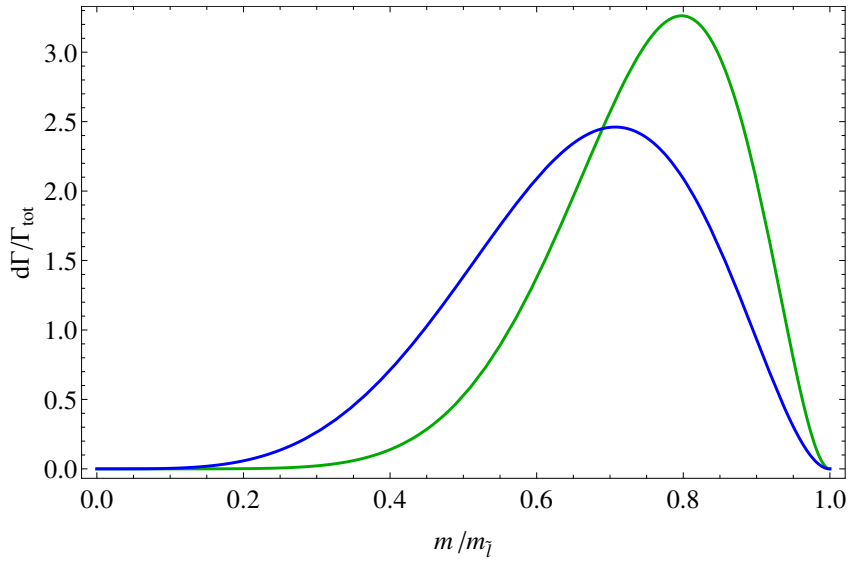

Figure 7.1: Differential decay rate for sleptons in an auto-concealed SUSY scenario. Here sleptons decay to the KK-tower of a bulk modulino LSP living in $d = 6$ (green) or $d = 3$ (blue) extra dimensions. The modulino mass is given as a ratio to the slepton mass $m_{\tilde{l}}$ on the horizontal axis. Since the number of KK-modes grows like $\sim m^{d-1}$, the $d = 6$ scenario results in a more compressed spectrum.

production and decay depends on the physical masses and the gauge couplings but not on soft SUSY parameters. Therefore, a spectrum generator was not used and we simply set the physical masses of the sparticles to their desired values in the MadGraph parameter card–the masses of the decoupled sparticles were set to 8 TeV.

In the auto-concealed SUSY scenario, sleptons are constrained to live on a brane in a $4+d$ dimensional bulk and can decay promptly to a lepton and a nearly continuous tower of bulk LSP KK-modes. As we saw in ch. 6, the branching ratio to modulino KK-modes with mass m is given by

$$\frac{d\Gamma}{\Gamma_{\text{tot}}} = \frac{1}{\Gamma_{\text{tot}}} \frac{\Omega_d}{(2\pi)^d} \frac{m_{\tilde{l}}^{d+3}}{8\pi M_*^{d+2}} \left(\frac{m}{m_{\tilde{l}}}\right)^{d+1} \left(1 - \frac{m^2}{m_{\tilde{l}}^2}\right)^2 \frac{dm}{m_{\tilde{l}}}, \tag{7.1}$$

where $m_{\tilde{l}}$ is the parent slepton mass, Ω_d is the surface area of a $(d-1)$-sphere, M_* is the fundamental gravitational scale, and Γ_{tot} is the slepton total decay width. Assuming the relevant scales are such that the slepton decay is prompt, this leads to a quasi-compressed spectrum as shown in fig. 7.1.

We approximate the continuous spectrum as in ch. 6 by introducing $N = 20$ new gauge neutral spin 1/2 states in Pythia. The masses of these states m_j fell into N evenly spaced bins from 0 to the slepton mass $m_{\tilde{l}}$. The mass m_j of the j^{th} state was given by the branching ratio-weighted average of masses in the j^{th} bin, and the branching fraction

to this state was determined by the integrated width over the bin.

7.2.3 Backgrounds

We estimate SM backgrounds in the 2 leptons + 1 jet + $E_{\mathrm{T}}^{\mathrm{miss}}$ channel by modeling the processes below. Tops and W's are decayed leptonically within MadGraph. In all processes except $(Z/\gamma^*)j$, leptonic decays include taus (which are then decayed in Tauola); $(Z/\gamma^*)j$ decaying to taus is included in the $\tau\tau j$ background. The backgrounds were:

1. $\tau^+\tau^- j$.
2. $t\bar{t}$.
3. $W^+W^- j$.
4. $l^+l^-(Z \to \nu\bar{\nu})j$ where the leptons are primarily from Z/γ^*. We will simply refer to this process as ZZj.
5. $l^+l^-W^{\pm}j$. Despite the fact that this process produces three visible leptons, its relatively large cross section combined with the possibility of losing a lepton makes this background more significant than ZZj. We will refer to this process as WZj.
6. tW with jets defined to come from light-flavor or b-quarks. To increase generation efficiency it is required that the jet p_{T} be greater than 80 GeV.
7. tq with jets defined to come from light-flavor or b-quarks and the same jet cut is imposed as in tW.
8. $l^+l^- j$ where the required missing transverse momentum comes primarily from mis-measured jets. We will refer to this process as Zj.

We also investigated the rare processes $t\bar{t}W$ and $t\bar{t}Z$ but found contributions from these processes were negligible.

At this point it is worth noting that these backgrounds are similar to what were considered in refs. [75, 167] which looked for Higgsino pair production plus an additional jet, although there are a few differences. First, like ref. [75], backgrounds from single-top and WZj processes, while sub-dominant, are non-negligible (refs. [167] did not consider

these backgrounds). Second, unlike ref. [75], we did not include a k-factor enhancement of the $t\bar{t}$ cross section for two reasons (ref. [75] included a NNLO+NNLL enhancement of 1.72). The first is that at least some of this enhancement will come from $t\bar{t}$ events with additional ISR which would then be preferentially rejected by our second-jet veto; thus it is questionable whether one should simply scale up the leading order cross section. The second reason is that we do not include NLO enhancements for any of our backgrounds or our signal, despite the fact that SUSY signal k-factors can be substantial.[2] Clearly, a better option would be to generate both signal and background events at NLO – an option we do not pursue for this first study.

Finally, although neither refs. [75] nor [167] considered the background from Zj plus mis-measured $E_{\mathrm{T}}^{\mathrm{miss}}$, we find that it provides a potentially substantial background; albeit one that is easily dealt with by requiring a large separation R between the leptons and a cut on reconstructed $m_{\tau\tau}^2$. Both studies used a $m_{\tau\tau}^2$ cut which would have likely dealt with the majority of this background, although their definitions of this reconstructed variable differ from each other as we discuss in sec. 7.3 below.

7.3 Beating the backgrounds

7.3.1 Key variables: $m_{\tau\tau}^2$ and $m_{\mathbf{T2}}$

The SM backgrounds discussed in sec. 7.2.3 are much greater than the SUSY signal we are seeking. To reduce the background we use a series of kinematic cuts, including cuts on the reconstructed $m_{\tau\tau}^2$ designed to separate the $\tau\tau j$ background, and on the 'stransverse mass' m_{T2}, with which we define our final signal windows.

To reconstruct the di-tau invariant mass squared $m_{\tau\tau}^2$ we follow ref. [75] and use the fact that taus recoiling against a 100 GeV jet are highly relativistic and their decay products will be nearly parallel. Thus in a fully leptonic di-tau decay we write the sum of the neutrinos' transverse momentums as

$$\vec{p}_{\mathrm{T}}^{\,\mathrm{miss}} = \xi_1 \vec{p}_{\mathrm{T}}^{\,l_1} + \xi_2 \vec{p}_{\mathrm{T}}^{\,l_2}, \tag{7.2}$$

where $\vec{p}_{\mathrm{T}}^{\,\mathrm{miss}}$ is the missing transverse momentum vector and ξ_n is a scale factor relating

[2] For instance, ref. [172] found a k-factor of 2.3 for neutralino pair + jet production.

the transverse momentums of the n^{th} tau daughter neutrinos to the transverse momentum of the daughter electron or muon $\vec{p}_{\text{T}}^{\,l_n}$. Using this set of two equations we solve for the unknowns ξ_1 and ξ_2, with which we find the four-momenta of the taus: $p_{\tau_n} = (1+\xi_n)p_{l_n}$. Then the di-tau invariant mass squared is

$$m_{\tau\tau}^2 = 2(1+\xi_1)(1+\xi_2)p_{l_1} \cdot p_{l_2}. \tag{7.3}$$

This definition differs from ref. [167] in that it allows for a negative invariant mass squared if $\xi < -1$ for a single ξ. From eq. (7.2) we see this can occur for a missing transverse momentum vector nearly opposite to a lepton's $\vec{p}_{\text{T}}$ and $\text{p}_{\text{T}}^{\text{miss}} > \text{p}_{\text{T}}^{l}$. For example, this may happen in WWj when a neutrino and a lepton (possibly coming from different W decays) are nearly back-to-back. Though having a negative invariant mass squared is clearly unphysical–which motivates ref. [167] to scale energy by $|\xi_i|$ rather than ξ_i–we do not concern ourselves with this fact since the approximation $\vec{p}_{\text{T}}^{\,\nu_1} \approx \xi_1 \vec{p}_{\text{T}}^{\,l_1}$ is not always valid and in practice we find this definition slightly more effective at separating signal from background.

To determine the final signal regions we use the kinematic variable m_{T2}, defined as

$$m_{\text{T2}}(p_{\text{T}}^{l_1}, p_{\text{T}}^{l_2}; m_{\tilde{\chi}_1^0}) = \min_{q_{\text{T}}} \Big[\max\Big(m_{\text{T}}(p_{\text{T}}^{l_1}, q_{\text{T}}; m_{\tilde{\chi}_1^0}), m_{\text{T}}(p_{\text{T}}^{l_2}, p_{\text{T}}^{\text{miss}} - q_{\text{T}}; m_{\tilde{\chi}_1^0})\Big)\Big] \tag{7.4}$$

where $m_{\tilde{\chi}_1^0}$ is the mass of the neutral particle which produces $E_{\text{T}}^{\text{miss}}$ and

$$m_{\text{T}}(p_{\text{T}}^{l}, q_{\text{T}}; m_{\tilde{\chi}_1^0}) = \sqrt{m_l^2 + m_{\tilde{\chi}_1^0}^2 + 2\left(E_{\text{T}}^{l} E_{\text{T}}^{q} - \vec{p}_{\text{T}} \cdot \vec{q}_{\text{T}}\right)}. \tag{7.5}$$

In a two-body semi-invisible decay, the stransverse mass variable m_{T2} provides an event-by-event bound in the space of masses of the parent and the invisible daughter particle. In practice, it is usually employed as a function which takes as an input the invisible particle's proposed mass, and returns the maximal lower bound on the mass of the parent particle. For example, in a pair-decay of sleptons of mass $m_{\tilde{l}}$ to leptons and LSPs of mass $m_{\tilde{\chi}_1^0}$ the function $m_{\text{T2}}(m_{\tilde{\chi}_1^0})$ is always smaller than $m_{\tilde{l}}$ when the correct LSP mass is input. Since the same is not necessarily true for background processes, we can preferentially select the signal by imposing a requirement that $m_{\text{T2}}(m_{\tilde{\chi}_1^0}) < m_{\tilde{l}}$ for our trial LSP and slepton masses. In this way, we can scan the $m_{\tilde{l}}$ – $m_{\tilde{\chi}_1^0}$ plane.

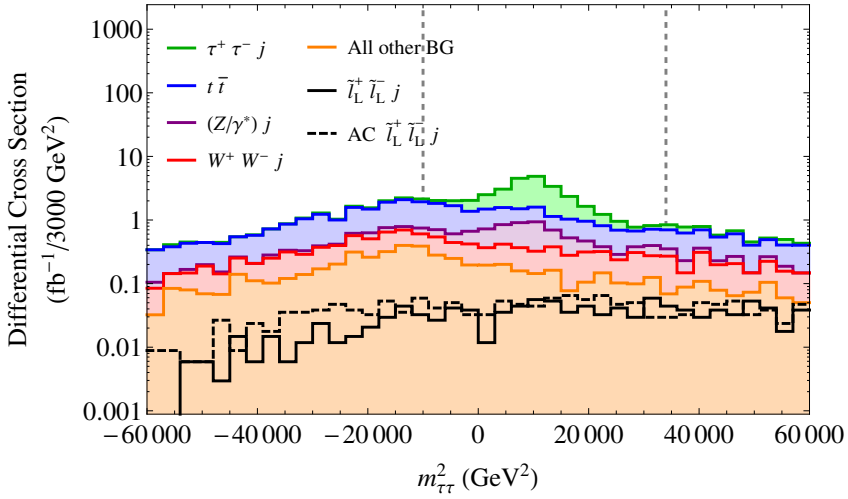

Figure 7.2: Reconstructed $m^2_{\tau\tau}$ distributions after cuts 1-4 for backgrounds (histograms stacked) and two different signal scenarios: degenerate left-handed selectrons and smuons with mass $m_{\tilde{l}_L} = 104$ GeV each decaying to a lepton plus either a 96 GeV neutralino LSP (solid black) or an auto-concealed modulino KK-tower (dashed black). The gray area indicates the region removed in step 5 of the analysis. This cut significantly reduces the $\tau\tau j$ and Zj backgrounds.

7.3.2 Analysis cuts

Using the variables $m^2_{\tau\tau}$ and m_{T2} as defined above we use the following analysis cuts to enhance the slepton signal relative to the much larger SM backgrounds which also produce 2 leptons + 1 jet + $E_{\mathrm{T}}^{\mathrm{miss}}$:

1. Veto events with a tagged b-jet to reduce backgrounds involving top quarks.

2. Require one hard central jet with $|\eta| < 2.5$ and $p_{\mathrm{T}} > 100$ GeV. Veto events with a second jet with $|\eta| < 4.5$ and $p_{\mathrm{T}} > 40$ GeV.

3. Require $E_{\mathrm{T}}^{\mathrm{miss}}$ of at least 100 GeV. Also require $|\Delta\phi| > 1.5$ between the hard jet and $\vec{p}_{\mathrm{T}}^{\,miss}$. This helps to reduce backgrounds from Zj with $E_{\mathrm{T}}^{\mathrm{miss}}$ coming from mis-measured jet energy.

4. Require two SFOS isolated leptons with $R > 1.3$ between them. The large R requirement significantly reduces backgrounds involving Z/γ^* (in particular the otherwise large WZj background in which one lepton escapes detection) and is more effective than a soft invariant mass veto since this would also veto signal leptons which tend to be soft.

5. Veto events with a reconstructed $m^2_{\tau\tau}$ between $-10,000\ \mathrm{GeV}^2 < m^2_{\tau\tau} < 34,000\ \mathrm{GeV}^2$. This is very effective at reducing the $\tau\tau j$ background and also helps pare down Zj.

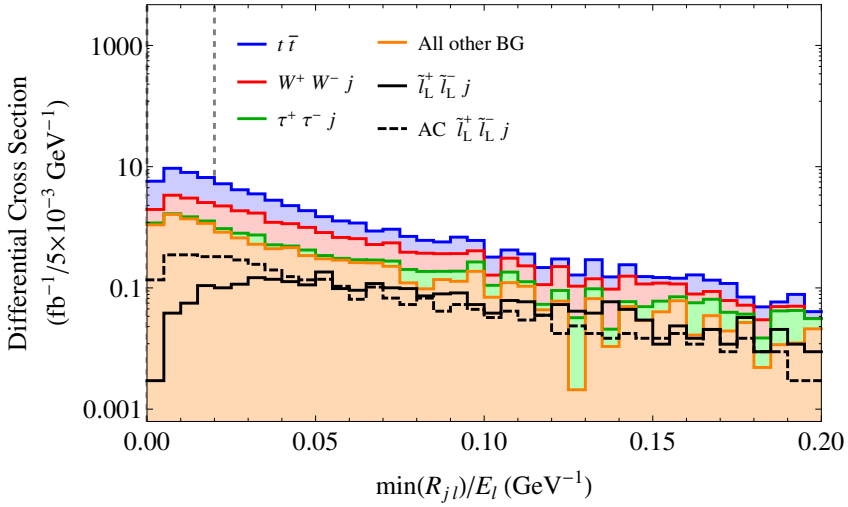

Figure 7.3: min$(R_{jl})/E_l$ distributions after cuts 1-5 for backgrounds (histograms stacked) and two different signal scenarios: degenerate left-handed selectrons and smuons with mass $m_{\tilde{l}_L} =$ 104 GeV each decaying to a lepton plus either a 96 GeV neutralino LSP (solid black) or an auto-concealed modulino KK-tower (dashed black). The gray area indicates the region removed in step 6 of the analysis.

The $m^2_{\tau\tau}$ distributions of backgrounds and representative signal models are shown in fig. 7.2.

6. Require min$(R_{jl})/E_l > 0.02$ where min(R_{jl}) gives the minimum distance R between the hard jet and the leptons and E_l is the energy of the lepton closest to the jet. Cutting small R_{jl} helps to isolate tops since their b-jets are closer to their leptons than the decay products from signal sleptons, which recoil against the hard ISR jet. This is more effective than an invariant mass cut on min(m_{jl}) since leptons from compressed spectra decays are softer than leptons from top/W decays and this partially compensates for the closer distance between the jet and lepton. We take advantage of this fact by dividing R_{jl} by the lepton energy, further differentiating tops from signal while also cutting into the WWj background. The min$(R_{jl})/E_l$ distributions of backgrounds and representative signal models are shown in fig. 7.3.

7. Require the two leptons' invariant mass $m_{ll} < 70$ GeV. This cuts away hard leptons from top and W decays. While cutting even lower on m_{ll} can slightly extend the mass reach of the search, this comes at the expense of weakening the reach for larger Δm, since sleptons further separated from the LSP will have harder leptons. The m_{ll} distributions of backgrounds and representative signal models are shown in fig. 7.4.

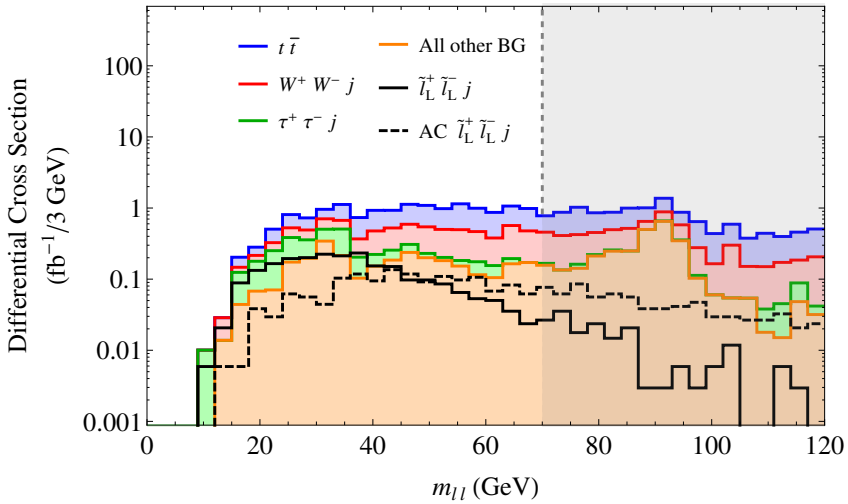

Figure 7.4: m_{ll} distributions after cuts 1-6 for backgrounds (histograms stacked) and two different signal scenarios: degenerate left-handed selectrons and smuons with mass $m_{\tilde{l}_L} = 104$ GeV each decaying to a lepton plus either a 96 GeV neutralino LSP (solid black) or an auto-concealed modulino KK-tower (dashed black). The gray area indicates the region removed in step 7 of the analysis.

8. The final signal regions are defined using the stransverse mass as a function of the trial LSP mass $m_{\mathrm{T2}}(\tilde{\chi}_1^0)$ as discussed in Sec. 7.3.1, requiring $m_{\mathrm{T2}}(\tilde{\chi}_1^0)$ to be less than the trial $m_{\tilde{l}}$. In this way, we scan the $m_{\tilde{l}}$ – $m_{\tilde{\chi}_1^0}$ plane. To evaluate the auto-concealed model, where multiple states play the role of LSP, we use three bins to evaluate the signal– $m_{\mathrm{T2}}(m_{\tilde{l}} - 24\ \mathrm{GeV})$, $m_{\mathrm{T2}}(m_{\tilde{l}} - 16\ \mathrm{GeV})$, $m_{\mathrm{T2}}(m_{\tilde{l}} - 8\ \mathrm{GeV}) < m_{\tilde{l}}$ –and choose the one with the largest signal significance. The m_{T2} distribution for $m_{\tilde{\chi}_1^0} = 96$ GeV is shown in fig. 7.5.

	$\tau\tau$	$t\bar{t}$	WWj	ZZj	WZj	tW	tq	Zj	$l_L^+l_L^-j$
MG cuts	3769013	5077488	74580	3478	21820	158000	2497581	4955268	10590
1) b-veto	3167916	902842	61618	2883	18187	38262	795944	4240902	9302
2) hard jet	417284	56546	19345	866	4548	8296	87754	1342713	1845
3) $E_{\mathrm{T}}^{\mathrm{miss}}$	130135	25823	9855	478	1723	2784	46904	46654	1477
4) SFOS ll	1751	4423	1726	186	289	553	169	570	327
5) $m_{\tau\tau}^2$	230	3511	1438	144	229	443	141	209	269
6) R_{jl_1}/E_l	196	1613	905	75	141	171	137	115	248
7) m_{ll}	174	713	397	8	25	85	113	60	229
8) m_{T2}	94	256	164	3	8	32	67	30	227

Table 7.1: Background and signal counts for pp collisions with $\sqrt{s} = 14$ TeV and an integrated luminosity of 100 fb^{-1}. This table shows the number of events which pass the MadGraph (MG) generator-level cuts described in sec. 7.2.3 and analysis cuts 1-8. The m_{T2} cut in this instance requires that $m_{\mathrm{T2}}(96\ \mathrm{GeV}) < 104$ GeV. This corresponds to the signal model $(m_{\tilde{l}}, m_{\tilde{\chi}_1^0}) = (104, 96)$ GeV. The far right column shows the cutflow for the matching model with degenerate left-handed selectrons and smuons with mass $m_{\tilde{l}_L} = 104$ GeV decaying to a SFOS lepton pair plus two neutralinos of mass 96 GeV.

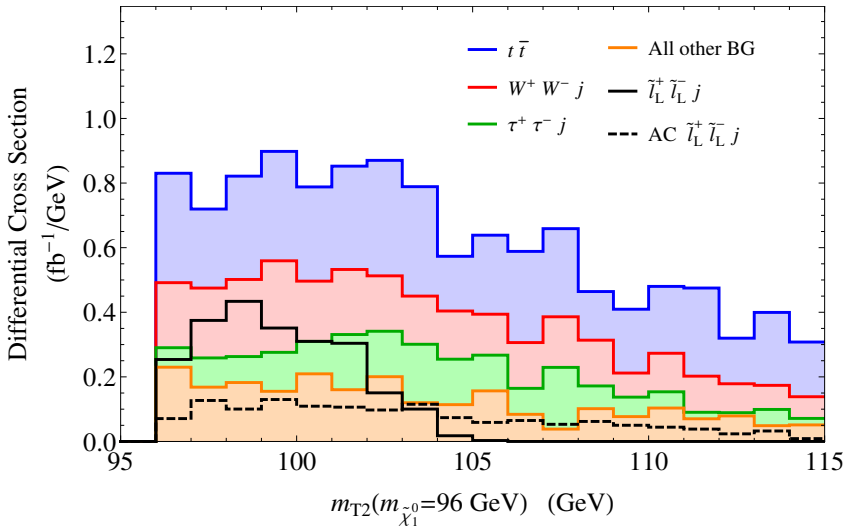

Figure 7.5: $m_{T2}(m_{\tilde{\chi}_1^0})$ distribution after cuts 1-7 for backgrounds (histograms stacked) and signal using $m_{\tilde{\chi}_1^0} = 96$ GeV for both. Note that the vertical axis is not log-scaled. Two different signal scenarios are shown: degenerate left-handed selectrons and smuons with mass $m_{\tilde{l}_L} = 104$ GeV each decaying to a lepton plus either a 96 GeV neutralino LSP (solid black) or an auto-concealed modulino KK-tower (dashed black). When scanning the $(m_{\tilde{l}}, m_{\tilde{\chi}_1^0})$ plane the expected signal and backgrounds at $(m_{\tilde{l}}, m_{\tilde{\chi}_1^0}) = (104, 96)$ GeV are evaluated in step 8 using $m_{T2}(96\text{ GeV}) < 104$ GeV. For the auto-concealed model, where multiple states play the role of the LSP, we use three bins to evaluate the signal – $m_{T2}(80\text{ GeV})$, $m_{T2}(88\text{ GeV})$, $m_{T2}(96\text{ GeV}) < 104$ GeV – and choose the one with the largest signal significance.

Cutflows for the background and representative signal samples are show in table 7.1. Unfortunately, even after cuts 1-8 a significant number of background events from $t\bar{t}$, WWj, and $\tau\tau j$ remain, as can be seen in fig. 7.5. Since we will evaluate the signal significance as $s = S/\sigma_B$ where S is the expected number of signal events and σ_B is the total background uncertainty, even a moderate σ_B ($\mathcal{O}(20\%)$) will overwhelm the signal. If we use

$$\sigma_B = \sqrt{B + \sigma_{B\,\text{sys}}^2} \tag{7.6}$$

where $\sigma_{B\,\text{sys}}$ is the systematic uncertainty of the background, and B is the expected number of background events,[3] then it is clearly necessary to have good control over background systematics to obtain a detectable signal significance. We attack this problem in the next section.

[3]Here and in what follows we will use the Gaussian limit to approximate Poisson statistical errors as $\sigma_{B\,\text{stat}} = \sqrt{B}$.

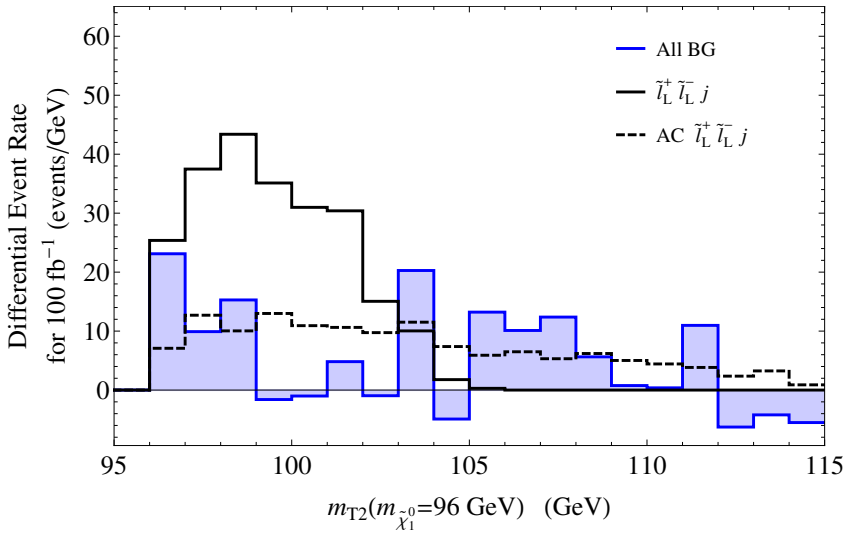

Figure 7.6: Different flavor subtracted $m_{\mathrm{T2}}(p_{\mathrm{T}}^{l_1}, p_{\mathrm{T}}^{l_2}; m_{\tilde{\chi}_1^0})$ distribution after cuts 1-7 for backgrounds and signal using $m_{\tilde{\chi}_1^0} = 96$ GeV for both. Two different signal scenarios are shown: degenerate left-handed selectrons and smuons with mass $m_{\tilde{l}_L} = 104$ GeV each decaying to a lepton plus either a 96 GeV neutralino LSP (solid black) or an auto-concealed modulino KK-tower (dashed black). Backgrounds are subtracted as described in Sec. 7.3.3. The results are shown in this figure, not including the m_{T2} cut described in step 8.

7.3.3 Controlling background systematics: SF-DF

To reduce background systematics, we estimate the size of the expected background using a different flavor (DF) di-lepton control region containing $e + \mu$ events which pass the equivalent of cuts 1-8. Since sleptons are produced in same flavor (SF) opposite sign pairs only, while the dominant backgrounds produce different flavor lepton pairs as often as same flavor pairs, the DF control sample can be used to estimate–and hence subtract–the majority of the remaining backgrounds.

To do so we use a background subtraction scheme similar to that used in a CMS BSM search [168]. Inside each signal region, we multiply the number of events in the DF control region B_{DF} by a normalization factor n to account for the different efficiencies in detecting muons and electrons. We then subtract the number of normalized control region events from the number of background signal region events B_{SF} to obtain the final background count: $B = B_{\mathrm{SF}} - n\, B_{\mathrm{DF}}$. The residual systematic uncertainty in the corresponding number of background events should now come from uncertainty in n, which was determined to within 4% in the CMS study. We therefore take this as an estimate of our systematic uncertainty. This comes at the cost of inflating the statistical uncertainty since the total background uncertainty is now

$$\begin{aligned}\sigma_B &= \sqrt{\left(\frac{\partial B}{\partial B_{\rm SF}}\right)^2 \sigma^2_{\rm SF\,stat} + \left(\frac{\partial B}{\partial B_{\rm DF}}\right)^2 \sigma^2_{\rm DF\,stat} + \left(\frac{\partial B}{\partial n}\right)^2 \sigma^2_n} \\ &= \sqrt{B_{\rm SF} + n^2 B_{\rm DF} + B^2_{\rm DF}\sigma^2_n} \end{aligned} \tag{7.7}$$

where $\sigma_{\rm SF\,stat}$, and $\sigma_{\rm DF\,stat}$ are the statistical uncertainties in $B_{\rm SF}$ and $B_{\rm DF}$ respectively and $\sigma_n = 0.04n$ is the total uncertainty in n assumed in this study. Despite the increased statistical error in this expression as compared to its non-background subtracted counterpart eq. (7.6), the lower systematic error more than compensates for this and reduces the total uncertainty. For example, if we estimate $\sigma_{B\,\rm sys} = 0.2B_{\rm SF}$ in (7.6), then for the typical backgrounds present in our study the background subtracted expression for σ_B in eq. (7.7) reduces the total error by more than 60%.

To summarize, we define our signal significance as $s = S/\sigma_B$ with $B = B_{\rm SF} - nB_{\rm DF}$ and σ_B defined in eq. (7.7). An example of the signal as compared to the remaining background is shown in fig. 7.6.

7.4 LHC14 reach with 100 fb^{-1}

To evaluate the potential 95% confidence level (CL) exclusion reach of this analysis we demand a signal significance of 1.96. As fig. 7.7 shows, LHC14 with 100 fb^{-1} of data will be sensitive to sleptons with 3 GeV $< \Delta m <$ 24 GeV up to nearly $m_{\tilde{l}_L} \simeq 150$ GeV. As can be seen from the figure, this analysis will allow the LHC to explore beyond $m_{\tilde{l}_L} > 100$ GeV in the compressed region for the first time, though it will not completely close the gap between the compressed region and current ATLAS limits ($\Delta m \gtrsim 60$ GeV). On the other hand, the production cross sections for right-handed sleptons are such that this analysis will only just reach $m_{\tilde{l}_R} = 100$ GeV with 100 fb^{-1}, and therefore will not improve on LEPII limits; at least until the LHC has more data.

The analysis is constrained to work in the region $\Delta m \lesssim 24$ GeV because it relies on $m_{\rm T2}$ to concentrate the signal events into a narrow mass range. The closer $m_{\tilde{l}}$ is to $m_{\tilde{\chi}^0_1}$ the more concentrated the signal events become and the better chance we have of beating the backgrounds. However this only works down to about $\Delta m \simeq 3$ GeV because below this fewer leptons have enough energy to be tagged by the detector–even considering the

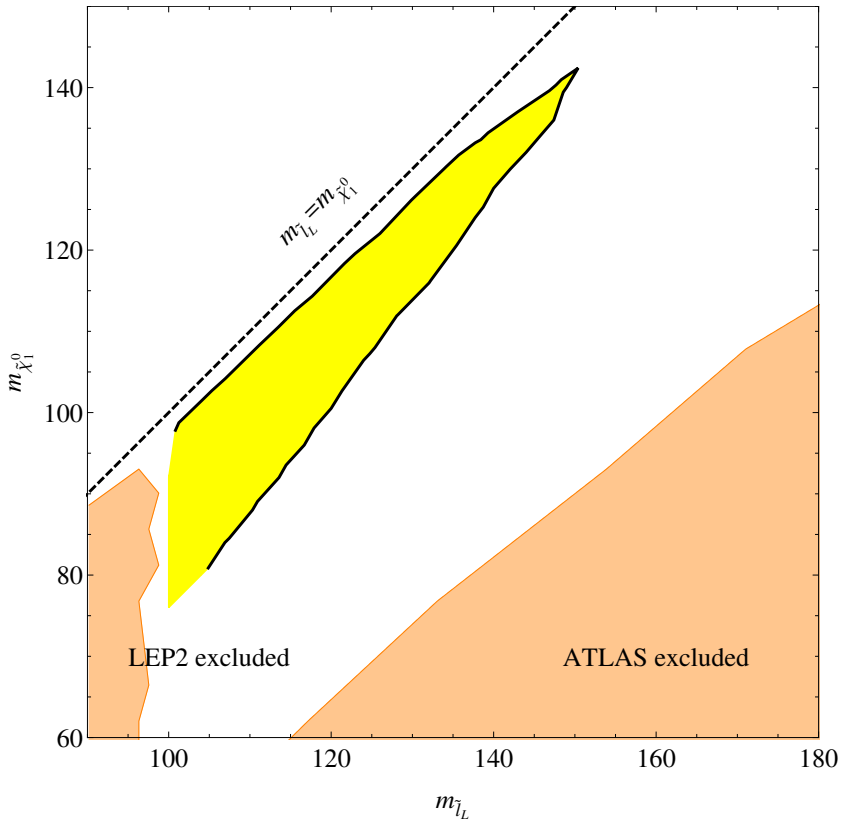

Figure 7.7: Potential 95% CL exclusion reach at LHC14 with 100 fb^{-1} for degenerate left-handed smuons and selectrons. Yellow area indicates the region excluded by this analysis, while orange areas indicate regions already excluded by LEPII [173] and ATLAS [72].

fact that their parent sleptons are boosted from jet recoil.

In the case of AC SUSY, detection becomes more challenging. Fig. 7.8 shows the expected LHC14 100 fb^{-1} reach for excluding the production cross section of AC sleptons decaying to the KK-tower of a modulino LSP which lives in either $d = 6$ or 3 extra dimensions. The analysis will be able to exclude left-handed AC sleptons in $d = 6$ (3) up to 110 (100) GeV. Again it will not be sensitive to right-handed AC sleptons except where LEPII should have already been able to discover them.

Clearly, AC sleptons present a bigger detection challenge than a normal compressed spectrum. The reason for this is twofold. First, the largest branching ratios are to particles with masses $\sim 80\%$ and $\sim 70\%$ of the slepton mass for $d = 6$ and 3 respectively (see fig. 7.1). For 100 GeV left-handed sleptons this puts Δm just inside the reach of the analysis in the first case, and just outside in the second. As $m_{\tilde{l}}$ increases, the effective Δm only gets larger taking the model outside of the detection range. The second challenge is that the differential branching ratio distributions are quite broad. Therefore m_{T2} is not able to concentrate signal events into a well defined window starting at the LSP mass.

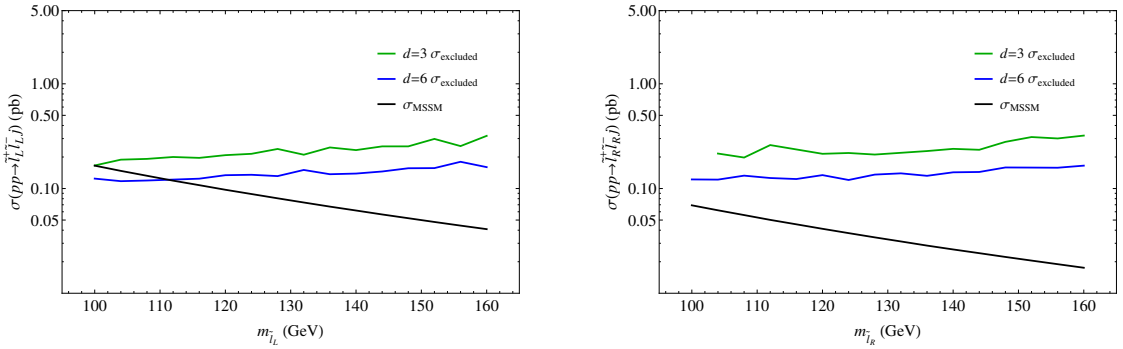

Figure 7.8: Potential 95% CL exclusion reach at LHC14 with 100 fb^{-1} for the production cross section of auto-concealed sleptons decaying to a modulino KK-tower in $d = 3$ (green) or $d = 6$ (blue) extra dimensions for left-handed (left plot) or right-handed (right plot) sleptons. The black line shows the tree level production cross section for $pp \to \tilde{l}^+\tilde{l}^- j$ indicating that, with this amount of data, the LHC should be sensitive to left-handed sleptons for $d = 6$ (3) up to 110 (100) GeV. The production cross section of right-handed sleptons is smaller, requiring more data for sensitivity.

Despite these challenges, it is encouraging to see that for the auto-concealed scenarios the sensitivity of the analysis improves as the number d of extra dimensions increases, in contrast to what was observed in ref. [6], where higher d cases were more difficult. Higher integrated luminosities and/or reduced systematic uncertainties would further increase sensitivity.

7.5 Conclusions

We have presented an analysis built to detect sleptons with small $m_{\tilde{l}} - m_{\tilde{\chi}_1^0}$. We use the $pp \to \tilde{l}^+\tilde{l}^- j \to l^+l^-\tilde{\chi}_1^0\tilde{\chi}_1^0 j$ channel, where the neutral, collider stable $\tilde{\chi}_1^0$s are inferred from $E_{\mathrm{T}}^{\mathrm{miss}}$ and the jet (which is required to have $p_{\mathrm{T}} > 100$ GeV) comes from ISR. The jet requirement distinguishes this search from 'classic' slepton analyses but is similar to monojet searches, and recent Higgsino search proposals [75, 167]. The jet requirement selects events with ISR, and thus boosted sleptons. The resulting events tend to have large $E_{\mathrm{T}}^{\mathrm{miss}}$ and daughter leptons with p_{T} above the detection threshold.

After a series of cuts to remove background events a significant number of unwanted backgrounds remain, most notably from the leptonic decays of $t\bar{t}$ and $W^+W^- j$. Two final steps help to distinguish the signal from these processes. First, we take advantage of the 'stransverse' mass m_{T2} to concentrate signal events into a window between the trial $m_{\tilde{l}}$ and $m_{\tilde{\chi}_1^0}$. Finally, we use the fact that signal leptons come in SFOS pairs while the major remaining backgrounds produce different flavor pairs as often as same flavor pairs.

We use the different flavor pairs to 'subtract away' the majority of the remaining background. Though this introduces additional statistical error, this data-driven technique significantly reduces the systematic uncertainty and makes the signal detectable.

The analysis presented in this chapter should allow LHC14 with 100 fb^{-1} to search for degenerate left-handed selectrons and smuons in the compressed region 3 GeV $< m_{\tilde{l}_L} - m_{\tilde{\chi}_1^0} < 24$ GeV for $m_{\tilde{l}_L} \lesssim 150$ GeV. This area is beyond LEPII limits and currently unexplored by the LHC. In addition, it should be sensitive to the challenging case of auto-concealed left-handed sleptons decaying to the KK-tower of a modulino LSP which lives in $d = 6$ extra dimensions up to $m_{\tilde{l}_L} \lesssim 110$ GeV. In both the compressed spectrum and auto-concealed scenarios this analysis will need more data to improve on LEPII limits for right-handed sleptons.

Chapter 8: Benchmark models for Maximally Natural Supersymmetry

This chapter is based on [174]*, work done in collaboration with Kiel Howe.*

As we discussed in ch. 4, collider searches for BSM physics necessarily rely on Monte Carlo programs to describe signal events and SM backgrounds. Such programs, in turn, typically rely on the Mathematica packages FeynRules [30] or SARAH [31] to efficiently convert a new BSM model Lagrangian into the Feynman rules necessary for the Monte Carlo to run. In this chapter we describe the implementation of MNSUSY in FeynRules, intended for eventual public release, and flesh out the model details. We also present benchmark models intended for future phenomenology studies and provide a short users manual for the model file.

MNSUSY is a five dimensional $\mathcal{N} = 1$ SUSY model (corresponding to $\mathcal{N} = 2$ four dimensional SUSY) compactified on a $S^1/\mathbb{Z}_2 \times \mathbb{Z}_2'$ orbifold using the Scherk-Schwarz Symmetry Breaking (SSSB) Mechanism. The compactification length scale $1/l$ is on the order of several TeV and the theory is not well approximated by 4D softly-broken $\mathcal{N} = 1$ SUSY. Higgsinos and gauginos are Dirac fermions. Higgsinos, gauginos, and first and second generation sfermions obtain masses at $m_l \equiv \pi/2l$, while third generation sfermion masses can be substantially below this since the latter particles will be brane localized. Soft SUSY breaking terms contain no large logarithms due to the super-softness of SSSB mechanism, protecting the Electroweak scale [175–177]. Only H_u obtains a Vacuum Expectation Value (VEV) and is automatically SM-like. Unlike the MSSM and its cousins, there is no μ term and Higgsinos need not be light to ensure low fine-tuning. Fine tuning of the model is $\mathcal{O}(50\%)$ [7].

We will begin our discussion of MNSUSY by briefly addressing conventions, before moving on to derive the 4D Lagrangian as well as describe the mass matrices necessary to implement the model in FeynRules. A description of benchmark models will follow this.

8.0.1 Conventions

We adopt the "mostly minus" metric of FeynRules $(+1,-1,-1,-1,...)$. Capitalized space-time indices M,N run over 0, 1, 2, 3, 4, while lowercase greek letters μ,ν run over 0, 1, 2, 3. We will often separate out the compactified fifth dimension as $\{x^\mu, y\}$. Consistent with the discussion in ch. 3, our basis for Dirac matrices is:

$$\gamma^M = \{\gamma^\mu, \gamma^y\} = \left\{ \begin{pmatrix} 0 & \sigma^\mu \\ \overline{\sigma}^\mu & 0 \end{pmatrix}, \begin{pmatrix} i & 0 \\ 0 & -i \end{pmatrix} \right\} \tag{8.1}$$

with $\sigma^\mu = (\mathbb{1}, \vec{\sigma})$ and $\overline{\sigma}^\mu = (\mathbb{1}, -\vec{\sigma})$. Note that in this basis, $i\gamma^y = \gamma_* \equiv i\gamma^0\gamma^1\gamma^2\gamma^3$ where γ_* is usually referred to as γ^5 in physics literature and is related to the projection matrices $P_R = (1+\gamma_*)/2$ and $P_L = (1-\gamma_*)/2$.

When considering Weyl spinor indices we will use the conventions of [10] and when we need to explicitly write the antisymmetric tensor ϵ^{ij} we use $\epsilon^{12} = -\epsilon^{21} = \epsilon_{21} = \epsilon_{12} = 1$. $\mathcal{N}=1$ superfields are written (using the FeynRules convention) as

$$V^a(V_\mu, \lambda) = -\theta^\dagger\overline{\sigma}^\mu\theta V_\mu^a - i\theta^{\dagger 2}\theta\lambda^a + i\theta^2\theta^\dagger\lambda^{a\dagger} + \frac{1}{2}\theta^2\theta^{\dagger 2}D^a, \tag{8.2}$$

$$\Phi(\varphi,\psi) = \varphi + \sqrt{2}\theta\psi - \theta^2 F + i\theta^\dagger\overline{\sigma}^\mu\theta\partial_\mu\varphi - \frac{i}{\sqrt{2}}\theta^2\theta^\dagger\overline{\sigma}^\mu\partial_\mu\psi - \frac{1}{4}\theta^2\theta^{\dagger 2}\partial_\mu\partial^\mu\varphi. \tag{8.3}$$

Non-abelian gauge fields appearing without a superscript are $V_M = gV_M^a T^a$ and similarly for their $\mathcal{N}=2$ superpartners and auxiliary fields. The gauge covariant derivatives for fields in the fundamental representation are $D_M\psi = \partial_M\psi - iV_M\psi$ and in the adjoint representation are $D_M\lambda = \partial_M\lambda - i[V_M,\lambda]$ where the implicit T^a is in the fundamental representation in both cases. When considering the trace of generators in the fundamental representation, we use the typical physics convention $\mathrm{Tr}[T_F^a T_F^a] = T_F\delta^{ab} = \delta^{ab}/2$.

Note that our conventions, while consistent with FeynRules, differ by factors of two and minus signs with several other popular works [10, 95, 97, 98].

8.1 Field content

8.1.1 5D SUSY field content

In five dimensions the smallest fermion is a Dirac spinor, equivalent to two 4D Weyl spinors $\psi_{i\alpha}$ labeled by $i = 1, 2$. We have explicitly written the spinor index α to emphasize that i is not a Weyl spinor index.

In 5D it is often convenient to write the Dirac spinor as a symplectic-Majorana spinor [26, 95, 98] carrying a $SU(2)$ index i related to the 4D Weyl spinor label and defined as

$$\Psi_i = \begin{pmatrix} \psi_{i\alpha} \\ \epsilon^{ij}\psi_j^{\dagger\dot{\alpha}} \end{pmatrix}. \tag{8.4}$$

The height of the indices $i,\ j$ only matters in ϵ^{ij}, for which we are consistent with our conventions in sec. 8.0.1; for fields we simply write them lowered. A very explicit example may be helpful in understanding symplectic-Majorana spinors – using 8.1 one can write the kinetic term for a 5D fermion as

$$\begin{aligned} \frac{i}{2}\overline{\Psi}_i\gamma^M D_M\Psi_i =& \frac{i}{2}\begin{pmatrix} \epsilon^{ij}\psi_j^{\alpha} & \psi^{\dagger}_{i\dot{\alpha}} \end{pmatrix}\begin{pmatrix} -i\delta^{\beta}_{\alpha}\ D_y & \sigma^{\mu}_{\alpha\dot{\beta}}\ D_\mu \\ \overline{\sigma}^{\mu\dot{\alpha}\beta}\ D_\mu & i\delta^{\dot{\alpha}}_{\dot{\beta}}\ D_y \end{pmatrix}\begin{pmatrix} \psi_{i\beta} \\ \epsilon^{ik}\psi_k^{\dagger\dot{\beta}} \end{pmatrix} \\ =& i\psi_i^{\dagger}\overline{\sigma}^{\mu}D_\mu\psi_i - \frac{1}{2}\epsilon^{ij}(\psi_i D_y\psi_j + \psi_i^{\dagger}D_y\psi_j^{\dagger}) \end{aligned} \tag{8.5}$$

with D_y the covariant derivative in the y direction. From this expression it is easier to see why the ϵ^{ij} is necessary in eq. 8.4 – its antisymmetry cancels the antisymmetry of the covariant derivative D_y (assuming proper boundary conditions) under the exchange $\psi_i D_y\psi_j \to -\psi_j D_y\psi_i$ and prevents the D_y term from vanishing.

Since the minimal 5D fermion is a Dirac spinor with four on-shell degrees of freedom (DOF), a 5D vector multiplet must contain a five dimensional vector field (three on-shell DOF), a Dirac fermion (equivalent to two 4D Weyl spinor fields with four on-shell DOF), and a real scalar field (one DOF). More succinctly, $\mathbb{V}^a = \{V_M^a, \lambda^a, \lambda'^a, \phi^a\}$ with $\lambda^a = \lambda_1^a$ and $\lambda'^a = \lambda_2^a$; the subscripts 1, 2 are the explicit index i. We use the λ' notation to match the conventions of refs. [8, 98]. Off-shell, three more auxiliary scalar degrees of freedom are required.

Similarly, an on-shell 5D hypermultiplet contains a Dirac fermion composed of two 4D

Weyl spinor fields and two complex scalar fields $\Phi = \{\psi, \psi^c, \varphi, \varphi^c\}$, where we have named $\psi^1 \to \psi$ and $\psi^2 \to \psi^c$. From 8.4 it is easy to see that ψ and $\psi^{c\dagger}$ have the same gauge transformation properties and therefore ψ and ψ^c must have conjugate transformations, justifying their names. Off-shell, four more axillary scalar degrees of freedom are required.

When writing the Lagrangian it will be convenient to write $\mathcal{N} = 2$ superfields using $\mathcal{N} = 1$ terminology. In this language gauge supermultiplets are

$$\mathbb{V}^a = \left\{ V^a(V^a_\mu, \lambda^a), \Sigma^a(\lambda'^a, \sigma^a) \right\} \tag{8.6}$$

with $\sigma^a = \frac{1}{\sqrt{2}}(\phi^a + iV^a_y)$ while matter hypermultiplets are

$$\Phi = \{\Phi(\psi, \varphi), \Phi^c(\psi^c, \varphi^c)\}\,. \tag{8.7}$$

For more information about supersymmetric transformations between these fields using either 5D or 4D language see refs. [26, 98, 178].

8.1.2 Scherk-Schwarz supersymmetry breaking

The $S_1/\mathbb{Z}_2 \times \mathbb{Z}'_2$ orbifold of MNSUSY is visualized by compactifying the 5^{th} dimension y on a circle as shown in fig. 8.1 where fields must satisfy $\psi(y) = P_{\mathbb{Z}_2}\psi(-y)$ and $\psi(l+y) = P_{\mathbb{Z}'_2}\psi(l-y)$ with the $\mathbb{Z}_2$ parities $P_{\mathbb{Z}_2} = \pm 1$. Equivalently, one may view the distance l as more fundamental than the orbifold and demand that fields have either Neumann or Dirichlet boundary conditions at $y = 0, l$ [178, 179]. Either way, after integrating the Lagrangian over the 5^{th} dimension y to obtain the effective 4D action, 5D Lorentz symmetry is broken down to 4D Lorentz symmetry plus a Kaluza-Klein (KK) tower of massive modes for each field due to their discrete momentum modes along y. The four possible combinations for $(P_{\mathbb{Z}_2}, P_{\mathbb{Z}'_2})$ result in the following field profiles along y

$$\begin{aligned}
\psi_{++m}(x^M) &= N(m)\cos\left(\frac{m\pi y}{l}\right)\psi_m(x^\mu) \\
\psi_{+-n}(x^M) &= N(n)\cos\left(\frac{(2n-1)\pi y}{2l}\right)\psi_n(x^\mu) \\
\psi_{-+n}(x^M) &= N(n)\sin\left(\frac{(2n-1)\pi y}{2l}\right)\psi_n(x^\mu) \\
\psi_{--n}(x^M) &= N(n)\sin\left(\frac{n\pi y}{l}\right)\psi_n(x^\mu)
\end{aligned} \tag{8.8}$$

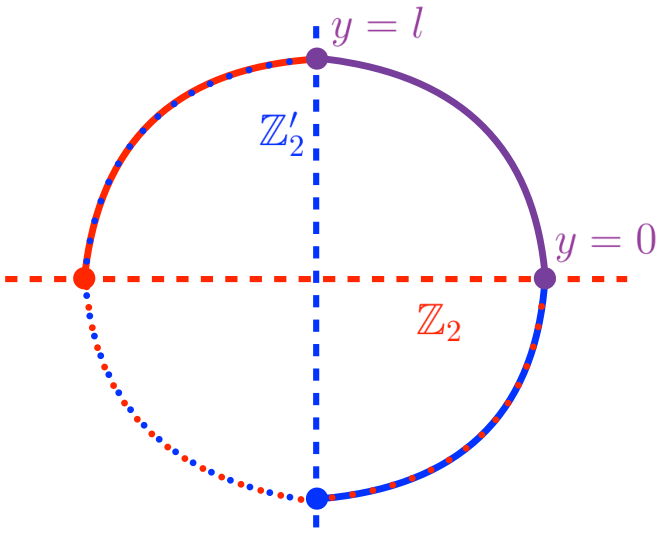

Figure 8.1: $S_1/\mathbb{Z}_2 \times \mathbb{Z}_2'$ orbifold of MNSUSY. Field profiles are constrained to be either symmetric or antisymmetric at the fixed points $y = 0$ and $y = l$.

for modes $n = \{1, 2, 3...\}$ and $m = \{0, n\}$. The field normalizations

$$N(m) = \begin{cases} 1/\sqrt{l}, & m = 0 \\ \sqrt{2/l}, & m = n \end{cases} \tag{8.9}$$

are necessary to keep the kinetic terms for $\psi_n(x^\mu)$ canonically normalized after integrating out the fifth dimension. Additionally, gauge couplings must be normalized as $g_5 = \sqrt{l}\, g_4$. We will usually keep these transformations implicit and simply refer to the couplings as g.

In SSSB each component field within a bulk $\mathcal{N} = 2$ supermultiplet has a different $(P_{\mathbb{Z}_2}, P_{\mathbb{Z}_2'})$ parity. The differing parities under one $\mathbb{Z}_2$ symmetry breaks $\mathcal{N} = 2$ SUSY into $\mathcal{N} = 1$ SUSY, while a second $\mathbb{Z}_2$ breaks the remaining $\mathcal{N} = 1$ SUSY. Due to the non-local nature of SSSB, loop corrections to the effective 4D soft terms come without cutoff-dependent *log* enhancements so fine tuning in the model remains exceptionally mild [7].

8.1.3 MNSUSY field content

MNSUSY contains one $\mathcal{N} = 2$ bulk vector superfield $\mathbb{V} = \{V(V_\mu, \lambda), \Sigma(\sigma, \lambda')\}$ for each of the SM gauge fields, one bulk hypermultiplet for an up-type Higgs and another for a down-type Higgs $\mathbb{H}_{u,d} = \{H_{u,d}(h_{u,d}, \tilde{h}_{u,d}),\ H^c_{u,d}(h^c_{u,d}, \tilde{h}^c_{u,d})\}$, and a bulk hypermultiplet for

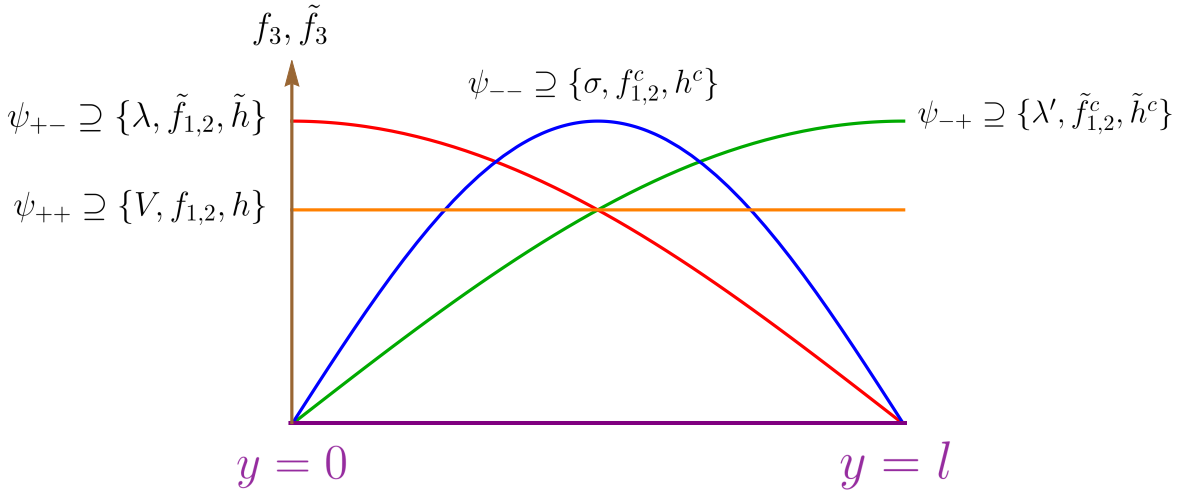

Figure 8.2: Lowest KK-modes of the minimal field content of MNSUSY. The $(\mathbb{Z}_2, \mathbb{Z}_2')$ parities of each of the fields is indicated by a pair of $\pm$ subscripts. Note that the SM fields are all massless before EWSB and loop corrections.

the first two generations of each of the SM fermions ($\overline{\mathbb{U}}_{1,2}$, $\overline{\mathbb{D}}_{1,2}$, $\overline{\mathbb{E}}_{1,2}$, $\mathbb{Q}_{1,2}$, $\mathbb{L}_{1,2}$), which we generically call $\mathbb{F}_{1,2} = \{F_{1,2}(\tilde{f}_{1,2}, f_{1,2}), F^c_{u,d}(\tilde{f}^c_{1,2}, f^c_{1,2})\}$. The third generation fields are brane localized and form 4D left-handed chiral supermultiplets $F_3(\tilde{f}_3, f_3)$. This is the minimal field content of MNSUSY.

The orbifold $\mathbb{Z}_2$ parities for each of the component fields is given in fig. 8.2, along with the resulting field profiles along y for the lowest modes. As can be seen from this figure, the bulk SM fields all have massless zero KK-modes.

As we will see in sec. 8.3, masses for scalar Higgs fields $h_{u,d}$ and third generation sfermions $\tilde{f}$ come from loop corrections and other interactions. SM fermions pick up their masses after EWSB in the usual way. Yukawa interactions must be brane localized due to the chiral nature of this interaction. Since third generation fields are brane localized the required normalizations between 5D and 4D Yukawa couplings are $\mathbf{y_5}_{ij} = l^{3/2}\mathbf{y_4}_{ij}$, $\mathbf{y_5}_{i3} = l\mathbf{y_4}_{i3}$, $\mathbf{y_5}_{33} = l^{1/2}\mathbf{y_4}_{33}$. This results in an automatic mass suppression of the first two generation's fermion field masses. As with gauge couplings, we will usually not distinguish between 5D and 4D Yukawa couplings and let context indicate which we mean.

In addition to the minimal field content already discussed, MNSUSY contains a gauge singlet brane localized chiral superfield X, which develops a vacuum expectation value (VEV) in its F term $\langle F_X \rangle$. As we will see in sec. 8.2.3.2, this allows one to write

Yukawa interactions using a single Higgs superfield H_u, with interactions involving down type quark superfields $\overline{D}$ and lepton superfields $\overline{E}$, L arising from higher dimensional operators [7, 8]. The benefits of this scheme are twofold. First, only one Higgs must obtain a VEV, $\langle h_u^0 \rangle = v/\sqrt{2}$ and h_u^0 is automatically SM-like. Second, the masses of the bottom and tau are suppressed as compared to the top due to the fact that they come from higher dimensional operators. Rather than including the X superfield in our FeynRules model file we add its effects using effective operators.

8.2 Lagrangian

8.2.1 Gauge multiplet Lagrangian

The 5D SUSY Yang-Mills Lagrangian can be written [97, 98]

$$\mathcal{L}_{\text{gauge}} = \frac{1}{T_F g^2}\left(\frac{1}{4}\,\text{Tr}(W^\alpha W_\alpha)\Big|_{\theta^2} + \text{h.c.} + \text{Tr}\left(\frac{1}{2}\{e^V, \partial_y e^{-V}\} + \frac{1}{\sqrt{2}}(e^V \Sigma^\dagger e^{-V} + e^{-V}\Sigma e^V)\right)^2\Big|_{\theta^4}\right) \tag{8.10}$$

with ∂_y the 5^{th} dimension partial derivative, $V \equiv gV^a T^a$, $\Sigma \equiv g\Sigma^a T^a$, $W_\alpha \equiv g W_\alpha^a T^a$, $\text{Tr}[T^a T^b] = T_F \delta^{ab}$, and T^a a generator in the fundamental representation. The typical physics convention (and the one used by FeynRules) is $T_F = 1/2$ so it is the one we adopt. This expression and the ones that follow are easily generalized to the abelian case by eliminating the trace along with any commutators and setting $T_F = 1$.

FeynRules includes functions to evaluate the kinetic term for Σ, therefore it is convenient to split the second term of 8.10 into the kinetic term and terms involving ∂_y. The second term becomes (in the Wess-Zumino gauge)

$$\mathcal{L}_{\text{gauge}} \supset \frac{1}{T_F g^2}\,\text{Tr}\left(e^V \Sigma^\dagger e^{-2V}\Sigma e^V + (\partial_y V)^2 - \left(\sqrt{2}\,(\partial_y V + [V, \partial_y V])\,\Sigma + \text{h.c.}\right)\right)\Big|_{\theta^4}. \tag{8.11}$$

The first term in this expression is easily handled by FeynRules.

To write the Lagrangian in terms of the component fields one performs the integrals over superspace coordinates and eliminates the auxiliary fields using their equations of motion

$$F_\Sigma = 0, \qquad D = -(\partial_y \phi - i[V_y, \phi]) = -D_y \phi \tag{8.12}$$

with $D \equiv gD^a T^a$, $\phi \equiv g\phi^a T^a$, and where D_y is the y component of the covariant deriva-

tive. Redefining $\lambda^1 \to i\lambda^1$ the Lagrangian takes the standard form for a 5D super-Yang-Mills multiplet[1] [95]

$$\mathcal{L}_{\text{gauge}} = \frac{1}{T_F g^2} \text{Tr}\left(-\frac{1}{4}F_{MN}^2 + \frac{1}{2}(D_M\phi)^2 + \frac{i}{2}\overline{\boldsymbol{\lambda}}_i\gamma^M D_M\boldsymbol{\lambda}_i - \frac{1}{2}\overline{\boldsymbol{\lambda}}_i[\phi,\boldsymbol{\lambda}_i]\right). \tag{8.13}$$

After Scherk-Schwarz symmetry breaking, the effective 4D Lagrangian for the lowest modes is

$$\begin{aligned}\mathcal{L}_{\text{gauge 4D}} = \frac{1}{T_F g^2} \text{Tr}\Bigg(&-\frac{1}{4}F_{\mu\nu}^2 + \frac{1}{2}(D_\mu\phi)^2 - \frac{1}{2}(2m_l)^2\phi^2 + \frac{1}{2}(D_\mu V_y)^2 - \frac{3}{4}[\phi,V_y]^2 \\ &+ \overline{\boldsymbol{\lambda}}(i\gamma^\mu D_\mu - m_l)\boldsymbol{\lambda} + \frac{1}{\sqrt{2}}\overline{\boldsymbol{\lambda}}\left([\phi,\boldsymbol{\lambda}] + i\gamma_*[V_y,\boldsymbol{\lambda}]\right)\Bigg).\end{aligned} \tag{8.14}$$

where $m_l \equiv \frac{\pi}{2l}$ and we have introduced the Dirac gaugino $\boldsymbol{\lambda} \equiv (\lambda\ \lambda^{c\dagger})^{\text{T}}$. Thus SSSB gives the gaugino $\boldsymbol{\lambda}$ a Dirac mass m_l and the scalar field ϕ a mass $2m_l$. The pseudoscalar V_y is "eaten" via the Higgs mechanism by the first non-zero mode of the vector field V_μ which also acquires a mass of $2m_l$. Only the lowest mode of the vector field remains massless. Another effect of SSSB is to change certain field interaction strengths by factors of $\sqrt{2}$ compared to generic 4D SUSY, as in the $\overline{\boldsymbol{\lambda}}[\phi,\boldsymbol{\lambda}]$ term for example.

8.2.2 Hypermultiplet Lagrangian

The 5D hypermultiplet Lagrangian is given by [98]

$$\mathcal{L}_{\text{hypermultiplet}} = (\Phi^\dagger e^{-2V}\Phi + \Phi^c e^{2V}\Phi^{c\dagger})\Big|_{\theta^4} - \left(\Phi^c\left(\partial_y - \sqrt{2}\Sigma\right)\Phi\Big|_{\theta^2} + \text{h.c.}\right). \tag{8.15}$$

Once again, performing the integration over superspace and eliminating the auxiliary fields using their equations of motion one obtains

$$\begin{aligned} F_\Phi &= (D_y + \phi)\varphi^{c\dagger}, \qquad & F_\Sigma^a &= \sqrt{2}g\varphi^\dagger T^a\varphi^{c\dagger}, \\ F_{\Phi^c}^\dagger &= -(D_y - \phi)\varphi, \qquad & D^a &= -(D_y\phi)^a + g(\varphi^\dagger T^a\varphi - \varphi^c T^a\varphi^{c\dagger}). \end{aligned} \tag{8.16}$$

with $(D_y\phi)^a = \partial_y\phi^a + gf^{abc}V_y^b\phi^c$, $D_M\varphi = \partial_M\varphi - iV_M\varphi$, and similarly for other fields in the fundamental representation. This is equivalent to the similar set of equations given in ref. [98] except for the term involving f^{abc}, which was omitted in that work.

After making the axillary field substitution the 5D Lagrangian can be put into canon-

[1]The phase transformation needed to put the Lagrangian into its canonical form depends on the choice of basis for γ^y.

ical form

$$\begin{aligned}\mathcal{L}_{\text{hypermultiplet}} =& D^M\varphi_i^\dagger D_M\varphi_i + i\overline{\Psi}\gamma^M D_M\Psi - \sqrt{2}(\varphi^c\overline{\boldsymbol{\lambda}}_1\Psi + \varphi^\dagger\overline{\boldsymbol{\lambda}}_2\Psi + \text{h.c.}) \\ & - \overline{\Psi}\phi\Psi - \varphi_i^\dagger\phi^2\varphi_i - \frac{g^2}{2}\sum_{m,a}(\varphi_i^\dagger(\sigma^m)_{ij}T^a\varphi_j)^2\end{aligned} \tag{8.17}$$

with $\Psi \equiv (\psi\ \psi^{c\dagger})^{\mathrm{T}}$, $\{\varphi_1, \varphi_2\} \equiv \{\varphi, \varphi^{c\dagger}\}$, and σ^m are the three Pauli matrices.

To derive the 4D effective theory there are two versions of SSSB we must consider: $\mathbb{H}$ field boundary conditions with a zero mode scalar and $\mathbb{F}$ field boundary conditions with a zero mode fermion. For the $\mathbb{H}$ type field, keeping only the lowest modes we obtain

$$\begin{aligned}\mathcal{L}_{\mathbb{H}4\text{D}} =& i\overline{\Psi}(\gamma^\mu D_\mu - m_l)\Psi - \frac{1}{\sqrt{2}}\overline{\Psi}(\phi - i\gamma^5 V_y)\Psi - (\varphi^c\overline{\boldsymbol{\lambda}}_1\Psi + \sqrt{2}\varphi^\dagger\overline{\boldsymbol{\lambda}}_2\Psi + \text{h.c.}) \\ & + |D_\mu\varphi^c|^2 - (2m_l)^2\varphi^{c\dagger}\varphi^c - \frac{3}{2}\varphi^c(\phi^2 + V_y^2)\varphi^{c\dagger} - \frac{3g^2}{4}(\varphi^c T^a\varphi^{c\dagger})^2 \\ & + |D_\mu\varphi|^2 - \varphi^\dagger(\phi^2 + V_y^2)\varphi - \frac{g^2}{2}(\varphi^\dagger T^a\varphi)^2 \\ & - 2g^2(\varphi^c T^a\varphi)(\varphi^\dagger T^a\varphi^{c\dagger}) + g^2(\varphi^\dagger T^a\varphi)(\varphi^c T^a\varphi^{c\dagger}).\end{aligned} \tag{8.18}$$

Similarly, for $\mathbb{F}$ type fields

$$\begin{aligned}\mathcal{L}_{\mathbb{F}4\text{D}} =& i\psi^\dagger\overline{\sigma}^\mu D_\mu\psi + \left(\sqrt{2}(\varphi^\dagger\lambda - \varphi^c\lambda')\psi + \text{h.c.}\right) \\ & + i\psi^{c\dagger}\overline{\sigma}^\mu D_\mu\psi^c - \left((\varphi^c\lambda^\dagger + \varphi^\dagger\lambda'^\dagger)\psi^{c\dagger} + \psi^c(\phi + iV_y)\psi + \text{h.c.}\right) \\ & + D^\mu\varphi_i^\dagger D_\mu\varphi_i - (m_l)^2\varphi_i^\dagger\varphi_i - \varphi_i^\dagger(\phi^2 + V_y^2)\varphi_i - \frac{3g^2}{4}(\varphi_i^\dagger T^a\varphi_i)^2 \\ & - g^2(\varphi^c T^a\varphi)(\varphi^\dagger T^a\varphi^{c\dagger}) + \frac{g^2}{2}(\varphi^\dagger T^a\varphi)(\varphi^c T^a\varphi^{c\dagger})\end{aligned} \tag{8.19}$$

Though it does not appear in the second expression, ψ^c obtains a Dirac mass of $2m_l$ with the first non-zero mode of ψ. Thus SSSB once again gives masses to the non-zero KK mode fields and changes the interaction strength in various terms as compared to generic 4D SUSY. Only the scalar Higgs bosons h and the SM fermions f remain massless after SSSB.

8.2.3 Brane localized terms

We now turn to the Lagrangian for brane localized fields. As we discussed in sec. 8.1, the chiral superfields F_3 and X are brane localized at $y = 0$. This leads to an action of the form

$$S = \int d^5x\,(\mathcal{L}_5 + \delta(y)\mathcal{L}_4)\,. \tag{8.20}$$

A minor complication arises after solving the auxiliary fields' equations of motion – one obtains terms in the action proportional to $\delta(y)^2$. As we shall see in the following section, these terms are removed using various field redefinitions. For more in-depth discussions of the field redefinitions we refer the reader to [95, 178, 180].

8.2.3.1 Brane localized third generation fields

The Lagrangian for the third generation brane localized fields is the standard one for a chiral superfield

$$\mathcal{L}_{F_3} = \delta(y)\Phi_3^\dagger e^{-2V}\Phi_3. \tag{8.21}$$

The subscript 3 reminds us that in MNSUSY it is the third generation superfields which live on the brane. Solving the auxiliary equation of motion for D as before we obtain

$$D^a = -(D_y\phi)^a + g(\varphi^\dagger T^a\varphi - \varphi^c T^a\varphi^{c\dagger} + \delta(y)\varphi_3^\dagger T^a\varphi_3). \tag{8.22}$$

where we have allowed for the presence of bulk scalar fields φ and their 5D partners φ^c as in sec. 8.2.2 along with the brane scalars φ_3. Thus the D-term Lagrangian is

$$\begin{aligned}\mathcal{L}_D =& -\frac{1}{2}D^aD^a \\ =& -\frac{1}{2}\left(-\partial_y\phi^a + g\delta(y)\varphi_3^\dagger T^a\varphi_3 + ...\right)^2.\end{aligned} \tag{8.23}$$

Since the term $\partial_y\phi^a$ appears nowhere else in the Lagrangian one can shift

$$\partial_y\phi^a \to \partial_y\phi^a + \left(\delta(y) - \frac{1}{2l}\right) g\varphi_3^\dagger T^a\varphi_3 \tag{8.24}$$

without much trouble. The factor of $1/2l$ is needed to maintain the $2l$ periodicity of the odd function ϕ (refer to figs. 8.1 and 8.2) since

$$\int_{-l}^{l}\partial_y\phi^a dy = 0 \to \int_{-l}^{l}\left[\partial_y\phi^a + \left(\delta(y) - \frac{1}{2l}\right) g\varphi_3^\dagger T^a\varphi_3\right] dy = 0. \tag{8.25}$$

Substituting 8.24 back into eq. 8.23 the singular terms cancel and one is left with

$$\begin{aligned}\mathcal{L}_D =& -\frac{1}{2}D^aD^a \\ =& -\frac{1}{2}\left(-(D_y\phi)^a + g(\varphi^\dagger T^a\varphi - \varphi^c T^a\varphi^{c\dagger} + \frac{1}{2l}\varphi_3^\dagger T^a\varphi_3)\right)^2.\end{aligned} \tag{8.26}$$

Note that this results in (otherwise absent) effective interactions between the brane localized fields φ_3 and the odd fields φ^c and ϕ.

8.2.3.2 Brane localized Yukawa interactions

Yukawa interactions involving chiral fields are forbidden in the bulk, therefore the SM Yukawa terms must be brane localized. MNSUSY uses the usual superpotential term to couple up-type quark superfields to H_u. Down-type quark and lepton superfields are coupled via higher dimensional operators with the brane localized singlet superfield X which, as we mentioned in sec. 8.1, develops a F term VEV $\langle F_X \rangle$ [7]. Therefore,

$$\mathcal{L}_{\text{Yukawa}} = \delta(y) \left(\overline{U} \mathbf{y_u} Q \cdot H_u \Big|_{\theta^2} + \frac{1}{M_*^2} (\overline{D} \mathbf{y_d} Q H_u^\dagger X^\dagger + \overline{E} \mathbf{y_e} L H_u^\dagger X^\dagger) \Big|_{\theta^4} + \text{h.c.} \right) \tag{8.27}$$

where $Q \cdot H_u$ is the usual $SU(2)$ invariant product $Q_i \epsilon^{ij} H_{uj} = Q_1 H_{u2} - Q_2 H_{u1}$. This has the advantages that only one Higgs field needs a VEV, so that H_u is automatically SM-like, and the tau and bottom masses are naturally suppressed compared to the top. The cost is the need to introduce the X field, since one cannot build a holomorphic superpotential out of $H_u^\dagger$. However from a practical standpoint, we need not include the gauge singlet X when coding the Lagrangian into FeynRules. Since $\langle F_X^\dagger \rangle$ will "eat up" the integrals over $\theta^{\dagger 2}$ we may drop X in eq. 8.27 and simply integrate over θ^2. Then $\mathcal{L}_{\text{Yukawa}}$ takes the general form.

$$\mathcal{L}_{\text{Yukawa}} = \delta(y) \Phi_i \mathbf{y}_{ij} \Phi_j H_u^{(\dagger)} \Big|_{\theta^2} + \text{h.c.} \tag{8.28}$$

where we have absorbed various factors of $\langle F_X \rangle$ and M^* into the definition of the Yukawa couplings, and the $^{(\dagger)}$ indicates that some terms contain the conjugated superfield H_u. The $SU(2)$ invariant product, where necessary, is left implicit.

In this case the auxiliary fields are given by

$$\begin{aligned} F_{\Phi_i} &= (D_y + \phi) \varphi_i^{c\dagger} + \delta(y) \mathbf{y}_{ij}^* \varphi_j^\dagger h_u^{(\dagger)\dagger} \\ F_{\Phi_3} &= \mathbf{y}_{3j}^* \varphi_j^\dagger h_u^{(\dagger)\dagger} \\ F_{H_{uj}} &= (D_y + \phi) h_u^{c\dagger} + \delta(y) \widetilde{\overline{u}}^\dagger \mathbf{y_u}^* \tilde{q}_i^\dagger \epsilon^{ij}. \end{aligned} \tag{8.29}$$

The bulk F-term Lagrangian includes $\delta(y)^2$ factors which can be handled in the same

manner as for D-terms.[2] For bulk sfermion fields one obtains

$$\begin{aligned}\mathcal{L}_{F_{\Phi_i}} &= -F^\dagger_{\Phi_i}F_{\Phi_i} \\ &= -\left|\partial_y\varphi^c_i + \delta(y)\mathbf{y}_{ij}\varphi_j h_u^{(\dagger)} + ...\right|^2 \\ &\to -\left|D_y\varphi^c_i + \varphi^c_i\phi + \frac{1}{2l}\mathbf{y}_{ij}\varphi_j h_u^{(\dagger)}\right|^2\end{aligned} \tag{8.30}$$

which, after SSSB gives the following cubic effective operators

$$\mathcal{L}_{F_{\Phi_i 4\mathrm{D}}} = -\frac{1}{\sqrt{2l}}\varphi^c_i\mathbf{y}^*_{ij}\varphi^\dagger_j h_u^{(\dagger)\dagger} - \frac{2}{3l}\varphi^c_i\mathbf{y}^*_{ij}\varphi^\dagger_{3j}h_u^{(\dagger)\dagger} + \text{h.c.} + ... \tag{8.31}$$

along with various quartic interactions.

8.3 Soft masses and field mixing

Since the third generation sfermions are brane localized, they do not pick up a mass at m_l in contrast to their first and second generation cousins, nor are the Higgs bosons $h_{u,d}$ massive at tree level. Instead, they pick up 1-loop soft-SUSY breaking masses given by [7, 181]

$$\delta\tilde{m}_i^2 = \frac{7\zeta(3)}{16\pi^2 l^2}\left(\sum_{I=1,2,3} C_I(i)g_I^2 + C_t(i)y_t^2\right) \tag{8.32}$$

where $\zeta(z)$ is the Riemann zeta function, y_t is the top Yukawa coupling, $g_{1,2,3}$ are the gauge couplings for $U(1)_Y$, $SU(2)_w$, and $SU(3)_c$ respectively and where

$$\begin{aligned} C(\tilde{t}_R) &= \{4/9, 0, 4/3, 1\} & C(\tilde{q}_3) &= \{1/36, 3/4, 4/3, 1/2\} \\ C(\tilde{b}_R) &= \{1/9, 0, 4/3, 0\} & C(\tilde{l}_3) &= \{1/4, 3/4, 0, 0\} \\ C(\tilde{\tau}_R) &= \{1, 0, 0, 0\} & C(h_{u,d}) &= \{1/4, 3/4, 0, 0\} \end{aligned}$$

with the C_I given by the first three numbers in each set (these are the squared hypercharges and quadratic Casimirs for $SU(2)$ and $SU(3)$ respectively) and C_t given by the last. In addition, higher dimensional operators including interactions with the brane-localized X can alter soft masses, trigger EWSB, and induce field mixing [7,8,182]. Without these additional interactions 8.32 implies the stau $\tilde{\tau}_R$ is the LSP. For the benchmark scenarios described in sec. 8.5 we will follow [7] and assume that additional interactions

[2] One may worry that $\mathbb{F}_{1,2}$ scalar fields will require a compensating factor other than $1/2l$ due to the $4l$ periodicity of $(+-)$ and $(-+)$ fields. This, however, is compensated by the fact that the orbifold conditions require a second delta function at $y = 2l$ and the factors of two conveniently cancel.

$\mathcal{N}=1$ Superfield	Boson	Fermion
$V(V_\mu, \lambda)$	0	+1
$\Sigma(\sigma, \lambda')$	0	−1
$H_{u,d}(h_{u,d}, \tilde{h}_{u,d})$	0	−1
$H^c_{u,d}(h^c_{u,d}, \tilde{h}^c_{u,d})$	+2	+1
$F_{1,2,3}(\tilde{f}_{1,2,3}, f_{1,2,3})$	+1	0
$F^c_{1,2}(\tilde{f}^c_{1,2}, f^c_{1,2})$	+1	0
$X = (x, \tilde{x})$	+2	+1

Table 8.1: R-charges of component fields. Table adapted from [8].

lift $\tilde{\tau}_R$ mass above $\tilde{l}_\tau$ so that $\tilde{\nu}_3$ is the LSP after EWSB. Other possibilities exist, such as a gravity sector LSP [7].

To understand the possible types of field mixings, we note that unbroken $\mathcal{N}=2$ SUSY includes a global $SU(2)_R$ symmetry, in an analogous way to the global $U(1)_R$ symmetry which exists in unbroken $\mathcal{N}=1$ SUSY [10]. In MNSUSY, after SSSB an accidental global $U(1)_R$ symmetry remains in the theory, which is exact in the absence of gravitational interactions [8]. The fields' R-charges affect which mixings are allowed and are useful in classifying the physical field content. We therefore list the fields and their R-charges in table 8.1 [8, 182].

From this table we see that interactions of the form

$$\delta(y)\frac{X^\dagger X}{M_*^2}(b_{H_u}H_u^\dagger H_u + b_{H_d}H_d^\dagger H_d + b_\mu H_u H_d + b_q Q_3^\dagger Q_3 + ...)\Big|_{\theta^4} \tag{8.33}$$

are allowed and generate soft-SUSY breaking scalar masses after X gets its F-term VEV $\langle F_X \rangle$. Rather than focus on specific sources of SUSY breaking we will simply parametrize possible mass/mixing terms allowed by all symmetries in the model using matrices $\mathbf{b}_\chi$ for each set of fields with a mass of around m_l or less.

We start by considering the neutralino and chargino sector. In MNSUSY, this sector is very similar to that of R-Symmetric models [182] but simpler since only h_u develops a VEV $\langle h \rangle = v/\sqrt{2}$ and interactions between $H_{u,d}$ and $\Sigma_{B,W}$ are governed by gauge couplings. From Table 8.1 we see that the R-symmetry prevents mixing between λ and λ' while allowing Dirac masses, as noted in sec. 8.2.1. While the same argument holds for higgsinos, mixing between gauginos and higgsinos is allowed – indeed EWSB generates such mixings.

Before examining the neutralino and chargino mass matrices it is convenient to first rotate the gauginos in the same way as their gauge field counterparts

$$\tilde{A} = (c_w\tilde{B} + s_w\tilde{W}_3) \qquad \tilde{W}^+ = \frac{1}{\sqrt{2}}(\tilde{W}_1 - i\tilde{W}_2)$$
$$\tilde{Z} = (-s_w\tilde{B} + c_w\tilde{W}_3) \qquad \tilde{W}^- = \frac{1}{\sqrt{2}}(\tilde{W}_1 + i\tilde{W}_2)$$

where c_w and s_w are cosine and sine of the weak mixing angle respectively. An identical set of equations holds for the fields $\tilde{B}'$ and $\tilde{W}'$. Then, in the basis $\chi^0_{R^+} = (-i\tilde{A}\ -i\tilde{Z}\ \tilde{h}^{c0}_u\ \tilde{h}^{c0}_d)^{\mathrm{T}}$, $\chi^0_{R^-} = (\tilde{A}'\ \tilde{Z}'\ \tilde{h}^0_u\ \tilde{h}^0_d)^T$ (the $R^\pm$ indicates the R charge of the Weyl spinor field) the 4D neutralino mass Lagrangian is:

$$\mathcal{L}_{m_{\chi^0}} = -\chi^{0\mathrm{T}}_{R^+}\left(\mathbf{M}_{\chi^0} + \mathbf{b}_{\chi^0}\right)\chi^0_{R^-} + \mathrm{h.c.} \tag{8.34}$$

with the tree level mass matrix

$$\mathbf{M}_{\chi^0} = \begin{pmatrix} m_l & 0 & 0 & 0 \\ 0 & m_l & m_Z & 0 \\ 0 & -m_Z & m_l & 0 \\ 0 & 0 & 0 & -m_l \end{pmatrix}. \tag{8.35}$$

where we have used the relation $m_Z = (v/2)\sqrt{g'^2 + g^2}$. Thus, in the limit that $\mathbf{b}_{\chi^0} = 0$, Ψ_A and Ψ_{H_d} decouple from the other neutralinos at tree level due to the fact that only h_u obtains a VEV. After the field rotations $U_{\chi^0_{R^-}}\chi^0_{R^-}$ and $U_{\chi^0_{R^+}}\chi^0_{R^+}$ with

$$U_{\chi^0_{R^-}} = \begin{pmatrix} 1 & 0 & 0 & 0 \\ 0 & c_\xi & -s_\xi & 0 \\ 0 & s_\xi & c_\xi & 0 \\ 0 & 0 & 0 & -1 \end{pmatrix}, \quad U_{\chi^0_{R^+}} = \begin{pmatrix} 1 & 0 & 0 & 0 \\ 0 & c_\xi & s_\xi & 0 \\ 0 & -s_\xi & c_\xi & 0 \\ 0 & 0 & 0 & 1 \end{pmatrix} \tag{8.36}$$

and

$$\xi \equiv \arctan(-m_Z/m_l)/2 \tag{8.37}$$

$\mathbf{M}_{\chi^0}$ is diagonalized with the real positive masses

$$\begin{aligned} m_{\tilde{A}} &= m_{\tilde{H}_d} = m_l \\ m_{\chi^0_2} &= m_{\chi^0_3} = \sqrt{m_l^2 + m_Z^2}. \end{aligned} \tag{8.38}$$

For $m_l > m_Z$ there is little mixing between the neutral higgsino and zino.

In what follows we will leave the soft SUSY breaking mass matrices $\mathbf{b}$ implicit and continue to evaluate the mass matrices in the limit that they vanish. For charginos in the basis $\chi^+_{R^+} = (-i\tilde{W}^+ \ \tilde{h}_d^{c+})^{\mathrm{T}}$, $\chi^-_{R^-} = (\tilde{W}'^- \ \tilde{h}_d^-)^{\mathrm{T}}$, $\chi^+_{R^-} = (\tilde{W}'^+ \ \tilde{h}_u^+)^{\mathrm{T}}$, $\chi^-_{R^+} = (-i\tilde{W}^- \ \tilde{h}_u^{c-})^{\mathrm{T}}$ the tree level chargino mass Lagrangian is

$$\mathcal{L} = -\chi^{-\mathrm{T}}_{R^-}\mathbf{M}_{\chi_d^\pm}\chi^+_{R^+} - \chi^{-\mathrm{T}}_{R^+}\mathbf{M}_{\chi_u^\pm}\chi^+_{R^-} + \mathrm{h.c.} \tag{8.39}$$

$$\mathbf{M}_{\chi_d^\pm} = \begin{pmatrix} m_l & 0 \\ 0 & m_l \end{pmatrix} \qquad \mathbf{M}_{\chi_u^\pm} = \begin{pmatrix} m_l & -\sqrt{2}m_W \\ -\sqrt{2}m_W & -m_l \end{pmatrix}. \tag{8.40}$$

The latter matrix is diagonalized in a similar manner to the neutralino case and the mixing angle is obtained via the replacement $m_Z \to \sqrt{2}m_W$ in eq. 8.37. The masses are

$$\begin{aligned} m_{\tilde{W}_1} &= m_{H_d} = m_l \\ m_{\tilde{W}_2} &= m_{H_u} = \sqrt{m_l^2 + 2m_w^2} \end{aligned} \tag{8.41}$$

and once again, there is little mixing between the gaugino Ψ_{W_2} and higgsino Ψ_{H_u}.

When considering sfermions it is conventional to work in the basis where the scalar fields undergo the same rotations as their fermion cousins: $\tilde{f} = U_f^\dagger \tilde{f}_{\mathrm{flavor}}$ where $f_{\mathrm{mass}} = U_f^\dagger f_{\mathrm{flavor}}$.[3] It is convenient to also make the change of basis $\tilde{f}_i^c = \tilde{f}^c_{\mathrm{flavor}\,j}(U_f)_{ji}$, where we have to be explicit about the indices since $\tilde{f}^c$ carries only two flavors. We then write fields with the same R-charges as $\tilde{f}_L = (\tilde{f}_1 \ \tilde{f}_2 \ \tilde{f}_3 \ \tilde{\bar{f}}_1^c \ \tilde{\bar{f}}_2^c)^{\mathrm{T}}$ and $\tilde{f}_R = (\tilde{\bar{f}}_1 \ \tilde{\bar{f}}_2 \ \tilde{\bar{f}}_3 \ \tilde{f}_1^c \ \tilde{f}_2^c)^\dagger$. Note that the dagger in the second expression gives $\tilde{f}_R$ the same electric charge as $\tilde{f}_L$ but opposite R-charge. In this basis the sfermion mass Lagrangian is

$$\mathcal{L} = -\tilde{f}_L^\dagger \mathbf{M}_{\tilde{f}_L}\tilde{f}_L - \tilde{f}_R^\dagger \mathbf{M}_{\tilde{f}_R}\tilde{f}_R \tag{8.42}$$

[3]The dagger on U_f is a matter of convention. In the quark sector, for instance, one usually chooses up like quarks to be diagonal in the mass and flavor basis. Then $d_{\mathrm{mass}} = V^{\mathrm{CKM}\dagger} d_{\mathrm{flavor}}$.

with

$$\mathbf{M}_{\tilde{f}_L} = \begin{pmatrix} m_l^2 + \delta m^2_{\tilde{f}_{L1}} & 0 & 0 & \frac{\sqrt{2}}{\pi} m_l m_{f_1} & 0 \\ 0 & m_l^2 + \delta m^2_{\tilde{f}_{L2}} & 0 & 0 & \frac{\sqrt{2}}{\pi} m_l m_{f_2} \\ 0 & 0 & \delta m^2_{\tilde{f}_3} + \delta m^2_{\tilde{f}_{L3}} & 0 & 0 \\ \frac{\sqrt{2}}{\pi} m_l m_{f_1} & 0 & 0 & m_l^2 + \delta m^2_{\tilde{f}^c_{R1}} & 0 \\ 0 & \frac{\sqrt{2}}{\pi} m_l m_{f_2} & 0 & 0 & m_l^2 + \delta m^2_{\tilde{f}^c_{R2}} \end{pmatrix} \tag{8.43}$$

and

$$\begin{aligned} \delta m^2_{\tilde{f}_{L1,2}} &= \frac{v^2 g_1^2}{4} Y_f \mp \frac{v^2 g_2^2}{8} + \frac{m^2_{f_{1,2}}}{4} \\ \delta m^2_{\tilde{f}_{L3}} &= \frac{v^2 g_1^2}{8} Y_f \mp \frac{v^2 g_2^2}{16} + m^2_{f_3} \\ \delta m^2_{\tilde{f}_{R1,2}} &= \frac{v^2 g_1^2}{4} Y_f \end{aligned} \tag{8.44}$$

where $\delta m^2_{\tilde{f}_3}$ is the loop induced squared mass from expression 8.32, $m_{f_{1,2}}$ are the $f_{1,2}$ fermion masses, Y_f is their hypercharge, and the minus sign in the $\mp v^2 g_2$ terms is for the upper component of the sfermion $SU(2)$ doublet while the plus is for the lower component. Similar expressions hold for $\mathbf{M}_{\tilde{f}_R}$.

In contrast to the neutralino/chargino cases, the near degeneracy of the diagonal terms result in almost maximal mixing between the fields $\tilde{f}_{Li}$ and $\tilde{f}^c_{Ri}$ (and similarly for $\tilde{f}_{Ri}$ and $\tilde{f}^c_{Li}$). The sparticles obtain an average mass squared of $m_l^2 + (\delta m^2_{\tilde{f}_{Li}} + \delta m^2_{\tilde{f}_{Ri}})/2$ with a splitting $2\sqrt{8(\frac{m_l m_{f_i}}{\pi})^2 + (\delta m^2_{\tilde{f}_{Li}} - \delta m^2_{\tilde{f}_{Ri}})^2}$.

Finally, we note that in the limit $\mathbf{b} \to 0$ there is no mixing between the scalars h_u and h_d. For simplicity, we have only implemented this limit in the MNSUSY FeynRules model file. In this case $\mathrm{Re}(h_u^0) = h$ becomes the physical Higgs at 125 GeV while h_u's other degrees of freedom are the Goldstone modes of the W and Z bosons. The masses of the neutral scalar $\mathrm{Re}(h_d^0)$ and pseudoscalar $\mathrm{Im}(h_d^0)$ are $\delta m^2_{h_d} - \frac{v^2}{8}(g_1^2 + g_2^2)$ while the mass of the charged scalar $h_d^\pm$ is $\delta m^2_{h_d} + \frac{v^2}{8}(-g_1^2 + g_2^2)$ where $\delta m^2_{h_d}$ is obtained from eq. 8.32.

We should mention that additional interactions are needed to induce EWSB and give h the correct mass and vacuum expectation value. One possibility is through a $U(1)'$ interaction as described in ref. [7]. In the FeynRules model file we remain agnostic to the mechanism and simply set the Higgs mass to its needed value and shift the value of the quartic coupling to be consistent with the VEV, which is set by the W mass.

In the next section we will describe how one can easily obtain the mass spectra and field mixings for a given MNSUSY parameter set using FeynRules and its associated tools.

8.4 FeynRules implementation and user manual

FeynRules is capable of computing the Feynman rules of a quantum field theory expressed in four-dimensional spacetime. Therefore, to implement MNSUSY within FeynRules required computing the effective 4D theory. To do so we wrote the Lagrangian in FeynRules using $\mathcal{N} = 1$ SUSY language, neglecting ∂_y terms. The bulk fields were then split into the product of the y profile of their lowest mode times their x^μ profile as in eq. 8.8. Then the extra dimension y was integrated out – this accounted for changes in coupling strengths by e.g. factors of $\sqrt{2}$ as covered in secs. 8.2.1-8.2.3. Operators involving ∂_y, including mass terms, were implemented using effective operators. Third generation superfields were included as separate fields from their first and second generation cousins; the CKM matrix only includes Cabibbo mixing due to complexities introduced by this aspect of the model.

To use the MNSUSY model file FeynRules must be loaded within a Mathematica notebook as usual, using the command

```
<< FeynRules`.
```

For more details on using FeynRules see ref. [30]. The MNSUSY model file is loaded with

```
LoadModel[MNSUSY.fr]
```

and the Lagrangian is obtained with the command

```
Lag
```

It should be noted that computing the Lagrangian can take several minutes and the output is very large so it is worth saving the results to file using

```
lagr = Lag;
Definition[lagr] >> lagr.dat
```

so that `lagr` can be accessed in future runs using

```
<< lagr.dat.
```

To obtain the mass spectrum for a given set of model parameters one can use the C++ add-on package ASperGe. The command

`WriteASperGe[lagr]`

writes the ASperGe source code into the folder `<modelname>_MD`. Model parameters are set in the file `<modelname>_MD/input/externals.dat`. Running

`RunASperGe[]`

computes field masses and mixings and loads these back into FeynRules. It also creates a SLHA file which can be used in Monte Carlos. Further information on ASperGe can be found in ref. [183].

To port the Feynman rules into Monte Carlos, such as MadGraph5_aMC@NLO, the command

`WriteUFO[lagr,<options>]`

writes model file information in the Universal FeynRules Output (UFO) format; `<options>` represents output options. For most tree level applications four scalar interaction vertices are unnecessary, therefore we recommend using the option `Exclude4Scalars -> True` which speeds up the output. Users should consider whether this is appropriate for their specific needs.

Once the UFO files are loaded into the Monte Carlo, one may conduct simulations of a given MNSUSY model with a specific mass spectrum. In the next section we present several simplified spectra which are of interest to the LHC.

8.5 Benchmark simplified models

The masses described in sec. 8.3 lead to a spectrum in which third generation sleptons and h_d have masses of about $\sim 0.1 m_l$ while third generation colored sparticles' masses are $\sim 0.25 m_l$. Higgsinos, gauginos, and first and second generation sparticles all have a mass of $\sim m_l$. As we have already discussed, the identity of the LSP is dependent on higher dimensional operators; for this work we assume the LSP is $\tilde{\nu}_\tau$. In this case the left-handed stau will be the next-to-lightest superpartner, with an EWSB mass splitting given by eq. 8.44. Given this, we lay out six simplified models as MNSUSY benchmark scenarios, shown in fig. 8.3. For each of these the most interesting scenario to consider for the LHC is third generation colored sparticle production followed by three-body decays via off-shell gauginos/higgsinos. The final states involve multiple jets (often including

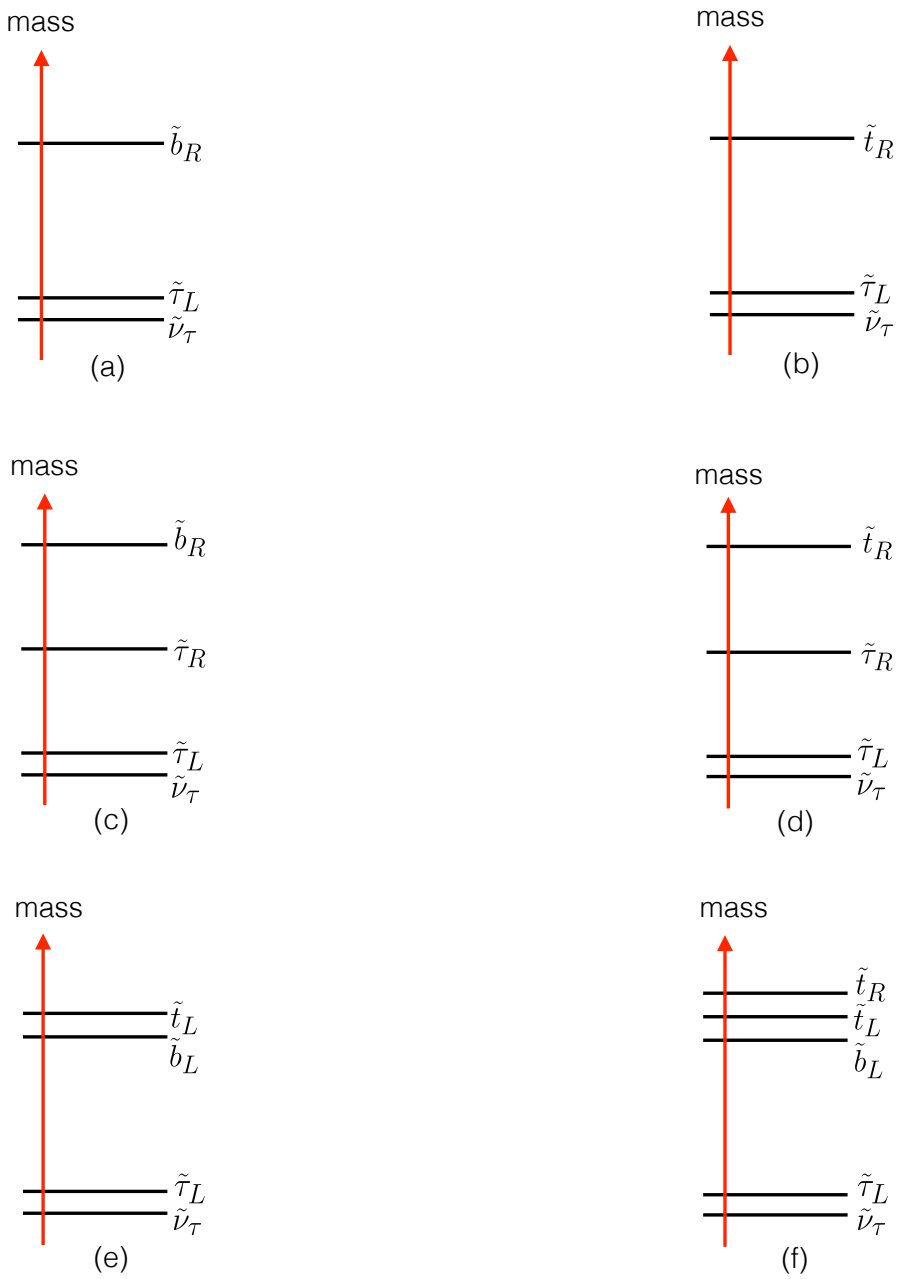

Figure 8.3: Benchmark simplified models for production of third generation colored states. Models (a) and (b) have a right-handed sbottom and stop respectively with third generation left-handed sleptons below, split by eq. 8.44. Cases (c) and (d) are similar but with intermediate right-handed staus. Case (e) contains left-handed squarks split by eq. 8.44. Case (f) contains both left and right-handed stops split by eq. 8.32, along with the left-handed sbottom.

several b and/or τ jets), along with missing energy.

For the simplified models we use $m_l = 2.5$ TeV; in this case eqs. 8.44 and 8.32 give $m_{\tilde{\nu}_\tau} = 212$ GeV, $m_{\tilde{\tau}} = 219$ GeV, $m_{\tilde{b}_L} = 616$ GeV, $m_{\tilde{t}_L} = 637$ GeV, and $m_{\tilde{t}_R} = 662$ GeV. This is the spectrum used in model (f) shown in fig. 8.3. Models (a)-(e) use the same left handed slepton masses but differ in their heavier sparticle spectra. For purposes of comparison, the lightest colored sparticle in each model was set to 616 GeV.

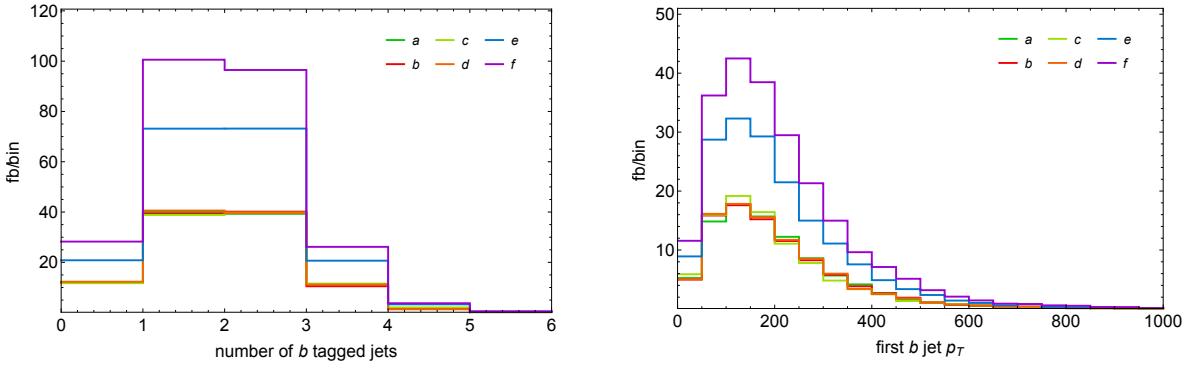

Figure 8.4: Number of b-tagged jets (left) and p_{T} of the leading b-tagged jet (right) for models (a)-(f). The larger colored state production cross sections of models (e) and (f) is readily evident, as is the fact that all models typically give at least one b-tagged jet.

Models (a) and (b) have third generation right-handed squark pair production with three-body decays to a quark plus a third generation lepton/slepton pair via an off-shell gaugino/higgsino. For (a) this gives the decay modes $\tilde{b}_R \to b+\tau+\tilde{\tau}_L^\dagger$ and $\tilde{b}_R \to b+\nu_\tau+\tilde{\nu}_\tau^\dagger$ while for (b) the large top Yukawa coupling causes $\tilde{t}_R \to b+\nu_\tau+\tilde{\tau}_L^\dagger$ to dominate, even for the small higgsino/gaugino mixing resulting from eq. 8.40. R charge is conserved since $\tilde{t}_R$, $\tilde{b}_R$, and $\tilde{\tau}_L^\dagger$ all have negative R charge. Staus undergo a further three-body decay via an off-shell W to the sneutrino and a jet pair or lepton pair.

Models (c) and (d) are similar to (a) and (b) except that they contain intermediate right-handed staus, which we set to a mass of $m_{\tilde{\tau}_R} = 300$ GeV. Cascade decays involving these intermediate staus result in higher multiplicity final states. For the masses we chose this has a greater effect in the $\tilde{b}_R$ model, which undergoes the decay $\tilde{b}_R \to b + \tau^+ + \tilde{\tau}_R$ about 50% of the time.

Model (e) has a left-handed third generation squark pair separated by the mass splitting given in 8.44; model (f) is as described three paragraphs earlier. Models (e) and (f) can also undergo cascade decays within the colored states resulting in higher multiplicity final states. The total production cross section of colored states in (e) and (f) are about 2 and 2.5 times the production cross sections of colored states in models (a)-(c).

Other important simplified models include bulk first and second generation colored sparticles with mass m_l. We do not consider these here but leave them for future work.

To determine the possible collider signatures of our simplified models we simulated pair production of the colored states using MadGraph5_aMC@NLO [35] with up to one additional jet. This was matched to Pythia6 [40] using the shower-k_{T} scheme [49] with

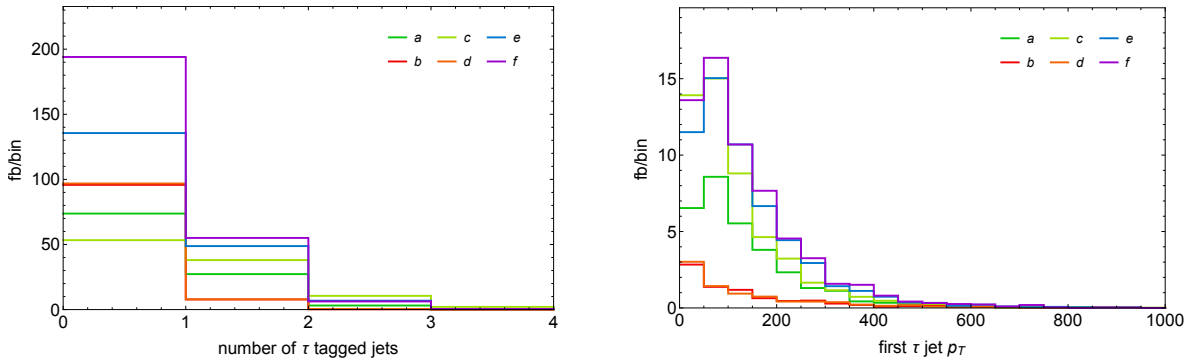

Figure 8.5: Number of τ-tagged jets (left) and p_{T} of the leading τ-tagged jet (right) for models (a)-(f). Models (a), (c), (e), and (f) will occasionally produce at least 1 τ-tagged jet. Model (c) produces more τ-jets than (a) due to cascade decays involving $\tilde{\tau}_R$. Models (b) and (d) produce fewer tau jets since the dominant decay mode is $\tilde{t}_R \to b + \nu_\tau + \tilde{\tau}_L^\dagger$ due to an off shell mixed higgsino/gaugino, as discussed in the text.

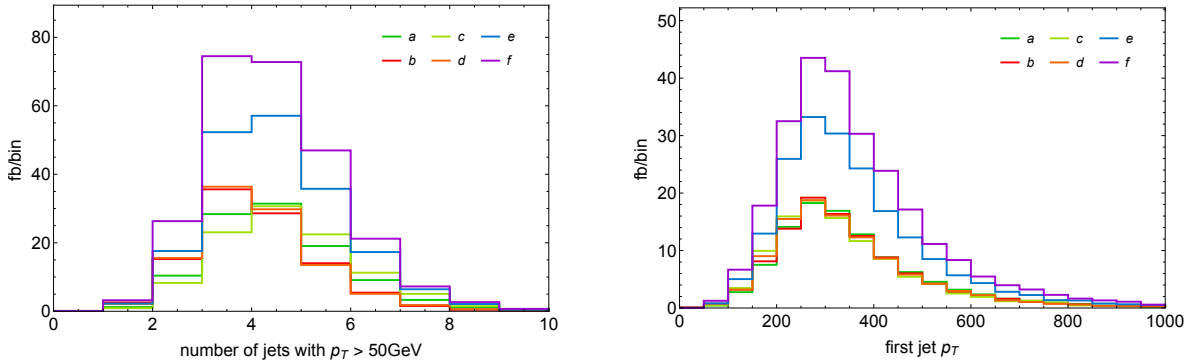

Figure 8.6: Number of jets with $p_{\mathrm{T}} > 50$ GeV (left) and p_{T} of the leading jet (right) for models (a)-(f). Each of the simplified models produces between 2-8 jets with p_{T} of the leading jet above about 200 GeV.

a matching scale of 200 GeV. The results were then fed into a Delphes simulation [52] of the ATLAS detector, within the program CheckMATE [55]. The CheckMATE team has more carefully tuned their detector simulation to match the performance of ATLAS.

We investigate b-tagged jets (fig. 8.4), τ-tagged jets (fig. 8.5), energetic jets with $p_{\mathrm{T}} > 50$ GeV (fig. 8.6), leptons (both muons and electrons) (fig. 8.7), and missing transverse energy (fig. 8.8). Jets were tagged using the anti-k_{T} algorithm with $R = 0.4$. b-jets were tagged with an efficiency of 0.8, while τ-jets were tagged using the "medium" identification criteria with an efficiency of about 0.6. Electrons were tagged using the "medium" identification criteria while muons required hits in both the muon chambers and inner tracker. For more information on object identification in the ATLAS detector simulation see ref. [52].

As can be seen in figs. 8.4-8.8, the most promising signals for each of the models are 2-8 hard jets ($p_{\mathrm{T}} > 50$ GeV) with at least one jet b-tagged, and large amounts of $E_{\mathrm{T}}^{\mathrm{miss}}$

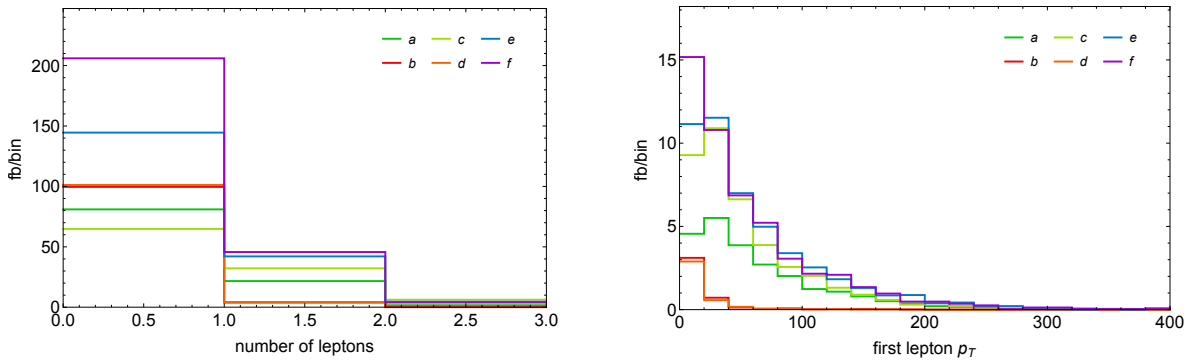

Figure 8.7: Number of leptons – both muons and electrons – (left) and p_{T} of the leading lepton (right) for models (a)-(f). Models (a), (c), (e), and (f) occasionally produce leptons; models with cascade decays produce more. Models (b) and (d) produce fewer leptons for the same reason as discussed in the caption in fig. 8.5.

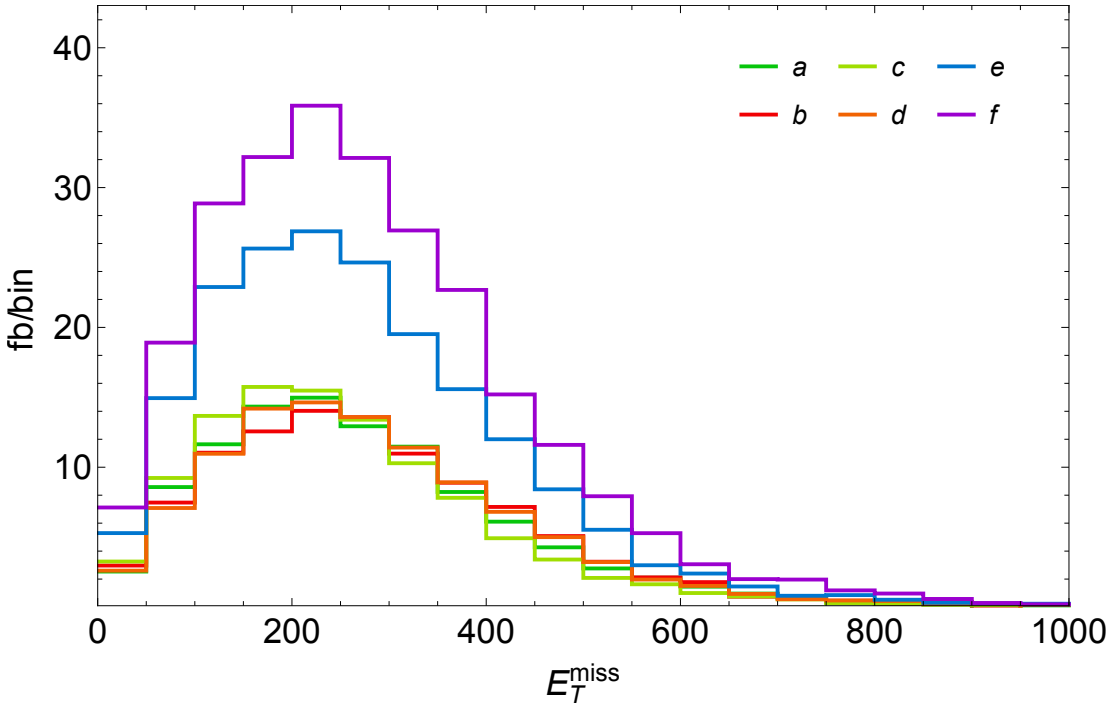

Figure 8.8: $E_{\mathrm{T}}^{\mathrm{miss}}$ for models (a)-(f). Models (b) and (d) produce more missing energy than those with cascade decays, in part because the majority of decays produce both neutrinos and sneutrinos. However, this is tempered by the fact that the vector sum of missing momentum from the three body decay involving both ν and $\tilde{\nu}$ is in less than or equal to the scalar sum of missing momentum carried by these particles. This is known as the hiding missing energy in missing energy effect and is described in detail in ref. [184].

(> 100 GeV). Leading backgrounds will include top production (both single and pair), $W +$ jets, $Z +$ jets and diboson. Though searching for τ-tagged jets and leptons could potentially improve the signal to background ratio this is not universally true for all of the simplified models.

When considering collider search limits of the simplified models we have described, it is worth noting that the three-body decay of light squarks can have important consequences. For instance, in the decay $\tilde{b}_R \to b + \nu_\tau + \tilde{\nu}_\tau^\dagger$ the vector sum of missing momentum from the three body decay involving both ν and $\tilde{\nu}$ is less than or equal to the scalar sum of missing momentum carried by these particles. Therefore, some of the event's energy will be "hidden" in $E_{\mathrm{T}}^{\mathrm{miss}}$. This is known as the hiding missing energy in missing energy effect and is described in detail in ref. [184]. Subtleties such as this might prevent one from obtaining MNSUSY limits by simply rescaling MSSM limits involving two body decays (like $\tilde{b} \to b + \tilde{\chi}_1^0$) according to the new model's production cross section and branching ratios; instead it may demand a recasting of existing searches or entirely new search strategies. Existing searches which may be sensitive to these benchmark models include [185–191]. Of course the current 13 TeV run of the LHC should be able to exclude similar simplified models with even higher values of m_l.

8.6 Conclusions

MNSUSY offers an intriguing answer to the question: why have we yet to see physics beyond the SM at the LHC? Naively using the current LHC limits on stops (~ 700 GeV) and gluinos (~ 1.4 TeV) MNSUSY has an exceptionally low fine tuning of one part in two due to the absence of large logarithms in its soft terms [7]. However, as we discussed in sec. 8.5 the limits on these particles are likely to shift in MNSUSY due to the unusual decay topologies for this model's typical low energy spectra. Setting more realistic limits requires recasting existing searches with detailed Monte Carlo simulations. This, in turn, requires a long list of Feynman rules which are most easily obtained via programs like SARAH [31] or FeynRules [30]. This is made especially challenging in the case of MNSUSY due to the unusual structure of its 4D effective theory.

In this chapter we announce the creation of a MNSUSY FeynRules model file along

with several benchmark models interesting for studying the collider phenomenology of this theory. Additionally, we give a detailed description of the model Lagrangian starting from its formulation in $\mathcal{N} = 1$ superfield language, through Scherk-Schwarz symmetry breaking, and ending with the 4D theory. We outline the masses and mixing matrices necessary to implement this model within FeynRules and describe the benchmark models which are of greatest interest. We also provide a short users manual for those wishing to use the MNSUSY FeynRules model file to set up collider simulations. Our hope is that this tool enables a recasting of existing searches for MNSUSY specific spectra and decay topologies, or better yet inspires new search strategies optimized for this theory.

Chapter 9: Summary and conclusions

The SM provides a remarkably successful description of fundamental particle interactions, though it leaves a number of open questions. One question that is particularly relevant in the LHC era is: what stabilizes the electroweak scale? As we have seen in ch. 2, the Higgs mass is very sensitive to high scale physics so that any new massive particles should pull the Higgs up to their scale. DM and gauge unification provide two compelling reasons to believe that new physics does indeed exist. Thus, if the Higgs is truly a fundamental scalar one is either led to believe that there is a remarkable accidental fine tuning of constants such that all large corrections to the Higgs mass cancel, or that the cancellation is a result of some new symmetry. SUSY, introduced in ch. 3, is an example of the latter and is all the more compelling since the LSP is a viable DM candidate and the MSSM seems to imply gauge coupling unification. Most SUSY models with low fine tuning predict that colored states should exist in the few hundred GeV to few TeV range – an exciting prospect given that this should be within reach of the LHC. Chapter 3 also introduced some of the basic concepts needed to understand extradimensional SUSY, which was the specific point of focus for this thesis.

To search for new physics at a collider requires separating the desired signal from large SM backgrounds. To do so usually requires Monte Carlo simulations, which were the focus of ch. 4. In that chapter we covered some of the tools which exist to recast existing LHC searches to hunt for new models, starting at the level of the Lagrangian written in $\mathcal{N} = 1$ superfield language, through detailed Monte Carlos and ending with the searches themselves.

Details of the LHC along with the ATLAS detector where given in ch. 5. Our discussion focused on the types of objects which are identifiable in the detector due to its construction. We also gave a very general overview of classic SUSY search strategies, giving an idea of how they worked and where they sometimes failed. In particular, we noted that regions in parameter space where sparticles are nearly degenerate to the LSP in mass (a compressed spectrum) are often difficult to detect since the decay products are not very energetic and the missing transverse momentum is reduced so that the signal can fail detector triggers or be buried under backgrounds.

In ch. 6 we went on to investigate the limits of a class of models which dynamically produce a quasi-compressed spectrum via the auto-concealment mechanism. In this, brane localized ordinary superpartners decay to the Kaluza-Klein tower of an extradimensional bulk superpartner. Since the number of KK states increases as $\sim m_n^{d-1}$ this favors decays to states closer to the mother particle in mass. We recast several searches to look for auto-concealed models and in all cases found that limits were weakened. In the most extreme example, right-handed slepton pair production, LHC limits disappeared entirely.

In ch. 7 we presented a new search designed not only to improve on auto-concealed slepton limits but also to help close off the 'classical' compressed slepton region which is currently unexplored by the LHC. Ultimately, the search proved more successful at detecting the compressed spectrum of MSSM-like models than the quasi-compressed auto-concealed spectra.

Finally, in ch. 8 we provided a detailed description of the Lagrangian and mass matrices of MNSUSY, an extradimensional SUSY model with exceptionally low fine tuning [7]. With this information we were able to code the theory as well as several benchmark models into FeynRules – both of which will eventually be public and will enable collider searches of this theory at the LHC.

Despite (or perhaps because) no signs of SUSY have been seen at the LHC, SUSY in higher dimensions is an intriguing alternative to 'classical' MSSM-like SUSY models. Auto-concealment loosens LHC limits while MNSUSY has lower fine-tuning that the MSSM. Therefore, some have argued that these extradimensional SUSY models are more compatible with current LHC data. It will be interesting to see how the tools presented in this thesis, from the compressed slepton search to the MNSUSY FeynRules model file, affect this statement in the upcoming runs of the LHC.

References

[1] **ATLAS** Collaboration, G. Aad *et. al.*, *Observation of a new particle in the search for the Standard Model Higgs boson with the ATLAS detector at the LHC*, *Phys. Lett.* **B716** (2012) 1–29, [arXiv:1207.7214].

[2] **CMS** Collaboration, S. Chatrchyan *et. al.*, *Observation of a new boson at a mass of 125 GeV with the CMS experiment at the LHC*, *Phys. Lett.* **B716** (2012) 30–61, [arXiv:1207.7235].

[3] **Particle Data Group** Collaboration, K. O. et al., *Searches for Monopoles, Supersymmetry, Technicolor, Compositeness, Extra Dimensions, etc.*, *Chin.Phys.* **C38** (2014) 090001.

[4] P. Bechtle, T. Plehn, and C. Sander, *Supersymmetry*, in *The Large Hadron Collider: Harvest of Run 1* (T. Schörner-Sadenius, ed.), pp. 421–462. 2015. arXiv:1506.0309.

[5] A. Arvanitaki, M. Baryakhtar, X. Huang, K. van Tilburg, and G. Villadoro, *The Last Vestiges of Naturalness*, *JHEP* **1403** (2014) 022, [arXiv:1309.3568].

[6] S. Dimopoulos, K. Howe, J. March-Russell, and J. Scoville, *Auto-Concealment of Supersymmetry in Extra Dimensions*, *JHEP* **1506** (2015) 041, [arXiv:1412.0805].

[7] S. Dimopoulos, K. Howe, and J. March-Russell, *Maximally Natural Supersymmetry*, *Phys.Rev.Lett.* **113** (2014) 111802, [arXiv:1404.7554].

[8] I. García García and J. March-Russell, *Rare Flavor Processes in Maximally Natural Supersymmetry*, *JHEP* **1501** (2015) 042, [arXiv:1409.5669].

[9] M. D. Schwartz, *Quantum Field Theory and the Standard Model*. Cambridge Univ. Pr., Cambridge, UK, 2013.

[10] S. P. Martin, *A Supersymmetry primer*, *Adv.Ser.Direct.High Energy Phys.* **21** (2010) 1–153, [hep-ph/9709356].

[11] J. Ellis, *Higgs Physics*, Tech. Rep. arXiv:1312.5672. KCL-PH-TH-2013-49. LCTS-2013-36. CERN-PH-TH-2013-315, Dec, 2013. 1522578.

[12] **Particle Data Group** Collaboration, K. Olive *et. al.*, *Review of Particle Physics*, *Chin.Phys.* **C38** (2014) 090001.

[13] K. G. Wilson, *The Renormalization Group and Critical Phenomena. I. Renormalization Group and the Kadanoff Scaling Picture*, *Phys. Rev. B* **4** (1971) 3174.

[14] G. 't Hooft, C. Itzykson, A. Jaffe, H. Lehmann, P. K. Mitter, I. M. Singer, and R. Stora, *Recent Developments in Gauge Theories. Proceedings, Nato Advanced Study Institute, Cargese, France, August 26 - September 8, 1979*, *NATO Sci. Ser. B* **59** (1980) pp.1–438.

[15] R. Barbieri and G. F. Giudice, *Upper Bounds on Supersymmetric Particle Masses*, *Nucl. Phys.* **B306** (1988) 63.

[16] K. D. Lane, *An Introduction to technicolor*, in *Theoretical Advanced Study Institute (TASI 93) in Elementary Particle Physics: The Building Blocks of Creation - From Microfermius to Megaparsecs Boulder, Colorado, June 6-July 2, 1993*, 1993. hep-ph/9401324.

[17] J. C. Pati and A. Salam, *Lepton Number as the Fourth Color*, *Phys.Rev.* **D10** (1974) 275–289.

[18] H. Georgi and S. Glashow, *Unity of All Elementary Particle Forces*, *Phys.Rev.Lett.* **32** (1974) 438–441.

[19] H. Georgi, H. R. Quinn, and S. Weinberg, *Hierarchy of Interactions in Unified Gauge Theories*, *Phys.Rev.Lett.* **33** (1974) 451–454.

[20] K. Garrett and G. Duda, *Dark Matter: A Primer*, *Adv.Astron.* **2011** (2011) 968283, [arXiv:1006.2483].

[21] D. Stockinger, *The Muon Magnetic Moment and Supersymmetry*, *J. Phys.* **G34** (2007) R45–R92, [hep-ph/0609168].

[22] L. E. Ibanez and G. G. Ross, *Supersymmetric Higgs and radiative electroweak breaking*, *Comptes Rendus Physique* **8** (2007) 1013–1028, [hep-ph/0702046].

[23] F. Quevedo, S. Krippendorf, and O. Schlotterer, *Cambridge Lectures on Supersymmetry and Extra Dimensions*, arXiv:1011.1491.

[24] J. Conlon, "Introduction to supersymmetry, lecture notes." http://www-thphys.physics.ox.ac.uk/people/JosephConlon/LectureNotes/SUSYLectures.pdf.

[25] J. Wess and B. Zumino, *Supergauge Transformations in Four-Dimensions*, *Nucl. Phys.* **B70** (1974) 39–50.

[26] D. Z. Freedman and A. Van Proeyen, *Supergravity*. Cambridge Univ. Pr., Cambridge, UK, 2012.

[27] J. Polchinski, *String theory. Vol. 2: Superstring theory and beyond*. Cambridge, UK.

[28] **Particle Data Group** Collaboration, J. Beringer *et. al.*, *Review of Particle Physics (RPP)*, *Phys.Rev.* **D86** (2012) 010001.

[29] P. C. West, *Introduction to supersymmetry and supergravity*. 1990.

[30] A. Alloul, N. D. Christensen, C. Degrande, C. Duhr, and B. Fuks, *FeynRules 2.0 - A complete toolbox for tree-level phenomenology*, *Comput.Phys.Commun.* **185** (2014) 2250–2300, [arXiv:1310.1921].

[31] F. Staub, *SARAH 4: A tool for (not only SUSY) model builders*, *Comput.Phys.Commun.* **185** (2014) 1773–1790, [arXiv:1309.7223].

[32] C. Degrande, *Automatic evaluation of UV and R2 terms for beyond the Standard Model Lagrangians: a proof-of-principle*, arXiv:1406.3030.

[33] W. Porod, *SPheno, a program for calculating supersymmetric spectra, SUSY particle decays and SUSY particle production at e+ e- colliders*, *Comput.Phys.Commun.* **153** (2003) 275–315, [hep-ph/0301101].

[34] W. Porod and F. Staub, *SPheno 3.1: Extensions including flavour, CP-phases and models beyond the MSSM*, *Comput.Phys.Commun.* **183** (2012) 2458–2469, [arXiv:1104.1573].

[35] J. Alwall, R. Frederix, S. Frixione, V. Hirschi, F. Maltoni, *et. al.*, *The automated computation of tree-level and next-to-leading order differential cross sections, and their matching to parton shower simulations*, *JHEP* **1407** (2014) 079, [arXiv:1405.0301].

[36] T. Gleisberg, S. Hoeche, F. Krauss, M. Schonherr, S. Schumann, *et. al.*, *Event generation with SHERPA 1.1*, *JHEP* **0902** (2009) 007, [arXiv:0811.4622].

[37] A. Belyaev, N. D. Christensen, and A. Pukhov, *CalcHEP 3.4 for collider physics within and beyond the Standard Model*, *Comput.Phys.Commun.* **184** (2013) 1729–1769, [arXiv:1207.6082].

[38] M. Moretti, T. Ohl, and J. Reuter, *O'Mega: An Optimizing matrix element generator*, hep-ph/0102195.

[39] W. Kilian, T. Ohl, and J. Reuter, *WHIZARD: Simulating Multi-Particle Processes at LHC and ILC*, *Eur.Phys.J.* **C71** (2011) 1742, [arXiv:0708.4233].

[40] T. Sjostrand, S. Mrenna, and P. Z. Skands, *PYTHIA 6.4 Physics and Manual*, *JHEP* **0605** (2006) 026, [hep-ph/0603175].

[41] M. Bahr, S. Gieseke, M. Gigg, D. Grellscheid, K. Hamilton, *et. al.*, *Herwig++ Physics and Manual*, *Eur.Phys.J.* **C58** (2008) 639–707, [arXiv:0803.0883].

[42] F. Maltoni and T. Stelzer, *MadEvent: Automatic event generation with MadGraph*, *JHEP* **0302** (2003) 027, [hep-ph/0208156].

[43] R. K. Ellis, W. J. Stirling, and B. Webber, *QCD and collider physics*, *Camb.Monogr.Part.Phys.Nucl.Phys.Cosmol.* **8** (1996) 1–435.

[44] J. I. Friedman and H. W. Kendall, *Deep inelastic electron scattering*, *Ann. Rev. Nucl. Part. Sci.* **22** (1972) 203–254.

[45] G. Altarelli and G. Parisi, *Asymptotic Freedom in Parton Language*, *Nucl. Phys.* **B126** (1977) 298.

[46] Y. L. Dokshitzer, *Calculation of the Structure Functions for Deep Inelastic Scattering and e+ e- Annihilation by Perturbation Theory in Quantum Chromodynamics.*, *Sov. Phys. JETP* **46** (1977) 641–653. [Zh. Eksp. Teor. Fiz.73,1216(1977)].

[47] V. N. Gribov and L. N. Lipatov, *Deep inelastic e p scattering in perturbation theory*, *Sov. J. Nucl. Phys.* **15** (1972) 438–450. [Yad. Fiz.15,781(1972)].

[48] **NNPDF** Collaboration, E. R. Nocera, R. D. Ball, S. Forte, G. Ridolfi, and J. Rojo, *A first unbiased global determination of polarized PDFs and their uncertainties*, *Nucl.Phys.* **B887** (2014) 276–308, [arXiv:1406.5539].

[49] J. Alwall, S. de Visscher, and F. Maltoni, *QCD radiation in the production of heavy colored particles at the LHC*, *JHEP* **0902** (2009) 017, [arXiv:0810.5350].

[50] H. K. Dreiner, M. Kramer, and J. Tattersall, *How low can SUSY go? Matching, monojets and compressed spectra*, *Europhys.Lett.* **99** (2012) 61001, [arXiv:1207.1613].

[51] B. Andersson, G. Gustafson, G. Ingelman, and T. Sjostrand, *Parton Fragmentation and String Dynamics*, *Phys.Rept.* **97** (1983) 31–145.

[52] **DELPHES 3** Collaboration, J. de Favereau *et. al.*, *DELPHES 3, A modular framework for fast simulation of a generic collider experiment*, *JHEP* **1402** (2014) 057, [arXiv:1307.6346].

[53] J. Conway, *Pgs 4 pretty good simulation of high energy collisions*, 2012.

[54] E. Richter-Was, *AcerDET: A Particle level fast simulation and reconstruction package for phenomenological studies on high p(T) physics at LHC*, hep-ph/0207355.

[55] M. Drees, H. Dreiner, D. Schmeier, J. Tattersall, and J. S. Kim, *CheckMATE: Confronting your Favourite New Physics Model with LHC Data*, arXiv:1312.2591.

[56] A. Buckley, J. Butterworth, L. Lonnblad, D. Grellscheid, H. Hoeth, *et. al.*, *Rivet user manual*, *Comput.Phys.Commun.* **184** (2013) 2803–2819, [arXiv:1003.0694].

[57] L. Rossi and O. Brüning, *The High Luminosity Large Hadron Collider: the new machine for illuminating the mysteries of Universe*. Advanced series on directions in high energy physics. World Scientific, Hackensack, NJ, 2015. Will also be published as a special issue of International journal of modern physics A.

[58] M. Lamont, *The LHC's first long run*, *CERN Courier* (Apr, 2013).

[59] **ATLAS** Collaboration, G. Aad *et. al.*, *The ATLAS Experiment at the CERN Large Hadron Collider*, *JINST* **3** (2008) S08003.

[60] M. Capeans, G. Darbo, K. Einsweiller, M. Elsing, T. Flick, M. Garcia-Sciveres, C. Gemme, H. Pernegger, O. Rohne, and R. Vuillermet, *ATLAS Insertable B-Layer Technical Design Report*, Tech. Rep. CERN-LHCC-2010-013. ATLAS-TDR-19, CERN, Geneva, Sep, 2010.

[61] **ATLAS** Collaboration, G. Aad *et. al.*, *Performance of the ATLAS Trigger System in 2010*, *Eur.Phys.J.* **C72** (2012) 1849, [arXiv:1110.1530].

[62] J. Pequenao and P. Schaffner, "A computer generated image representing how ATLAS detects particles." Jan, 2013.

[63] **ATLAS** Collaboration, G. Aad *et. al.*, *Electron reconstruction and identification efficiency measurements with the ATLAS detector using the 2011 LHC proton-proton collision data*, *Eur.Phys.J.* **C74** (2014), no. 7 2941, [arXiv:1404.2240].

[64] **ATLAS** Collaboration, G. Aad *et. al.*, *Measurement of the inclusive isolated prompt photon cross section in pp collisions at $\sqrt{s} = 7$ TeV with the ATLAS detector*, *Phys.Rev.* **D83** (2011) 052005, [arXiv:1012.4389].

[65] M. Cacciari and G. P. Salam, *Dispelling the N^3 myth for the k_t jet-finder*, *Phys.Lett.* **B641** (2006) 57–61, [hep-ph/0512210].

[66] M. Cacciari, G. P. Salam, and G. Soyez, *The Anti-k(t) jet clustering algorithm*, *JHEP* **0804** (2008) 063, [arXiv:0802.1189].

[67] **ATLAS** Collaboration, *Commissioning of the ATLAS high-performance b-tagging algorithms in the 7 TeV collision data*, Tech. Rep. ATLAS-CONF-2011-102, CERN, Geneva, Jul, 2011.

[68] M. Testa, *Refined reconstruction and calibration of the missing transverse energy in the ATLAS detector*, .

[69] A. Barr, C. Lester, and P. Stephens, *m(T2): The Truth behind the glamour*, *J.Phys.* **G29** (2003) 2343–2363, [hep-ph/0304226].

[70] C. Lester and D. Summers, *Measuring masses of semiinvisibly decaying particles pair produced at hadron colliders*, *Phys.Lett.* **B463** (1999) 99–103, [hep-ph/9906349].

[71] H.-C. Cheng and Z. Han, *Minimal Kinematic Constraints and m(T2)*, *JHEP* **0812** (2008) 063, [arXiv:0810.5178].

[72] **ATLAS** Collaboration, G. Aad *et. al.*, *Search for direct production of charginos, neutralinos and sleptons in final states with two leptons and missing transverse momentum in pp collisions at $\sqrt{s} = 8$ TeV with the ATLAS detector*, *JHEP* **05** (2014) 071, [arXiv:1403.5294].

[73] **CMS** Collaboration, V. Khachatryan *et. al.*, *Search for dark matter, extra dimensions, and unparticles in monojet events in proton–proton collisions at $\sqrt{s} = 8$ TeV*, *Eur. Phys. J.* **C75** (2015), no. 5 235, [arXiv:1408.3583].

[74] **ATLAS** Collaboration, G. Aad *et. al.*, *Search for new phenomena in final states with an energetic jet and large missing transverse momentum in pp collisions at $\sqrt{s} = 8$ TeV with the ATLAS detector*, *Eur. Phys. J.* **C75** (2015), no. 7 299, [arXiv:1502.0151].

[75] H. Baer, A. Mustafayev, and X. Tata, *Monojet plus soft dilepton signal from light higgsino pair production at LHC14*, arXiv:1409.7058.

[76] Z. Han and Y. Liu, *MT2 to the Rescue – Searching for Sleptons in Compressed Spectra at the LHC*, arXiv:1412.0618.

[77] A. Barr and J. Scoville, *A boost for the EW SUSY hunt: monojet-like search for compressed sleptons at LHC14 with 100 /fb*, *JHEP* **04** (2015) 147, [arXiv:1501.0251].

[78] D. Atwood, C. Burgess, E. Filotas, F. Leblond, D. London, *et. al.*, *Supersymmetric large extra dimensions are small and/or numerous*, *Phys.Rev.* **D63** (2001) 025007, [hep-ph/0007178].

[79] C. Burgess, J. Matias, and F. Quevedo, *MSLED: A Minimal supersymmetric large extra dimensions scenario*, *Nucl.Phys.* **B706** (2005) 71–99, [hep-ph/0404135].

[80] J. Matias and C. Burgess, *MSLED, neutrino oscillations and the cosmological constant*, *JHEP* **0509** (2005) 052, [hep-ph/0508156].

[81] M. Cicoli, C. Burgess, and F. Quevedo, *Anisotropic Modulus Stabilisation: Strings at LHC Scales with Micron-sized Extra Dimensions*, *JHEP* **1110** (2011) 119, [arXiv:1105.2107].

[82] I. Antoniadis, K. Benakli, and A. Laugier, *D-brane models with nonlinear supersymmetry*, *Nucl.Phys.* **B631** (2002) 3–42, [hep-th/0111209].

[83] E. Dudas and J. Mourad, *Consistent gravitino couplings in nonsupersymmetric strings*, *Phys.Lett.* **B514** (2001) 173–182, [hep-th/0012071].

[84] M. Klein, *Couplings in pseudosupersymmetry*, *Phys.Rev.* **D66** (2002) 055009, [hep-th/0205300].

[85] I. Antoniadis and M. Tuckmantel, *Nonlinear supersymmetry and intersecting D-branes*, *Nucl.Phys.* **B697** (2004) 3–47, [hep-th/0406010].

[86] E. Izaguirre, M. Manhart, and J. G. Wacker, *Bigger, Better, Faster, More at the LHC*, *JHEP* **1012** (2010) 030, [arXiv:1003.3886].

[87] T. J. LeCompte and S. P. Martin, *Compressed supersymmetry after 1/fb at the Large Hadron Collider*, *Phys.Rev.* **D85** (2012) 035023, [arXiv:1111.6897].

[88] T. J. LeCompte and S. P. Martin, *Large Hadron Collider reach for supersymmetric models with compressed mass spectra*, *Phys.Rev.* **D84** (2011) 015004, [arXiv:1105.4304].

[89] B. Bhattacherjee and K. Ghosh, *Degenerate SUSY search at the 8 TeV LHC*, arXiv:1207.6289.

[90] M. Drees, M. Hanussek, and J. S. Kim, *Light Stop Searches at the LHC with Monojet Events*, *Phys.Rev.* **D86** (2012) 035024, [arXiv:1201.5714].

[91] G. Belanger, M. Heikinheimo, and V. Sanz, *Model-Independent Bounds on Squarks from Monophoton Searches*, *JHEP* **1208** (2012) 151, [arXiv:1205.1463].

[92] B. Bhattacherjee, A. Choudhury, K. Ghosh, and S. Poddar, *Compressed supersymmetry at 14 TeV LHC*, *Phys.Rev.* **D89** (2014), no. 3 037702, [arXiv:1308.1526].

[93] K. R. Dienes, S. Su, and B. Thomas, *Distinguishing Dynamical Dark Matter at the LHC*, *Phys.Rev.* **D86** (2012) 054008, [arXiv:1204.4183].

[94] K. R. Dienes, S. Su, and B. Thomas, *Strategies for Probing Non-Minimal Dark Sectors at Colliders: The Interplay Between Cuts and Kinematic Distributions*, arXiv:1407.2606.

[95] E. A. Mirabelli and M. E. Peskin, *Transmission of supersymmetry breaking from a four-dimensional boundary*, *Phys.Rev.* **D58** (1998) 065002, [hep-th/9712214].

[96] R. Sundrum, *Effective field theory for a three-brane universe*, *Phys.Rev.* **D59** (1999) 085009, [hep-ph/9805471].

[97] N. Arkani-Hamed, T. Gregoire, and J. G. Wacker, *Higher dimensional supersymmetry in 4-D superspace*, *JHEP* **0203** (2002) 055, [hep-th/0101233].

[98] D. Marti and A. Pomarol, *Supersymmetric theories with compact extra dimensions in N=1 superfields*, *Phys.Rev.* **D64** (2001) 105025, [hep-th/0106256].

[99] A. Hebecker, *5-D superYang-Mills theory in 4-D superspace, superfield brane operators, and applications to orbifold GUTs*, *Nucl.Phys.* **B632** (2002) 101–113, [hep-ph/0112230].

[100] I. Linch, William Divine, M. A. Luty, and J. Phillips, *Five-dimensional supergravity in N=1 superspace*, *Phys.Rev.* **D68** (2003) 025008, [hep-th/0209060].

[101] J. L. Hewett and D. Sadri, *Supersymmetric extra dimensions: Gravitino effects in selectron pair production*, *Phys.Rev.* **D69** (2004) 015001, [hep-ph/0204063].

[102] N. Kaloper, J. March-Russell, G. D. Starkman, and M. Trodden, *Compact hyperbolic extra dimensions: Branes, Kaluza-Klein modes and cosmology*, *Phys.Rev.Lett.* **85** (2000) 928–931, [hep-ph/0002001].

[103] J. Alwall, M. Herquet, F. Maltoni, O. Mattelaer, and T. Stelzer, *MadGraph 5 : Going Beyond*, *JHEP* **1106** (2011) 128, [arXiv:1106.0522].

[104] **ATLAS** Collaboration, G. Aad *et. al.*, *Search for direct top-squark pair production in final states with two leptons in pp collisions at $\sqrt{s}$ = 8TeV with the ATLAS detector*, *JHEP* **1406** (2014) 124, [arXiv:1403.4853].

[105] M. Cacciari, G. P. Salam, and G. Soyez, *FastJet User Manual*, *Eur.Phys.J.* **C72** (2012) 1896, [arXiv:1111.6097].

[106] A. L. Read, *Presentation of search results: The CL(s) technique*, *J.Phys.* **G28** (2002) 2693–2704.

[107] **ATLAS** Collaboration, *Search for direct-slepton and direct-chargino production in final states with two opposite-sign leptons, missing transverse momentum and no jets in 20/fb of pp collisions at sqrt(s) = 8 TeV with the ATLAS detector*, Tech. Rep. ATLAS-CONF-2013-049, ATLAS-COM-CONF-2013-050, CERN, Geneva, May, 2013.

[108] **ATLAS** Collaboration, *Search for strongly produced supersymmetric particles in decays with two leptons at $\sqrt{s}$ = 8 TeV*, Tech. Rep. ATLAS-CONF-2013-089, ATLAS-COM-CONF-2013-109, CERN, Geneva, August, 2013.

[109] **ATLAS** Collaboration, *Search for New Phenomena in Monojet plus Missing Transverse Momentum Final States using 10fb-1 of pp Collisions at sqrts=8 TeV with the ATLAS detector at the LHC*, Tech. Rep. ATLAS-CONF-2012-147, ATLAS-COM-CONF-2012-190, CERN, Geneva, May, 2012.

[110] W. Beenakker, M. Klasen, M. Kramer, T. Plehn, M. Spira, *et. al.*, *The Production of charginos / neutralinos and sleptons at hadron colliders*, *Phys.Rev.Lett.* **83** (1999) 3780–3783, [hep-ph/9906298].

[111] **LEPSUSYWG,ALEPH,DELPHI,L3, and OPAL experiments** Collaboration, *Combined LEP Selectron/Smuon/Stau Results, 183-208 GeV*, Tech. Rep. LEPSUSYWG/04-01.1, CERN, Geneva, June, 2004.

[112] **ALEPH** Collaboration, A. Heister *et. al.*, *Search for scalar leptons in e+ e- collisions at center-of-mass energies up to 209-GeV*, *Phys.Lett.* **B526** (2002) 206–220, [hep-ex/0112011].

[113] **L3** Collaboration, P. Achard *et. al.*, *Search for scalar leptons and scalar quarks at LEP*, *Phys.Lett.* **B580** (2004) 37–49, [hep-ex/0310007].

[114] **OPAL** Collaboration, G. Abbiendi *et. al.*, *Search for anomalous production of dilepton events with missing transverse momentum in e+ e- collisions at s**(1/2) = 183-Gev to 209-GeV*, *Eur.Phys.J.* **C32** (2004) 453–473, [hep-ex/0309014].

[115] **DELPHI** Collaboration, J. Abdallah *et. al.*, *Searches for supersymmetric particles in e+ e- collisions up to 208-GeV and interpretation of the results within the MSSM*, *Eur.Phys.J.* **C31** (2003) 421–479, [hep-ex/0311019].

[116] **ATLAS** Collaboration, *Search for direct production of the top squark in the all-hadronic ttbar + etmiss final state in 21 fb-1 of p-pcollisions at sqrt(s)=8 TeV with the ATLAS detector*, Tech. Rep. ATLAS-CONF-2013-024, ATLAS-COM-CONF-2013-011, CERN, Geneva, March, 2013.

[117] **ATLAS** Collaboration, G. Aad *et. al.*, *Search for top squark pair production in final states with one isolated lepton, jets, and missing transverse momentum in $\sqrt{s} = 8$ TeV pp collisions with the ATLAS detector*, arXiv:1407.0583.

[118] **ATLAS** Collaboration, *Search for pair-produced third-generation squarks decaying via charm quarks or in compressed supersymmetric scenarios in pp collisions at $\sqrt{s} = 8$ TeV with the ATLAS detector*, *Phys.Rev.* **D90** (2014) 052008, [arXiv:1407.0608].

[119] "LHC SUSY Cross Section Working Group." https://twiki.cern.ch/twiki/bin/view/LHCPhysics/SUSYCrossSections.

[120] M. Kramer, A. Kulesza, R. van der Leeuw, M. Mangano, S. Padhi, *et. al.*, *Supersymmetry production cross sections in pp collisions at $\sqrt{s} = 7$ TeV*, arXiv:1206.2892.

[121] **CMS** Collaboration, *Exclusion limits on gluino and top-squark pair production in natural SUSY scenarios with inclusive razor and exclusive single-lepton searches at 8 TeV.*, Tech. Rep. CMS-PAS-SUS-14-011, CERN, Geneva, 2014.

[122] **ATLAS** Collaboration, G. Aad *et. al.*, *Search for direct pair production of the top squark in all-hadronic final states in proton-proton collisions at $\sqrt{s} = 8$ TeV with the ATLAS detector*, *JHEP* **1409** (2014) 015, [arXiv:1406.1122].

[123] **ATLAS** Collaboration, *Search for squarks and gluinos with the ATLAS detector in final states with jets and missing transverse momentum and 20.3 fb^{-1} of $\sqrt{s} = 8$ TeV proton-proton collision data*, Tech. Rep. ATLAS-CONF-2013-047, ATLAS-COM-CONF-2013-049, CERN, Geneva, May, 2013.

[124] M. R. Buckley, J. D. Lykken, C. Rogan, and M. Spiropulu, *Super-Razor and Searches for Sleptons and Charginos at the LHC*, *Phys.Rev.* **D89** (2014) 055020, [arXiv:1310.4827].

[125] K. Rolbiecki and K. Sakurai, *Constraining compressed supersymmetry using leptonic signatures*, *JHEP* **1210** (2012) 071, [arXiv:1206.6767].

[126] G. F. Giudice, T. Han, K. Wang, and L.-T. Wang, *Nearly Degenerate Gauginos and Dark Matter at the LHC*, *Phys.Rev.* **D81** (2010) 115011, [arXiv:1004.4902].

[127] P. Schwaller and J. Zurita, *Compressed electroweakino spectra at the LHC*, *JHEP* **1403** (2014) 060, [arXiv:1312.7350].

[128] **ATLAS** Collaboration, G. Aad *et. al.*, *Search for contact interactions and large extra dimensions in the dilepton channel using proton-proton collisions at $\sqrt{s} = 8$ TeV with the ATLAS detector*, arXiv:1407.2410.

[129] **ATLAS** Collaboration, G. Aad *et. al.*, *Search for dark matter candidates and large extra dimensions in events with a jet and missing transverse momentum with the ATLAS detector*, *JHEP* **1304** (2013) 075, [arXiv:1210.4491].

[130] S. Baek, S. C. Park, and J.-h. Song, *Kaluza-Klein gravitino production with a single photon at e+ e- colliders*, *Phys.Rev.* **D66** (2002) 056004, [hep-ph/0206008].

[131] G. F. Giudice, R. Rattazzi, and J. D. Wells, *Quantum gravity and extra dimensions at high-energy colliders*, *Nucl.Phys.* **B544** (1999) 3–38, [hep-ph/9811291].

[132] J. L. Hewett, *Indirect collider signals for extra dimensions*, *Phys.Rev.Lett.* **82** (1999) 4765–4768, [hep-ph/9811356].

[133] E. A. Mirabelli, M. Perelstein, and M. E. Peskin, *Collider signatures of new large space dimensions*, *Phys.Rev.Lett.* **82** (1999) 2236–2239, [hep-ph/9811337].

[134] T. Han, J. D. Lykken, and R.-J. Zhang, *On Kaluza-Klein states from large extra dimensions*, *Phys.Rev.* **D59** (1999) 105006, [hep-ph/9811350].

[135] R. Contino, L. Pilo, R. Rattazzi, and A. Strumia, *Graviton loops and brane observables*, *JHEP* **0106** (2001) 005, [hep-ph/0103104].

[136] G. F. Giudice and A. Strumia, *Constraints on extra dimensional theories from virtual graviton exchange*, *Nucl.Phys.* **B663** (2003) 377–393, [hep-ph/0301232].

[137] G. F. Giudice, T. Plehn, and A. Strumia, *Graviton collider effects in one and more large extra dimensions*, *Nucl.Phys.* **B706** (2005) 455–483, [hep-ph/0408320].

[138] R. Diener and C. Burgess, *Bulk Stabilization, the Extra-Dimensional Higgs Portal and Missing Energy in Higgs Events*, *JHEP* **1305** (2013) 078, [arXiv:1302.6486].

[139] S. Hannestad and G. G. Raffelt, *Supernova and neutron star limits on large extra dimensions reexamined*, *Phys.Rev.* **D67** (2003) 125008, [hep-ph/0304029].

[140] A. J. Barr and C. G. Lester, *A Review of the Mass Measurement Techniques proposed for the Large Hadron Collider*, *J.Phys.* **G37** (2010) 123001, [arXiv:1004.2732].

[141] G. Moortgat-Pick, *LHC/ILC Interplay in SUSY Searches*, *J.Phys.Conf.Ser.* **110** (2008) 072027, [arXiv:0801.2414].

[142] **ILC** Collaboration, G. Aarons *et. al.*, *International Linear Collider Reference Design Report Volume 2: Physics at the ILC*, arXiv:0709.1893.

[143] H.-U. Martyn, *Detection of sleptons at a linear collider in models with small slepton-neutralino mass differences*, hep-ph/0408226.

[144] H.-U. Martyn, *Study of sleptons at a linear collider - supersymmetry scenario SPS 1a*, hep-ph/0406123.

[145] S. Asai, K. Hamaguchi, and S. Shirai, *Measuring lifetimes of long-lived charged massive particles stopped in LHC detectors*, *Phys.Rev.Lett.* **103** (2009) 141803, [arXiv:0902.3754].

[146] J. Pinfold and L. Sibley, *Measuring the Lifetime of Trapped Sleptons Using the General Purpose LHC Detectors*, *Phys.Rev.* **D83** (2011) 035021, [arXiv:1006.3293].

[147] T. Ito, K. Nakaji, and S. Shirai, *Identifying the Origin of Longevity of Metastable Stau at the LHC*, *Phys.Lett.* **B706** (2012) 314–319, [arXiv:1104.2101].

[148] I. Hinchliffe and F. Paige, *Measurements in gauge mediated SUSY breaking models at CERN LHC*, *Phys.Rev.* **D60** (1999) 095002, [hep-ph/9812233].

[149] W. Kilian, T. Plehn, P. Richardson, and E. Schmidt, *Split supersymmetry at colliders*, *Eur.Phys.J.* **C39** (2005) 229–243, [hep-ph/0408088].

[150] B. Allanach, C. Harris, M. A. Parker, P. Richardson, and B. Webber, *Detecting exotic heavy leptons at the large hadron collider*, *JHEP* **0108** (2001) 051, [hep-ph/0108097].

[151] A. Rajaraman and B. T. Smith, *Determining Spins of Metastable Sleptons at the Large Hadron Collider*, *Phys.Rev.* **D76** (2007) 115004, [arXiv:0708.3100].

[152] R. Kitano, *Study of chargino-neutralino production at hadron colliders in a long-lived slepton scenario*, *JHEP* **0811** (2008) 045, [arXiv:0806.1057].

[153] J. L. Feng, S. T. French, C. G. Lester, Y. Nir, and Y. Shadmi, *The Shifted Peak: Resolving Nearly Degenerate Particles at the LHC*, *Phys.Rev.* **D80** (2009) 114004, [arXiv:0906.4215].

[154] M. A. Luty and D. J. Phalen, *Higgsstrahlung from R-hadrons*, *JHEP* **1111** (2011) 019, [arXiv:1105.1166].

[155] S. Chang, C. Kilic, and T. Okui, *Measuring Top Squark Interactions With The Standard Model Through Associated Production*, *Phys.Rev.* **D84** (2011) 035015, [arXiv:1105.1332].

[156] W. Buchmuller, K. Hamaguchi, M. Ratz, and T. Yanagida, *Gravitino and goldstino at colliders*, hep-ph/0403203.

[157] W. Buchmuller, K. Hamaguchi, M. Ratz, and T. Yanagida, *Supergravity at colliders*, *Phys.Lett.* **B588** (2004) 90–98, [hep-ph/0402179].

[158] P. W. Graham, K. Howe, S. Rajendran, and D. Stolarski, *New Measurements with Stopped Particles at the LHC*, *Phys.Rev.* **D86** (2012) 034020, [arXiv:1111.4176].

[159] K. Hamaguchi, Y. Kuno, T. Nakaya, and M. M. Nojiri, *A Study of late decaying charged particles at future colliders*, *Phys.Rev.* **D70** (2004) 115007, [hep-ph/0409248].

[160] J. L. Feng and B. T. Smith, *Slepton trapping at the large hadron and international linear colliders*, *Phys.Rev.* **D71** (2005) 015004, [hep-ph/0409278].

[161] **ATLAS, CMS** Collaboration, P. de Jong, *Supersymmetry searches at the LHC*, arXiv:1211.3887.

[162] **CMS** Collaboration, *Searches for electroweak production of charginos, neutralinos, and sleptons decaying to leptons and W, Z, and Higgs bosons in pp collisions at 8 TeV*, *Eur.Phys.J.* **C74** (2014), no. 9 3036, [arXiv:1405.7570].

[163] J. F. Gunion and S. Mrenna, *A Study of SUSY signatures at the Tevatron in models with near mass degeneracy of the lightest chargino and neutralino*, *Phys.Rev.* **D62** (2000) 015002, [hep-ph/9906270].

[164] S. Mukhopadhyay, M. M. Nojiri, and T. T. Yanagida, *Compressed SUSY search at the 13 TeV LHC using kinematic correlations and structure of ISR jets*, *JHEP* **1410** (2014) 12, [arXiv:1403.6028].

[165] C. Han, A. Kobakhidze, N. Liu, A. Saavedra, L. Wu, and J. M. Yang, *Probing Light Higgsinos in Natural SUSY from Monojet Signals at the LHC*, *JHEP* **02** (2014) 049, [arXiv:1310.4274].

[166] **CMS** Collaboration, *Search for top squarks decaying to a charm quark and a neutralino in events with a jet and missing transverse momentum*, CMS-PAS-SUS-13-009.

[167] Z. Han, G. D. Kribs, A. Martin, and A. Menon, *Hunting quasidegenerate Higgsinos*, *Phys.Rev.* **D89** (2014) 075007, [arXiv:1401.1235].

[168] **CMS** Collaboration, *Search for physics beyond the standard model in events with two opposite-sign same-flavor leptons, jets, and missing transverse energy in pp collisions at sqrt[s] = 8 TeV*, CMS-PAS-SUS-12-019.

[169] B. Dutta, T. Ghosh, A. Gurrola, W. Johns, T. Kamon, *et. al.*, *Probing Compressed Sleptons at the LHC using Vector Boson Fusion Processes*, arXiv:1411.6043.

[170] O. Shekhovtsova, I. Nugent, T. Przedzinski, P. Roig, and Z. Was, *MC generator TAUOLA: implementation of Resonance Chiral Theory for two and three meson modes. Comparison with experiment*, *AIP Conf.Proc.* **1492** (2012) 62–66, [arXiv:1208.5420].

[171] **ATLAS** Collaboration, *Search for direct-slepton and direct-chargino production in final states with two opposite-sign leptons, missing transverse momentum and no jets in 20/fb of pp collisions at sqrt(s) = 8 TeV with the ATLAS detector*, ATLAS-CONF-2013-049.

[172] G. Cullen, N. Greiner, and G. Heinrich, *Susy-QCD corrections to neutralino pair production in association with a jet*, *Eur. Phys. J.* **C73** (2013), no. 4 2388, [arXiv:1212.5154].

[173] **LEP SUSY Working Group (ALEPH, DELPHI, L3, OPAL)** Collaboration, "Notes LEPSUSYWG/01-03.1, 04-01.1." http://lepsusy.web.cern.ch/lepsusy/Welcome.html.

[174] K. Howe and J. Scoville, *Benchmark Models for Maximally Natural Supersymmetry*, *In preparation* (2015).

[175] A. Delgado, G. von Gersdorff, P. John, and M. Quiros, *One loop Higgs mass finiteness in supersymmetric Kaluza-Klein theories*, *Phys. Lett.* **B517** (2001) 445–449, [hep-ph/0104112].

[176] R. Contino and L. Pilo, *A Note on regularization methods in Kaluza-Klein theories*, *Phys. Lett.* **B523** (2001) 347–350, [hep-ph/0104130].

[177] N. Weiner, *Ineffective supersymmetry: Electroweak symmetry breaking from extra dimensions*, in *36th Rencontres de Moriond on Electroweak Interactions and Unified Theories Les Arcs, France, March 10-17, 2001*, 2001. hep-ph/0106021.

[178] D. V. Belyaev, *Boundary conditions in the Mirabelli and Peskin model*, *JHEP* **0601** (2006) 046, [hep-th/0509171].

[179] R. Barbieri, L. J. Hall, and Y. Nomura, *A Constrained standard model from a compact extra dimension*, *Phys.Rev.* **D63** (2001) 105007, [hep-ph/0011311].

[180] T. Gherghetta and A. Riotto, *Gravity mediated supersymmetry breaking in the brane world*, *Nucl.Phys.* **B623** (2002) 97–125, [hep-th/0110022].

[181] I. Antoniadis, S. Dimopoulos, A. Pomarol, and M. Quiros, *Soft masses in theories with supersymmetry breaking by TeV compactification*, *Nucl.Phys.* **B544** (1999) 503–519, [hep-ph/9810410].

[182] S. Choi, D. Choudhury, A. Freitas, J. Kalinowski, and P. Zerwas, *The Extended Higgs System in R-symmetric Supersymmetry Theories*, *Phys.Lett.* **B697** (2011) 215–221, [arXiv:1012.2688].

[183] A. Alloul, J. D'Hondt, K. De Causmaecker, B. Fuks, and M. Rausch de Traubenberg, *Automated mass spectrum generation for new physics*, *Eur.Phys.J.* **C73** (2013), no. 2 2325, [arXiv:1301.5932].

[184] D. S. M. Alves, J. Liu, and N. Weiner, *Hiding Missing Energy in Missing Energy*, *JHEP* **04** (2015) 088, [arXiv:1312.4965].

[185] **ATLAS** Collaboration, G. Aad *et. al.*, *Search for direct scalar top pair production in final states with two tau leptons in pp collisions at $\sqrt{s} = 8$ TeV with the ATLAS detector*, arXiv:1509.0497.

[186] **ATLAS** Collaboration, G. Aad *et. al.*, *Search for massive supersymmetric particles decaying to many jets using the ATLAS detector in pp collisions at $\sqrt{s} = 8$ TeV*, *Phys. Rev.* **D91** (2015), no. 11 112016, [arXiv:1502.0568].

[187] **ATLAS** Collaboration, G. Aad *et. al.*, *Search for squarks and gluinos with the ATLAS detector in final states with jets and missing transverse momentum using $\sqrt{s} = 8$ TeV proton–proton collision data*, *JHEP* **09** (2014) 176, [arXiv:1405.7875].

[188] **ATLAS** Collaboration, G. Aad *et. al.*, *Search for new phenomena in final states with large jet multiplicities and missing transverse momentum at $\sqrt{s}$=8 TeV proton-proton collisions using the ATLAS experiment*, *JHEP* **10** (2013) 130, [arXiv:1308.1841]. [Erratum: JHEP01,109(2014)].

[189] **CMS** Collaboration, V. Khachatryan *et. al.*, *Searches for third-generation squark production in fully hadronic final states in proton-proton collisions at $\sqrt{s} = 8$ TeV*, *JHEP* **06** (2015) 116, [arXiv:1503.0803].

[190] **CMS** Collaboration, S. Chatrchyan *et. al.*, *Search for new physics in the multijet and missing transverse momentum final state in proton-proton collisions at $\sqrt{s}$= 8 TeV*, *JHEP* **06** (2014) 055, [arXiv:1402.4770].

[191] **CMS** Collaboration, S. Chatrchyan *et. al.*, *Search for supersymmetry in hadronic final states with missing transverse energy using the variables α_T and b-quark multiplicity in pp collisions at $\sqrt{s} = 8$ TeV*, *Eur. Phys. J.* **C73** (2013), no. 9 2568, [arXiv:1303.2985].